MCDONNELL DOUGLAS TECHNICAL SERVICES CO.
HOUSTON ASTRONAUTICS DIVISION

SPACE SHUTTLE ENGINEERING AND OPERATIONS SUPPORT

1.2-DN-B0603-007

TRACKER IMPLEMENTATION FOR THE ORBITER Ku-BAND COMMUNICATIONS ANTENNA

ENGINEERING SYSTEMS ANALYSIS

1 OCTOBER 1976

This Design Note is Submitted to NASA Under Task Order No. B0603, Contract NAS 9-14960.

PREPARED BY: J. F. Rudnicki
J. F. Rudnicki
Electronics Engineer
488-5660 Ext. 256

PREPARED BY: J. F. Lindsey
J. F. Lindsey
Task Manager
488-5660 Ext. 252

APPROVED BY: L. R. Blanke
L. R. Blanke
Technical Manager
488-5660 Ext. 261

APPROVED BY: R. F. Pannett
R. F. Pannett
Project Manager
488-5660 Ext. 258

TABLE OF CONTENTS (CONTINUED)

LIST OF FIGURES

APPENDIX A

LIST OF FIGURES (CONT.)

LIST OF FIGURES (CONT)

LIST OF FIGURES (CONT.)

APPENDIX B

LIST OF TABLES

1.0 SUMMARY

The purpose of this design note is to evaluate possible implementations and make recommendations for the Space Shuttle Ku-Band Integrated Communications/ Radar Antenna Tracking system. The study emphasizes communication aspects involving the Tracking Data Relay Satellite (TDRS)/Orbiter Ku-Band link. Detailed analysis of antenna sizes, gains and signal-to-noise ratios shows the desirability of using maximum size 36-inch diameter dish and a triple channel monopulse. The use of the original baselined 20 inch dish is found to result in excessive acquisition time since the despread signal would be used in the tracking loop. Evaluation of vehicle dynamics shows typical communication timelines for various on-orbit activities and relatively slow look angle rate changes over 90 percent of the on-orbit activities during a mission. An evaluation of scan procedures which includes vehicle dynamics, designation error, time for acquisition and probability of acquisition shows that the conical scan is preferred since the time for lock-on for relatively slow look angle rates will be significantly shorter than the raster scan. An evaluation of Orbiter body and yoke blockage shows that significant improvement in spherical coverage may be obtained by reorienting the antenna gimbal to obtain maximum blockage overlap. Also, a simplified evaluation has shown that multipath will have some limiting effects on communications; however, additional study is suggested to more accurately determine these effects. Also, it is suggested that the allowed Doppler shift may be reduced to minimize lock-on time during acquisition.

2.0 INTRODUCTION

The purpose of this design note is to evaluate and trade-off significant design parameters and make recommendations for the implementation of the tracker for the Space Shuttle Orbiter Ku-Band Communications Antenna System. First, background information is given to show the present status of the development of the Ku-Band System. This is followed by a detailed discussion of significant parameters which relate to tracker implementation. Factors included in the discussion are: (1) antenna power gain as related to beamwidth and antenna size (2) tracking loop signal-to-noise ratio considerations (3) effects of spread spectrum and Doppler phenomenon on tracking and acquisition (4) vehicle dynamics effects on acquisition and tracking (5) scan parameters for acquisition and tracking including antenna location and gimbal orientations as related to spherical coverage factors (6) effects of multipath on performance and (7) single versus triple channel monopulse. Specific recommendations may not be given in the discussion subsections since many factors are interrelated. The individual factors and parameters developed in the discussion subsections are combined and interrelated in the results section to illustrate the rationale for the recommended implementation The results of this study are intended to influence the optimum choice for the design, specification and implementation of the Ku-Band tracker system. Finally, concise recommendations are given in the conclusion section which is followed by a listing of the references used in this design note.

The illustrations in this paper in figure form are compiled in Appendix A and the computer programs are compiled in Appendix B for the reader's convenience

3.0 BACKGROUND

The Ku-Band Communications Antenna System will initially consist of a single antenna on the Space Shuttle Orbiter. This antenna will be capable of automatically acquiring and tracking an appropriate synchronous orbit Tracking and Data Relay Satellite (TDRS). This capability is scheduled to begin on the fourth operational flight test (OFT-4) and current planning entails the addition of a second antenna for increased coverage on OFT-17 (Reference A). The antennas will be stowed within the payload bay during ascent and descent. The first antenna to be used beginning on OFT-4 will deploy from the right side of the Orbiter and will serve both communication and radar functions. The second antenna beginning with OFT-17 will deploy from the left side of the Orbiter and serve only a communications function Detailed specifications for the antenna and associated equipment are given in Reference B, which was issued in March of 1976. Subsequently proposals were written and submitted to Rockwell and the selection process is currently in progress. The detailed design and implementation for the Ku-Band Antenna and tracker has not been fully established.

A number of studies have been performed to date involving the Ku-Band System. A study was made by Rockwell in 1973 (Reference C) to determine requirements and constraints for the Ku-Band integrated communications/radar system. Studies by Hughes, Axiomatics and Dynamic Development Corporation (References D, E, and F), principally involved with radar optimization, were completed in 1975 and 1976. Also, recent studies have been performed by Lockheed in Houston (Reference G and H) concerning acquisition and tracking aspects of the Ku-Band system. Lastly, some detailed studies relating to this subject have been performed at McDonnell Douglas in Houston (References I, J, K, L, M and N).

Significant factors relating to the Orbiter Ku-Band Antenna System are given in Table I and a functional block diagram based on Reference B is given in Figure 1. Significant aspects of the six McDonnell Douglas working papers are combined and summarized in this report.

PARAMETER	VALUE OR RANGE
Orbiter Transmitter Output Power	50 W (minimum)
Forward Link Frequency Band	13.75-13.80 GHz
Return Link Frequency Band	14.896-15.121 GHz
Center Frequency	13.775 GHz (Forward Link) 15.0085 GHz (Return Link)
Specified r.f. Bandwidth	50 MHz (Forward Link) 225 MHz (Return Link)
Assumed Spread Spectrum Bandwidth	25 MHz
Spread Spectrum Degradation in PN Despreader (assumed)	-1.5 dB
Orbiter Orbital Altitudes	100-600 n mi. (nominally circular)
Maximum Doppler (Forward Link)	$\pm$500 kHz
Antenna Efficiency	55%
Orbiter Antenna Power Gain	$\geq$34.5 dB (receive at 13.775 GHz) $\geq$35.4 dB (transmit at 15.0085 GHz)
Antenna Sidelobes	18 dB down from peak
Polarization	RHCP (Communications) Linear (Radar)
Antenna Pointing Angle Computer Update	2 seconds
Scan Region for Acquisition	20 by 20 degree search field
Designation Error-Orbiter Antenna	2.8 degrees (maximum)
Scan Rate	10 degrees/second (maximum)
Orbiter Antenna Acquisition Time	60 seconds (maximum)
Orbiter Antenna Reacquisition Time	30 seconds (maximum)
TDRS Effective Isotropic Radiated Power (EIRP)	48.0 dBw (minimum)
TDRS Orbital Altitude	19,323 n.mi (nominally circular)

Table 1 Pertinent Ku-Band Antenna Parameters

4.0 DISCUSSION

The discussion section is divided into seven subsections in which specific parameters are developed. In the first subsection, 4.1, the power gain and beamwidth parameters are determined for four dish sizes ranging from the baselined diameter of 20 inches to the maximum permitted size of 36 inches. The power gain significantly affects signal-to-noise ratios, and the beamwidth affects the length of time required for a scan cycle during acquisition of the TDRS by the Orbiter antenna. The second subsection, 4.2, deals with the signal-to-noise ratio in the tracking loop as related to antenna power gain, the use of a spread or despread signal and the variation in slant range of the Orbiter from the TDRS. The factors in this subsection are significantly related to the selection of the dish size. Subsection 4.3 defines the amplitude versus frequency content of the spread spectrum signal received by the Orbiter. Also, Doppler shift and Doppler rates are calculated for Orbiter altitudes of 100 n.mi. and 600 n.mi. The results of this section affect the design of the automatic frequency control, amplifiers, and filters used by the Orbiter receiver in the tracking loop. Subsection 4.4 shows the relationship between Orbiter vehicle dynamics for planned attitudes and look angle changes between the Orbiter Ku-Band Antenna and the TDRS. Typical communication timelines for various planned activities are also developed to show expected operational limitations. Subsection 4.5 deals with scan parameters and includes an evaluation of the limitations for spherical coverage imposed by the antenna yoke and Orbiter body. This subsection also includes an estimation of detection time and probability of detection as related to the raster and conical scan, designation error and vehicle dynamics (look angle rate). The results of this section will show operational limitations, a recommended gimbal orientation and a recommended

scanning procedure. In Subsection 4.6 a simplified model is developed to determine possible multipath effects on tracking as related to operational limitations and finally in Subsection 4.7 the relative merits of the three channel monopulse feed system versus the single channel feed system are given to make a recommendation for the tracking system implementation.

In most cases final conclusions are not drawn in the discussion subsections since multiple factors need to be considered. Since many of the subsections in the discussion are interrelated, the development and rationale for specific recommendations are given in Section 5 0, entitled Results.

4.1 Antenna Patterns

An important aspect to investigate relative to the Ku-Band Shuttle Orbiter tracking and acquisition implementation is the radiation pattern of a parabolic reflector. Antenna patterns for 20, 26, 30 and 36 inch reflectors are calculated as a function of boresight angle for the normalized electric field magnitude and the relative power. From these patterns the half power beamwidth (HPBW), antenna power gains, and side lobe levels will be obtained for the four respective circular reflectors. These parameters are useful in the calculation of the signal-to-noise ratio and scanning procedures for the Ku-Band Antenna.

The normalized electric field magnitude and relative power patterns were produced using the calculator program found in Figure 84 of Appendix B. The normalized electric field pattern is calculated with the use of the Bessel function in the equation for a uniformally illuminated circular aperture. The equation for the normalized field pattern E (Ø) is (Reference 0):

$$E(\emptyset) = \left| \frac{2\lambda}{\pi D} \left(\frac{J_1\left[\left(\frac{\pi D_r}{\lambda}\right) \sin \emptyset\right]}{\sin \emptyset} \right) \right| \qquad (1)$$

*λ = free space wavelength (meters)

D_r = diameter of reflector (meters)

π = 3.14159

Ø = angle with respect to the normal of the reflector (designated "Boresight Angle (Degrees)" on plots)

J_1 = first order Bessel function

$\left[\left(\frac{\pi D}{\lambda}\right) \sin \emptyset\right]$ = argument for the Bessel function

* NOTE: G represents the wavelength in Figures 2-17

The relative power as a function of boresight angle is calculated by the following equation:

$$P_{rel}\ (dB) = 20 \log E(\emptyset) \qquad (2)$$

Both the electric field and relative power patterns are calculated for the forward and return link frequencies of the Orbiter/TDRS Communication System of 13.775 GHz and 15.0085 GHz respectively.

Plots of the normalized electric field as a function of boresight angle for twenty, twenty-six, thirty, and thirty-six inch reflectors for the forward link frequency are found in Figures 2-5 and for the return link frequency in Figures 6-9. These eight plots illustrate the pattern for the main lobe, first side lobe, and second side lobe (forward link and 20 inch return link only). These plots show that the position of the first null varies up to 1.43° due to the change in frequency and reflector diameter in Figures 2-9.

The relative power expressed in dB as a function of boresight angle is illustrated in Figures 10-17 for each reflector size and each respective link frequency The figures show the main lobe and first lobe (levels in decibels directly from the plots). The side lobe level in dB can be calculated in Figures 2-9 by use of the following equation.

$$\text{S.L. (dB)} = 20 \log \left(\frac{\text{side lobe field level}}{\text{main-lobe field level}} \right) \qquad (3)$$

The calculated first side lobe level for each link frequency and each reflector is at -17.60 dB with respect to the main lobe. The Ku-Band Specification for the first side lobe level is set at -18 dB (Reference B) which is reasonable considering that some tapered illumination will cause side lobe reduction. Tables 2-9 contain a listing of the specific data points for each reflector at the forward and return link frequencies.

PAD. PATTERN DATA FOR 20IN. REFLECTOR AT 13.775GHZ

ANGLE FROM BORESIGHT(DEG.)	NORM. ELEC. FIELD MAG.	RELATIVE POWER(DB)
.1	9.97955681E-01	-.0
.2	9.91843444E-01	-.1
.3	9.81710275E-01	-.2
.4	9.67629929E-01	-.3
.5	9.49747027E-01	-.4
.6	9.28176982E-01	-.6
.7	9.03104422E-01	-.9
.8	8.74731453E-01	-1.2
.9	8.43285597E-01	-1.5
1.0	8.09017489E-01	-1.9
1.1	7.72198346E-01	-2.2
1.2	7.33112528E-01	-2.7
1.3	6.92078246E-01	-3.2
1.4	6.49397324E-01	-3.7
1.5	6.05295512E-01	-4.4
1.6	5.60014684E-01	-5.0
1.7	5.14776347E-01	-5.8
1.8	4.69815461E-01	-6.6
1.9	4.25361251E-01	-7.5
2.0	3.81237958E-01	-8.5
2.1	3.38251653E-01	-9.6
2.2	2.96693235E-01	-10.8
2.3	2.45737711E-01	-12.2
2.4	2.04013674E-01	-13.8
2.5	1.64422943E-01	-15.7
2.6	1.26765873E-01	-17.9
2.7	9.12677981E-02	-20.9
2.8	5.68849023E-02	-24.9
2.9	2.73813096E-02	-31.3
3.0	7.26277701E-04	-62.8
3.1	2.61470624E-02	-31.7
3.2	4.88160361E-02	-26.2
3.3	5.89639675E-02	-25.3
3.4	5.57785164E-02	-25.3
3.5	1.00021213E-01	-20.0
3.6	1.11645756E-01	-19.0
3.7	1.20543657E-01	-18.4
3.8	1.26863244E-01	-17.9
3.9	1.30718279E-01	-17.7
4.0	1.32241578E-01	-17.6
4.1	1.31582977E-01	-17.6
4.2	1.28906137E-01	-17.8
4.3	1.24355744E-01	-18.1
4.4	1.18235221E-01	-18.5
4.5	1.10624276E-01	-19.1
4.6	1.01766435E-01	-19.8
4.7	9.18685716E-02	-20.7
4.8	8.11384634E-02	-21.8
4.9	6.97824236E-02	-23.1
5.0	5.80056076E-02	-24.7

ORIGINAL PAGE IS
OF POOR QUALITY

TABLE 2

RAD. PATTERN DATA FOR 26IN. REFLECTOR AT 13.775GHZ

ANGLE FROM BORESIGHT±DEG.	NORM. ELEC. FIELD MAG	RELATIVE POWER DB
.1	9.965E3590E-01	-.0
.2	9.862579116-01	-.1
.3	9.69257302E-01	-.3
.4	9.45795639E-01	-.5
.5	9.161E3004E-01	-.8
.6	8.807E3163E-01	-1.1
.7	8.401591506-01	-1.5
.8	7.948029726-01	-2.0
.9	7.45228125E-01	-2.5
1.0	6.923992046-01	-3.2
1.1	6.366139256-01	-3.9
1.2	5.798961946-01	-4.7
1.3	5.197634256-01	-5.7
1.4	4.580647016-01	-6.7
1.5	4.004590246-01	-7.9
1.6	3.416E2990E-01	-9.3
1.7	2.843443596-01	-10.9
1.8	2.301250076-01	-12.8
1.9	1.785752046-01	-15.1
2.0	1.272093766-01	-17.9
2.1	8.147237986-02	-21.8
2.2	3.973111696-02	-28.0
2.3	2.305440666-03	-52.7
2.4	2.866587316-02	-30.3
2.5	5.885557606-02	-24.6
2.6	8.238274006-02	-21.7
2.7	1.012340006-01	-19.9
2.8	1.154104436-01	-18.7
2.9	1.251632196-01	-18.1
3.0	1.306E7984E-01	-17.7
3.1	1.322688336-01	-17.6
3.2	1.302386406-01	-17.7
3.3	1.249744196-01	-18.1
3.4	1.168356336-01	-18.6
3.5	1.064096916-01	-19.5
3.6	9.355376636-02	-20.5
3.7	8.009536456-02	-21.9
3.8	6.516340026-02	-23.7
3.9	4.965566966-02	-26.1
4.0	3.388021066-02	-29.4
4.1	1.854110226-02	-34.6
4.2	3.700330746-03	-48.6
4.3	1.021397226-02	-34.8
4.4	2.292053596-02	-32.8
4.5	3.418266196-02	-29.3
4.6	4.381266246-02	-27.2
4.7	5.167328746-02	-25.7
4.8	5.767763996-02	-24.8
4.9	6.178E7459E-02	-24.2
5.0	6.401603F6E-02	-23.9

TABLE 3

FAR. PATTERN DATA FOR JOIN. REFLECTOR AT 17.775GHZ

ANGLE FROM BOREsIGHT*DEG.)	NORM. ELEC. FIELD MAG.	RELATIVE POWER DB)
.1	9.95406447E-01	-.0
.2	9.81710193E-01	-.2
.3	9.59162449E-01	-.4
.4	9.28177559E-01	-.6
.5	8.89113461E-01	-1.0
.6	8.43278831E-01	-1.5
.7	7.90287089E-01	-2.0
.8	7.33037698E-01	-2.7
.9	6.70893257E-01	-3.5
1.0	6.05356895E-01	-4.4
1.1	5.37590552E-01	-5.4
1.2	4.68740744E-01	-6.6
1.3	3.99894293E-01	-8.0
1.4	3.32135373E-01	-9.6
1.5	2.66462244E-01	-11.5
1.6	2.03675735E-01	-13.8
1.7	1.45163673E-01	-16.8
1.8	9.10736567E-02	-20.8
1.9	4.22156622E-02	-27.5
2.0	9.30361016E-04	-60.6
2.1	2.80295031E-02	-28.4
2.2	5.66836319E-02	-23.2
2.3	8.34411743E-02	-20.6
2.4	1.11791215E-01	-19.0
2.5	1.34112863E-01	-17.1
2.6	1.50762735E-01	-16.4
2.7	1.62152123E-01	-15.8
2.8	1.68831821E-01	-15.5
2.9	1.71365316E-01	-15.3
3.0	1.70410779E-01	-15.4
3.1	1.66524035E-02	-20.3
3.2	8.67915873E-02	-21.9
3.3	6.25264551E-02	-23.9
3.4	4.55442110E-02	-26.8
3.5	3.74047604E-02	-31.2
3.6	9.94599150E-03	-40.0
3.7	6.53994254E-03	-43.7
3.8	2.15108734E-02	-33.3
3.9	3.45895973E-02	-29.2
4.0	4.54632670E-02	-26.8
4.1	5.29881358E-02	-25.4
4.2	5.99927037E-02	-24.4
4.3	6.34695469E-02	-23.9
4.4	6.44748139E-02	-23.8
4.5	6.21394134E-02	-24.0
4.6	5.96622789E-02	-24.5
4.7	5.42987355E-02	-25.3
4.8	4.73492247E-02	-26.5
4.9	3.91480676E-02	-28.1
5.0	3.08505494E-02	-30.4

TABLE 4

RAD. PATTERN BOTH FOR 15IN. REFLECTOR AT 13.775GHZ

ANGLE FROM BORESIGHT*DEG.	NORM. ELEC. FIELD MAG.	RELATIVE POWER*DB*
.1	9.93345515E-01	-.1
.2	9.73756425E-01	-.2
.3	9.41600963E-01	-.5
.4	8.97759573E-01	-.9
.5	8.43409702E-01	-1.5
.6	7.79913083E-01	-2.2
.7	7.08907125E-01	-3.0
.8	6.32199203E-01	-4.0
.9	5.51581232E-01	-5.2
1.0	4.69094685E-01	-6.6
1.1	3.86591853E-01	-8.2
1.2	3.05951782E-01	-10.3
1.3	2.28824912E-01	-12.9
1.4	1.56915247E-01	-16.1
1.5	9.14344616E-02	-20.8
1.6	3.24445311E-02	-29.5
1.7	1.62221463E-02	-35.8
1.8	5.70597932E-02	-24.9
1.9	8.88459135E-02	-21.0
2.0	1.11653178E-01	-19.0
2.1	1.25813875E-01	-18.0
2.2	1.31908653E-01	-17.6
2.3	1.33736369E-01	-17.7
2.4	1.32205539E-01	-18.2
2.5	1.10522219E-01	-19.1
2.6	9.37630003E-02	-20.6
2.7	7.41692647E-02	-22.6
2.8	5.29413786E-02	-25.5
2.9	3.13228843E-02	-30.1
3.0	1.00917190E-02	-39.9
3.1	9.53902662E-03	-40.4
3.2	2.68801636E-02	-31.4
3.3	4.13197268E-02	-27.7
3.4	5.24277547E-02	-25.6
3.5	5.99599382E-02	-24.4
3.6	6.38529962E-02	-23.9
3.7	6.42181520E-02	-23.8
3.8	6.13143563E-02	-24.2
3.9	5.55354548E-02	-25.1
4.0	4.73785877E-02	-26.5
4.1	3.74157730E-02	-28.5
4.2	2.62630992E-02	-31.6
4.3	1.45493043E-02	-36.7
4.4	2.88924038E-03	-50.9
4.5	8.14915E04E-02	-41.8
4.6	1.80623712E-02	-34.9
4.7	2.54234481E-02	-31.8
4.8	3.29455381E-02	-29.6
4.9	3.73907061E-02	-28.5
5.0	3.96732712E-02	-28.0

TABLE 5

RAD. PATTERN DATA FOR 26IN. REFLECTOR AT 15.0085GHZ

ANGLE FROM BORESIGHT(DEG.)	NORM ELEC. FIELD MAG.	RELATIVE POWER DB
.1	9.97574760E-01	-.0
.2	9.90322192E-01	-.1
.3	9.78312471E-01	-.3
.4	9.61661293E-01	-.5
.5	9.40553402E-01	-.9
.6	9.15128616E-01	-1.3
.7	8.85693959E-01	-1.8
.8	8.52560899E-01	-2.4
.9	8.15873366E-01	-3.0
1.0	7.76154094E-01	-3.8
1.1	7.33713822E-01	-4.7
1.2	6.88941092E-01	-5.7
1.3	6.42243552E-01	-6.8
1.4	5.94056570E-01	-8.0
1.5	5.44732815E-01	-9.3
1.6	4.94263254E-01	-10.7
1.7	4.44773958E-01	-12.0
1.8	3.94951610E-01	-13.5
1.9	3.45568850E-01	-15.1
2.0	2.97284839E-01	-16.5
2.1	2.50361035E-01	-18.0
2.2	2.05204640E-01	-19.8
2.3	1.62074530E-01	-21.8
2.4	1.21276779E-01	-23.8
2.5	8.30717340E-02	-25.6
2.6	4.76719210E-02	-26.4
2.7	1.52601321E-02	-36.3
2.8	1.40204768E-02	-37.1
2.9	4.00675266E-02	-27.9
3.0	6.25170723E-02	-24.0
3.1	8.22463115E-02	-21.7
3.2	9.93629523E-02	-20.1
3.3	1.11223026E-01	-19.1
3.4	1.20909906E-01	-18.4
3.5	1.27541714E-01	-17.9
3.6	1.31235632E-01	-17.6
3.7	1.32251093E-01	-17.6
3.8	1.30724154E-01	-17.7
3.9	1.26876965E-01	-17.9
4.0	1.20957379E-01	-18.3
4.1	1.13216673E-01	-18.9
4.2	1.03915916E-01	-19.7
4.3	9.32139941E-02	-20.6
4.4	8.17039280E-02	-21.8
4.5	6.93916953E-02	-23.2
4.6	5.64600680E-02	-25.0
4.7	4.33935215E-02	-27.3
4.8	3.02436520E-02	-30.4
4.9	1.73649499E-02	-35.2
5.0	4.92771769E-03	-46.1

TABLE 6

RAD. PATTERN DATA FOR CEIR. REFLECTOR AT 15.0025GHZ

ANGLE FROM BORESIGHT(DEG.)	NORM. ELEC. FIELD MAG.	RELATIVE POWER(DB)
.1	9.95986433E-01	-.0
.2	9.827A0655E-01	-.1
.3	9.635762D0E-01	-.3
.4	9.35663155E-01	-.6
.5	9.010:1232E-01	-.9
.6	0.56592851E-01	-1.3
.7	9.13241609E-01	-1.8
.8	7.59728877E-01	-2.4
.9	7.03538704E-01	-3.1
1.0	6.42601266E-01	-3.8
1.1	5.79765951E-01	-4.7
1.2	5.15362051E-01	-5.8
1.3	4.50243081E-01	-6.9
1.4	3.95425513E-01	-8.1
1.5	3.21773524E-01	-9.8
1.6	2.80133131E-01	-11.1
1.7	2.01285463E-01	-13.9
1.8	1.45934567E-01	-16.7
1.9	9.46947493E-02	-20.5
2.0	4.80932E3EE-02	-26.4
2.1	6.51108503E-03	-43.7
2.2	2.972020913-02	-30.5
2.3	6.042170382-02	-24.4
2.4	8.551562D5E-02	-21.4
2.5	1.050337105-01	-19.6
2.6	1.19111668E-01	-18.5
2.7	1.279822502-01	-17.9
2.8	1.319962332-01	-17.6
2.9	1.314E1841E-01	-17.6
3.0	1.269327242-01	-17.9
3.1	1.18895027E-01	-18.5
3.2	1.079036772-01	-19.3
3.3	9.453833E1E-02	-20.5
3.4	7.939[illegible]731E-02	-22.0
3.5	6.304299832-02	-24.0
3.6	4.607315802-02	-26.7
3.7	2.902012332-02	-30.7
3.8	1.238772282-02	-38.1
3.9	3.369478702-03	-49.4
4.0	1.785424252-02	-35.0
4.1	3.073245042-02	-30.2
4.2	4.173771172-02	-27.6
4.3	5.067410912-02	-25.9
4.4	5.741677092-02	-24.8
4.5	6.191032052-02	-24.2
4.6	6.416686072-02	-23.9
4.7	6.426E1473E-02	-23.8
4.8	6.233556922-02	-24.1
4.9	5.856010432-02	-24.6
5.0	5.316523812-02	-25.5

TABLE 7

RAD. PATTERN DATA FOR 20IN. REFLECTOR AT 15.0025GHZ

ANGLE FROM BORESIGHT(±DEG.)	NORM. ELEC. FIELD MAG.	RELATIVE POWER DB
.1	9.94548507E-01	-.0
.2	9.78312961E-01	-.2
.3	9.51645320E-01	-.4
.4	9.15126940E-01	-.8
.5	8.69541334E-01	-1.2
.6	8.15865674E-01	-1.8
.7	7.55215943E-01	-2.4
.8	6.88916983E-01	-3.2
.9	6.19280364E-01	-4.2
1.0	5.44745533E-01	-5.3
1.1	4.69766120E-01	-6.6
1.2	3.94773677E-01	-8.1
1.3	3.21175540E-01	-9.9
1.4	2.50290625E-01	-12.0
1.5	1.82226345E-0.	-14.7
1.6	1.21124509E-01	-18.3
1.7	6.48491105E-02	-23.8
1.8	1.50889065E-02	-36.4
1.9	2.76233234E-02	-31.2
2.0	6.29777687E-01	-24.0
2.1	9.62571340E-02	-20.6
2.2	1.11227121E-01	-19.1
2.3	1.24675754E-01	-18.1
2.4	1.31297364E-01	-17.7
2.5	1.31772301E-01	-17.6
2.6	1.25794142E-01	-17.9
2.7	1.17152583E-01	-18.5
2.8	1.07796349E-01	-19.3
2.9	8.73532851E-02	-21.2
3.0	6.90026259E-02	-23.2
3.1	4.95467416E-02	-26.1
3.2	2.98353168E-02	-30.5
3.3	1.06520056E-02	-39.5
3.4	7.13559151E-03	-42.9
3.5	2.24423108E-02	-33.0
3.6	3.72791947E-02	-28.6
3.7	4.94574191E-02	-26.3
3.8	5.87463058E-02	-24.9
3.9	6.20400950E-02	-24.1
4.0	6.23534986E-02	-23.8
4.1	6.38129920E-02	-23.9
4.2	6.06447416E-02	-24.3
4.3	5.51589257E-02	-25.2
4.4	4.77578020E-02	-26.4
4.5	3.88073401E-02	-28.2
4.6	2.88293635E-02	-30.8
4.7	1.82715102E-02	-34.8
4.8	7.60284610E-03	-42.4
4.9	2.738.9166E-03	-51.2
5.0	1.23505852E-02	-38.2

TABLE 6

PAD. PATTERN PATH FOR MAIN. REFLECTOR AT 15.000 GHZ

ANGLE FROM BORESIGHT@DEG.	NORM. ELEC. FIELD MAG.	RELATIVE POWER DB
.1	9.92162973E-01	-.1
.2	9.68897364E-01	-.3
.3	9.30929686E-01	-.6
.4	8.79440152E-01	-1.1
.5	8.16014[illegible]-01	-1.8
.6	7.42585349E-01	-2.6
.7	6.61355115E-01	-3.6
.8	5.74713912E-01	-4.8
.9	4.85149673E-01	-6.3
1.0	3.95151164E-01	-8.1
1.1	3.07127468E-01	-10.3
1.2	2.23313022E-01	-13.0
1.3	1.45656398E-01	-16.7
1.4	7.52571689E-02	-22.4
1.5	1.54116950E-02	-36.2
1.6	3.50146701E-02	-29.1
1.7	7.43034406E-02	-22.5
1.8	1.05854474E-01	-19.5
1.9	1.32469199E-01	-18.2
2.0	1.31289294E-01	-17.6
2.1	1.31218185E-01	-17.6
2.2	1.23539519E-01	-18.2
2.3	1.09602259E-01	-19.2
2.4	9.09647305E-02	-20.8
2.5	6.91729571E-02	-23.2
2.6	4.57754625E-02	-26.8
2.7	2.22297665E-02	-33.1
2.8	1.52851648E-01	-76.3
2.9	3.02508350E-01	-33.9
3.0	3.71720577E-02	-28.6
3.1	5.02752375E-02	-26.0
3.2	5.91800295E-02	-24.6
3.3	6.37644613E-02	-23.9
3.4	6.41498029E-02	-23.9
3.5	6.06749045E-02	-24.3
3.6	5.38615142E-02	-25.4
3.7	4.45732702E-02	-27.1
3.8	3.29684827E-02	-29.6
3.9	2.04556251E-02	-33.8
4.0	7.64354573E-03	-42.3
4.1	4.70097508E-03	-46.6
4.2	1.58923082E-02	-36.0
4.3	2.53575439E-02	-31.9
4.4	3.26614568E-02	-29.7
4.5	3.75206420E-02	-28.5
4.6	3.98100077E-02	-28.0
4.7	3.95597181E-02	-28.1
4.8	3.69439153E-02	-28.6
4.9	3.22625175E-02	-29.8
5.0	2.59156632E-02	-31.7

TABLE 9

The directive gain and power gain for each of the parabolic reflectors may be calculated from equations (4) and (5) respectively assuming an efficiency of 55%:

$$D_G = \left(\frac{\pi D}{\lambda}\right)^2 \qquad (4)\ \text{(Reference C)}$$

$$G_A = \eta D_G \qquad (5)\ \text{(Reference C)}$$

η = efficiency

D_r = diameter of reflector (meters)

D_G = directive gain

G_A = antenna power gain

π = 3.14159

λ = free space wavelength (meters)

A tabulation of the antenna power gain and beamwidth for each appropriate frequency and reflector size is given in Table 10 The power gains are obtained from Equations (4) and (5) and the beamwidths are obtained from the patterns. The 36 inch dish is noted to have an approximate 5 dB gain over the 20 inch dish at the forward frequency. The beamwidth narrows from 2.52 degrees for the 20 inch dish to 1.41 degrees for the 36 inch dish.

Also, it should be mentioned that the difference pattern may be obtained by subtracting two sum patterns displaced in space, and the width of the nulls by a fixed power level varies as a function of the antenna size. The relative null widths for a fixed power level of 32.74 dB yields .65, .39, .36, and .19 degrees for the respective dish sizes of 20, 26, 30, and 36 inches. This result shows that tracking uncertainties due to the low amplitude of the difference pattern on boresite will be minimized with the largest dish.

DISH SIZE (IN.)	* GAIN (dB)	BEAMWIDTH (DEG).	FREQ. (GHZ)	1ST SIDE LOBE (dB)	2ND SIDE LOBE (dB)
20	34.74	2.52°	13.775	-17 6	-
20	35.49	2.36°	15.0085	-17.6	-
26	36.972	1.94°	13.775	-17.6	-23.8
26	37.72	1.75°	15.0085	-17.6	-23.8
30	38.267	1.72°	13.775	-17.6	-23.8
30	39.017	1.54°	15.0085	-17 6	-23 8
36	39.799	1.41°	13.775	-17.6	-23.8
36	40.549	1.30°	15.0085	-17.6	-23.8

Table 10 Antenna Pattern Parameters

* ASSUMES 55% EFFICIENCY

4.2 Tracking Loop Signal-to-Noise Ratio Evaluation

The Ku-Band tracking system is part of an integrated radar/communication system which is being designed to automatically acquire and track a TDRS in the communications mode. The tracking loop operates with the Orbiter receiver carrier frequency of 13.775 GHz over a specified maximum r.f. bandwidth of 50 MHz from the TDRS to the Orbiter (forward link). The conceptual baseline entails a three channel monopulse system that utilizes a Cassegrain fed parabolic dish antenna. The three channels include sum tracking, difference azimuth, and difference elevation which are shown in the conceptual block diagram of Figure 18 (Reference B). The sum channel is separated from the r.f. sum data channel at the power divider with the difference channels coming directly from the monopulse type hybrid circuit through a transmit/receive (T/R) switch. Several parameters may vary in the tracking loop that should be considered. Some of these parameters include:

(1) Signal level at the Orbiter as the slant range changes

(2) Change in the power gain of the antenna

(3) Amplifier bandwidth

(4) Use of spread or despread signals in tracking loop

(5) Use of triple or single channel monopulse type tracking signals

(6) Use of parametric amplifier, a preamplifier or a direct mixer at the front end

(7) Circuit losses due to transmission lines, switches, pointing, rotary joints, and polarization.

The signal-to-noise ratio calculations in this section are discussed in relation to the antenna size and the option of using the despread signal versus the spread signal in the tracking loop. The despread signal considered has a bandwidth of 1 MHz, and a bandwidth of 25 MHz for the spread signal is assumed.

The signal-to-noise ratio calculations are based on minimum and maximum slant range parameters which are shown in Figure 19. The level of the radiated signal at the surface of the Earth required to meet the recommendations set by the International Radio Consultive Communication Union (CCIR) is -152 $dB_W/m^2/4$ kHz from a TDRS satellite in synchronous orbit, 19,323 n.mi., above the Earth. The power level calculation (flux density) is defined in a 4 kHz bandwidth to conform to CCIR guidelines (Reference C).

The level of the TDRS signal at the Orbiter varies from -152.0 $dBW/m^2/4$ kHz to -153.7 $dBW/m^2/4$ kHz for typical slant range variation obtained from the following equation.

$$\text{FLUX DENSITY } \left(\frac{\text{WATTS}}{m^2/4 \text{ kHz}}\right) = \frac{EIRP\ (4 \times 10^3)}{4\pi R^2 BW_{SS}} \qquad (6)$$

where:

EIRP = effective isotropic radiated power (assumed 6 31 x 10^4 watts)

R = range (TDRS - SSO) in meters

BW_{SS} = bandwidth of spread spectrum (assumed 25 x 10^6 Hz)

π = 3.14159

4×10^3 = CCIR bandwidth in Hertz

The flux density may be expressed in $dBw/m^2/4kHz$ by taking 10 times the log of the flux density.

Several parameters are considered for the signal-to-noise ratio calculation which include the transmit power, the TDRS transmit and Orbiter receive antenna power gains; wavelength, transmit and receive circuit losses which also include the pointing, transmission line and polarization losses, noise figure; antenna temperature; and the transmit bandwidth. The equation used for the signal-to-noise ratio calcuations is the following:

$$S/N = \frac{EIRP\ G_r \lambda^2\ L_T}{(4\pi R)^2 K\ T_{sys}\ B} \qquad (7)$$

where:

- EIRP = effective isotropic radiated power for TDRS (assumed 48.0 dBw)
- G_r = receive antenna power gain for Orbiter (See Subsection 4.1, Table 10)
- λ = wavelength in meters assumed 0.0218 meters for forward frequency of 13.775 GHz
- L_T = loss factors assumed 5.71 dB (Reference J)
- R = range in meters, TDRS-SSO (assumed 4.337×10^7 meters for maximum and 3.556×10^7 meters for minimum)
- T_{sys} = equivalent system temperature (assumed $856.9^{\circ}K$)
- B = bandwidth in Hertz (assumed 25 MHz for spread and 1 MHz for despread)
- k = 1.38×10^{-23} joules/°K(Boltzmann's constant)

4.2 1 Antenna Size Considerations

The reflector diameters considered in Section 4.1 were twenty, twenty-six, thirty and thirty-six inches. It was shown in that section that the larger the reflector the higher the power gain and the narrower the beamwidth. Although the narrower beamwidth will require a longer acquisition time, the interference from reflected signals from the Orbiter, Earth, payloads, etc and the higher power gain of the larger antenna reflector tend to provide better S/N margins for tracking loop considerations The gain advantage of the 36 inch dish is approximately 5 dB over the 20 inch dish.

4.2.2 Spread vs. Despread System Considerations

The general definition of the term spread spectrum according to Reference P is a transmitted waveform which occupies a bandwidth far exceeding that of the input/output baseband signal. The Orbiter utilizes this spread spectrum effect with phase modulation and a pseudo noise code for spreading. In this paper a 216 KBPS data rate is assumed to be transmitted in an approximate 25 MHz r.f. bandwidth.

If the tracking loop were implemented with the despread signal, rather than the spread signal, it would result in a higher signal-to-noise ratio as depicted in Tables 11-12. However, use of the despread signal will result in a longer acquisition time because of increased lock-up time required for PN code synchronization. This is because despreading of the spread signal in the sum data channel degrades the (S/N) by approximately 1.5 dB (Reference Q). However, the decrease in bandwidth enhances the signal-to-noise ratio by $[10 \log (\frac{25}{1})]$,13.9 dB. Therefore, while the spread signal permits quicker acquisition time, the despread signal provides better S/N margin for tracking after lock-up. Unfortunately, the acquisition time for lock-up of the despread signal has been estimated to take as long as five minutes, which exceeds the specified value of 60 seconds (Reference B). Since the despread signal is not considered to be suitable for the tracking loop it will not be discussed in subsequent sections.

TABLE 11

SUM TRACKING CHANNEL (INPUT OF AGC)

RANGE	REFLECTOR DIAMETER (INCHES)	* DESPREAD S/N (dB) B = 1 MHz	SPREAD S/N (dB) B = 25 MHz
MIN.	20	10.07	-3.91
MAX.	20	8.35	-5.63
MIN.	26	12.30	-1.68
MAX.	26	10.58	-3.40
MIN.	30	13.60	- .38
MAX.	30	11.88	-2.10
MIN.	36	15.13	+1.15
MAX.	36	13.41	- .57

Assumptions:

L_T = -5.71 dB (Reference J)

T_{sys} = 856.9°K (Reference J)

MIN. = 3.556×10^7 meters

MAX. = 4.337×10^7 meters

* 1.5 dB degradation for despreader included with bandwidth enhancement.

NOTE: Sum pattern S/N calculations assume the peak power levels for respective reflectors.

TABLE 12

DIFFERENCE AZIMUTH OR ELEVATION TRACKING CHANNEL
(INPUT OF ANGLE TRACKING ELECTRONICS)

RANGE	REFLECTOR DIAMETER (INCHES)	*DESPREAD S/N (dB) B = 1 Mhz	SPREAD S/N (dB) B = 25 MHz
MIN.	20	8.57	-5.41
MAX.	20	6.85	-7.14
MIN.	26	10.80	-3.18
MAX.	26	9.08	-4.90
MIN.	30	12.10	-1.88
MAX.	30	10.38	-3.60
MIN.	36	13.63	- .35
MAX.	36	11.91	-2.07

Assumptions: L_T = -5.71 dB (Reference J)

T_{sys} = 856.9^{o}K (Reference J)

MIN. = 3.556 x 10^7 meters

MAX. = 4.337 x 10^7 meters

* 1.5 dB degradation for despreader included with bandwidth enhancement.

NOTE: Difference pattern S/N calculations are assumed to be at a power level of 1.5 dB down from that for the sum pattern.

4.3 Characteristics of the TDRS Spread Spectrum Ku-Band Tracking Signal

This section develops characteristics of the tracking signal transmitted by the TDRS as seen by the Orbiter. This involves consideration of the effects of Doppler shift and Doppler rates as seen by the Orbiter from acquisition-of-signal (AOS) to loss-of-signal (LOS) A frequency plot of the transmitted spread spectrum signal is also included in this section for evaluation of automatic frequency control (AFC) requirements. The spread spectrum which results from a pseudo noise (PN) code makes up the signal transmitted by the TDRS for normal operation. The PN code is based on a random noise sequence of 2047 symbols

The geometry of the Orbiter and TDRS used to derive the parameters for the Doppler calculations is shown in Figure 20 The Doppler shift results in a variation of the Orbiter receive frequency in which the TDRS is considered to be a stationary point and the Orbiter is in a circular orbit with a constant tangential velocity (V_o) at altitudes of 100 n.mi, 237.57 n.mi. (Reference R) and 600 n.mi The calculations presented represent the worst-case Doppler shift and Doppler rate, since the TDRS is assumed to be in the orbital plane.

4.3.1 Doppler Shift and Doppler Rate Calculations

The Doppler rate and Doppler shift calculations are based on the following parameters: orbital time, Orbiter and TDRS locations relative to the center of the Earth, carrier frequency, and instantaneous radial component of the Orbiter velocity (V_r) directed toward the TDRS. The period T in seconds of a circular orbit made by the Orbiter at a given altitude is calculated using the equation:

$$T = 2\pi \sqrt{\frac{(R_e + SSO)^3}{\mu}} \qquad \text{[Ref S]} \quad (8)$$

where:

μ = gravitational acceleration of the Earth (3.98×10^{14} m^3/sec^2)

R_e = radius of the Earth (6.37×10^6 meters)

SSO = Orbiter's altitude from the Earth's surface in meters

Calculations of the Orbiter tangential velocity (V_o) in meters per second and radial component (V_r) in meters per second for the respective altitudes are performed by use of the following equations:

$$V_o = R_e \sqrt{\left(\frac{g}{R_e + SSO}\right)} \qquad \text{[Ref S]} \qquad (9)$$

where:

g = gravitational acceleration at Earth's surface (9.81 meters/sec^2)

$$V_r = V_o \cos \theta_L \qquad (10)$$

where:

θ_L = angle between Orbiter velocity vector and line joining the Orbiter TDRS (See Figure 20 in Appendix A)

$$\theta_L = n(t) - \tan^{-1}\left[\frac{R_o \sin(90° - n(t))}{R_{TDRS} - R_o \cos(90 - n(t))}\right] \qquad (11)$$

where:

$n(t)$ = angle change of Orbiter = $(\frac{2\pi}{T})\,t$

t = time in seconds

R_o = Orbiter radius from center of Earth

R_{TDRS} = TDRS radius from center of Earth

T = period of circular orbit in seconds

The calculated velocities and time periods that result from Equations (8) and (9) are given in Table 13.

Alt. (n.mi.)	T(sec.)	V_o (meters/sec.)
100	5282.958	7.793×10^3
237.57	5594.087	7.645×10^3
600	6441.192	7.294×10^3

TABLE 13. ORBITAL PARAMETERS

The equation for Doppler shift f_d in Hertz is:

$$f_d = \frac{V_r}{\lambda} \qquad (12)$$

where: λ = free space wavelength in meters

V_r = Orbiter radial velocity component toward TDRS in meters per second.

The Doppler shifts for the selected altitudes are shown in Figure 21-23. The maximum Doppler shift of 357.8 kHz occurs at an altitude of 100 n mi. The maximum Doppler shift limit specified in Reference B is ±500 kHz. The Doppler rate is the derivative of the Doppler shift which is calculated using the numerical differentiation with closely spaced points such that:

$$\frac{\Delta f_d(t)}{\Delta t} = \frac{f_d(t_1)-f_d(t_2)}{t_2 - t_1} \qquad (13)$$

The Doppler rates for the respective altitudes from AOS to LOS are shown in Figures 24-26. The worst case Doppler rate is found to be -507.5 kHz/min. at an altitude of 100 n.mi. The worst case Doppler shifts and Doppler rates for the carrier frequency (13.775 GHz) and the sample altitudes are tabulated in Table 14. The maximum Doppler shifts for the high and low side of the TDRS spread spectrum signal are also calculated using Equations (8) - (13) which are tabulated in Table 14. The Doppler effects at the high and low end of the spectrum differs in a non-linear fashion. The HP 9821A calculator and plotter programs used to calculate the Doppler shift and rate are found in Figure 85 and Figure 86 respectively in Appendix B.

ALT. (n mi.)	* CARRIER DOPPLER SHIFT (kHz)	* CARRIER DOPPLER RATE (kHz/min.)	** HIGH SIDE DOPPLER SHIFT (kHz)	*** LOW SIDE DOPPLER SHIFT (kHz)
100	357 815	-507.5	358.385	357 243
237.57	351.055	-472.5	351.614	350 493
600	334.937	-390	335.470	334.40

* WORST CASE

** WORST CASE AT 13 797 GHz

*** WORST CASE AT 13 753 GHz

TABLE 14. CARRIER DOPPLER SHIFT & DOPPLER RATE

4.3.2 Frequency Spectrum of TDRS Signal

This section shows the expected frequency content of the spread spectrum signal which will be used in the tracking loop. The current baselined signal from the TDRS is a spread spectrum of 22 464 MHz bandwidth to meet the specification recommended by the International Radio Consultive Communication Union (CCIR) of -152 dBw/m^2/4 kHz from a satellite in geosynchronous orbit 19,323 n.mi. above the Earth [Ref C]. The frequency spectrum equation that represents the double-sided TDRS spectrum signal using a PN code is [Ref B].

$$S(\omega) = \frac{p+1}{p^2}\left(\frac{\sin\frac{\omega\tau}{2}}{\frac{\omega\tau}{2}}\right)^2 + \sum_{\substack{n=+\infty \\ n=-\infty \\ n\neq 0}} \delta\left(\omega - \frac{2\pi n}{p\tau}\right) + \frac{1}{p^2}\delta(\tilde{\omega}) \qquad (14)$$

where : $\omega = \frac{2\pi n}{p \cdot \tau}$

ω = radian frequency off-set from carrier

p = PN code length (2047 symbols)

δ = Dirac delta function

n = PN code sideband order

τ = 1/chip rate ($1/11.232 \times 10^6$ = 89 nanoseconds)

A plot of the double-sided spread frequency spectrum is illustrated in Figure 27. The spectrum is a series of impulses with a separation between sidebands of 5.486 kHz. However, since the Doppler change varies over the bandwidth as indicated in Table 14, the spacing between PN sidebands will also vary slightly during the mission. This variable spacing could affect the design of a special tracking loop filter. The relative power for the carrier and nearby sideband frequencies is seen to be 4.89×10^{-4} in Figure 27 which results directly from Equation (14). The magnitude of the impulses decrease to zero as the frequency reaches $\pm$ 11.232 MHz. The corresponding information data rate for the

22.464 MHz spread spectrum r.f. bandwidth is 216 kbps. It follows that one half of the spread bandwidth corresponds to 11.232 megachips/second. Filtering in the tracking loop may be possible to enhance the periodcially occuring sidebands generated by the PN code which occupies an r.f. noise bandwidth that is significantly greater than the minimum bandwidth required to generate a 216 kbps rate. The special filter would improve the signal-to-noise ratio performance. Some form of frequency control to account for Doppler would be required to enable the filter and spectrum characteristics to be matched. The computer plot program used to obtain the charactertistics of the TDRS transmitted signal given in Figure 27 is found in Figure 87 of Appendix B.

4.4 Evaluation of Vehicle Dynamics Effects

This section determines the dynamic movement effects of the Orbiter relative to the Ku-Band antenna and TDRS. The aspects investigated are: (1) the Orbiter-to-TDRS look angle variations with the TDRS assumed to be in the orbital plane, (2) a mathematical relationship for the elevation and azimuth gimbal angles as a function of the Orbiter look angles to the TDRS, and (3) an estimate of the communications time line of the Orbiter (per revolution) in pitch, yaw, and roll look angle changes. Three configurations are considered in this section: star tracking (inertial hold), local-vertical/local horizontal (LVLH), i.e. heads up and heads down, and "barbecue" (solar inertial). The geometry used to illustrate the parameters for the Orbiter look angle calculation is the same as that used for the Doppler geometry in Figure 20 in Appendix A.

4.4.1 Orbiter-to-TDRS Look Angle Variations

The Inertial Hold (IH) configuration is based on a fixed Earth centered inertial system. In this case the Orbiter X-axis is assumed to be perpendicular to the orbital plane. The IH configuration is illustrated in Figure 28. The variations of the Orbiter look angle rates may be obtained by taking the derivative of the look angle α with respect to time (See Figure 20) in the IH mode for the three assumed altitudes The maximum values are shown in Table 15. The maximum variations for the respective altitudes only vary .0005 degrees/second in the IH configuration, as noted in Table 15. The computer program used to obtain the results in Table 15 is given in Figure 88 of Appendix B. For the IH configuration the look angle does change with respect to distant stars and is found to change only slightly with respect to the distant TDRS.

Altitude (n.mi.)	Maximum Orbiter Look Angle Rate (DEG./SEC.) for Inertial Hold
100	.0124
237.57	.0123
600	.0119

TABLE 15. Inertial Hold Look Angle Variation

LVLH

The LVLH heads down configuration is illustrated in Figure 29. The orbiter look angle variation in the LVLH mode is calculated using equations (15) and (16).

$$\theta_L = n(t) - \tan^{-1}\left[\frac{R_0 \sin(90-n(t))}{R_{TDRS}-R_0\cos(90-n(t))}\right] \qquad (15)$$

where: $n(t)$ = angle change of Orbiter = $(\frac{2\pi}{T})t$

t = time in seconds referenced to point 1

R_0 = radius from center of Earth to Orbiter in meters

T = period of circular orbit in seconds

R_{TDRS} = radius from center of Earth to TDRS in meters

θ_L = angle between Orbiter velocity vector and line joining the Orbiter/TDRS

$$\frac{\Delta\Theta_L}{\Delta t} = \frac{\theta_{2L}-\theta_{1L}}{t_2-t_1} \qquad (16)$$

$\frac{\Delta\Theta_L}{\Delta t}$ = change in angle with respect to time that is between the Orbiter velocity vector and line joining the Orbiter/TDRS in the LVLH configuration.

The HP program found in Figure 88 of Appendix B is used to calculate the maximum IH and LVLH Orbiter look angle variations The Orbiter look angle rates for the selected altitudes are shown in Figures 30-32 for the LVLH attitude configuration The look angle rates decrease as a function of attitude as shown in the respective figures and the rates vary between AOS and LOS as illustrated in Figures 30-32. The maximum look angle rate occurs when the Orbiter is directly beneath the TDRS (θ_L = 90°).

It is further pointed out that the worst case angle rate for maneuvers is 2.0 degrees/second [Reference T]. The combined effects of the Orbiter angle rates due to orbit movement in the LVLH configuration for vehicle roll, pitch or yaw variations at the three altitudes of 100 n.mi., 237.57 n.mi., and 600 n.mi. are tabulated in Table 16 for a worst case condition. The look angles rates of this Table also represent the fastest look angle rates seen by the antenna since the moment arm of the antenna from the Orbiter center of mass is very short compared with the distance between the Orbiter and the TDRS.

Altitude (n.mi)	Orbital Look Angle Rate (DEG /MIN.) (LVLH)	Body Vehicle Look Angle Rate (DEG./SEC.)	Orbital & Vehicle Rate (DEG./SEC.)
100	4.833	2	2.081
237.57	4.597	2	2.077
600	4.069	2	2.068

Table 16 Worst Case, Orbiter-to-TDRS Look Angle Variations

Thermal Conditioning

In the "barbecue" configuration one of the Orbiter's axes is perpendicular to the Orbiter-sunline. The "barbecue" configuration is illustrated in Figure 33. The barbecue rate is typically 0.5 degrees per second [Reference U]. This type of attitude is used for thermal conditioning of the Orbiter in conjunction with an inertial hold. The barbecue attitude will typically occur only 10% or less of a total mission. At this time little transmission of the 50 Mbps data would probably take place since most high data rate experiments would not use this attitude.

The three principal activities and typical Orbiter look angle rates are tabulated below in Table 17

Activity	Orbiter Look Angle Rate (DEG./SEC.)
LVLH	.081
Inertial Hold	.012
Barbecue (.5+.012)	.512

Table 17 Typical Orbiter Look Angle Rates

4.4.2 Transformation from Orbiter-to-Antenna Gimbal Angles

The antenna gimbal axes were initially specified to correspond to the roll (Φ) and pitch (θ) angles of the Orbiter body coordinates with the (Φ= 0°, θ = 0°) point corresponding to the -Z body axis [Reference B]. For the initially specified system, the antenna gimbal limits do not optimally match the vehicle blockage limts. To maximize antenna coverage the boom should be deployed at some optimum angle, and this gimbal should also have an optimum orientation. For this case, the antenna elevation and azimuth will be related to the Orbiter body roll and pitch angles by a direction cosine transformation matrix The relation between the Orbiter body and antenna gimbal coordinates is shown in Figure34. The Orbiter body X, Y, and Z look angle components are given by.

$$\vec{T} = \sin\theta_o \hat{x} - \cos\theta_o \sin\Phi_o \hat{y} - \cos\theta_o \cos\Phi_o \hat{z} \qquad (17)$$

where:

Φ_c = roll component of Orbiter look angle

θ_o = pitch component of Orbiter look angle

The antenna azimuth and elevation angles are then given by:

$$\beta = \tan^{-1}\left(\frac{Ty'}{Tz'}\right) \qquad (18)$$

$$\alpha = \sin^{-1}(Tx')$$

where, Tx', Ty' and Tz' are obtained from the direction cosine matrix A, such that:

$$\vec{T}' = A\vec{T} \qquad (19)$$

The translation matrix A may be used to determine antenna gimbal angle rates for azimuth and elevation for any defined gimbal orientation and may also be used by the Orbiter computer software for designation error correction. Designation error correction would be made after an initial acquisition is established.

4.4.3 Orbiter Shadowing/Communications Time

The Orbiter Ku-Band antenna will not always have communications locked on with the TDRS due to the shadowing by the Orbiter at different roll, pitch, and yaw attitudes while in orbit around the Earth. The time apertures for communications have been determined by using the shadowing of the Orbiter shown on the antenna management display Figure 35 [Reference V] The Orbiter look angle is assumed to change 360° in either a pitch, roll, or yaw attitude at .5, 2, and 0.081 degrees/second which are the rates for typical barbecue, Orbiter worst case maneuver, and typical (LVLH). The results of the evaluation displayed in Table 18, Orbiter Shadow Time, have been formulated by taking the indicated paths illustrated in Figure 36, Path/Attitude Look Angle Variation, for the pitch, roll, and yaw attitudes through an excursion of 360° at the respective Orbiter look angle rates. The shadow/communications times shown in Table 18 only consider shadowing from the Orbiter The worst case look angle variations (Table 19) occur for a combination pitch and yaw look angle change with a communications loss of 53.79 sec. at the rate of 2.83 degrees per second The rates in Table 19 are root sum squared (RSS) to obtain a resultant Orbiter rate from a combination of pitch and roll rates

Pitch Rate (DEG./SEC.)	Roll Rate (DEG./SEC.)	Yaw Rate (DEG./SEC.)	Rotation Time (SEC.)	Shadowed Time (SEC.) from Orbiter	Communications (SEC.)
.5	-	-	720	133	587
2	-	-	180	33	147
.081	-	-	4444.44	814.82	3629.62
-	.5	-	720	19.11	700.89
-	2	-	180	47.77	132.23
-	.081	-	4444.44	1185.18	3259.26
-	-	.5	720	188.44	531.56
-	-	2	180	47.11	132.89
-		.081	4444.44	1163.21	3281.23

* Does not include earth shadowing

Table 18 Orbiter Shadow Time (LVLH)

RSS Pitch and Yaw (DEG./SEC)	360° Rotation Time (SEC.)	Shadowed Time (SEC)	Communications (SEC.)*
.707	720.11	215 30	510 81
2.83	179.90	53.79	126.11
.115	4427.13	1323.65	3103 48

* Does not include earth shadowing

Table 19 Orbiter Worst Case Shadow Time (LVLH)

The Orbiter inertial hold configuration evaluation is formulated in a similar fashion as that done for the LVLH configuration. The inertial hold configuration has large time spans as shown in Table 20.

Pitch Rate (DEG./SEC.)	Roll Rate (DEG./SEC.)	Yaw Rate (DEG./SEC)	360° Rotation Time (SEC.)	Shadowed Time From Orbiter (SEC.)	Communicatio (SEC.)
.012	-	-	30000	5500.00	24500 00
-	.012	-	30000	7962.50	22037.50
-	-	.012	30000	8375.00	21625.00

* Does not include Earth shadowing

Table 20 Orbiter Shadow Time (IH)

The Orbiter worst case condition shown in Table 21 is obtained by taking the root sum square of the pitch and yaw rates from Table 20. The resultant amount of shadowing increases while the communication times become shorter when compared with those of Table 13. The attitude and paths considered for these calculations are those indicated in Figure 36.

RSS Pitch and Yaw (DEG /SEC)	360° Rotation Time (SEC)	Shadow Time (SEC.)	Communications * (SEC)
.01697	21213.90	9192.59	12021.32

* Does not include Earth shadowing

Table 21 Orbiter Worst Case Time (IH)

4.5 Evaluation of Scan Parameters

The scan parameters are discussed in relation to yoke blockage and the orientation of the gimbal axes to the Orbiter vehicle The raster and conical scan procedures are then discussed in relation to the time to acquire a target for both scan procedures utilizing the four respective reflector sizes (20, 26, 30, and 36 inches) The scan limits will depend on the blockage from the yoke of the Ku-Band antenna, the orientation of the antenna gimbal axes, and the deployment of the boom. The results of this section should be useful in determining an optimum gimbal orientation and in selecting a scan procedure for acquisition The present baseline deployment for the Ku-Band Antenna System is shown in Figure 37 for a single antenna and in Figure 38 for the dual antenna configuration.

4.5.1 Gimbal Limits in Relation to Antenna Yoke

The yoke will cause a cone of communication blockage to be formed when the antenna elevation angle (α) is varied such that the beam is pointing towards the rear of the Orbiter. The elevation angle limit for communication coverage is estimated to be $\alpha \leq 40°$ which results in a half angle cone of 50° caused by yoke blockage illustrated by Figure 39.

The percent of the total spherical coverage due to yoke blockage is calculated by the following equation:

$$BF = \left(\frac{1 - \cos \theta_h}{2}\right) \times 100\% \qquad (20)$$

where:

BF = blockage factor (percent spherical coverage)

θ_h = half angle of blockage cone made by antenna yoke

Using Equation (20) and a half cone angle of 50 degrees, the resultant blockage imposed by the yoke is 17.9% of the sphere. This blockage will occur when the Ku-Band Antenna is pointed towards the tail section of the Orbiter with the present baseline boom deployment.

4.5.2 Gimbal Limit in Relation to Gimbal Orientation

With the present baseline configurations illustrated in Figures 37 and 38 there will be blockage from both the yoke plus the Orbiter The percent of coverage, C, may be determined by the following equation.

$$C = 100\% - BF_{yoke} - BF_{Orbiter} \qquad (21)$$

where

BF = blockage factors in percent

The baseline deployment of the single Ku-Band Antenna is found to provide about 68% coverage with the yoke blockage occuring when the antenna is pointed toward the tail section. This blockage is indicated in Figure 40, which is an antenna management graph showing Orbiter and yoke blockage from a single Ku-Band Antenna in the baseline configuration. The cross hatched lines indicate the amount of yoke and orbiter blockage with the antenna deployed in the present baseline orientation.

Optimum deployment for the single antenna configuration would be similar to that shown in Figure 41. The change in the orientation of the gimbal azimuth and elevation angles would place the cone produced from yoke blockage mostly in the Orbiter blockage as shown by circle A in the blockage plot of Figure 42. The yoke blockage factor of this orientation and deployment of the boom would be about 8.3% in addition to that of the Orbiter blockage which would be 14.1%. The coverage represented by this configuration is about 78%.

The two antenna Ku-Band system employing the present baseline orientation for each antenna in Figure 38 would result in the blockage illustrated in Figure 43. This represents about 82% coverage, with the majority of the blockage in the rear section of the Orbiter. Figure 44 illustrates the corresponding blockage employing the optimum configuration for the two antenna configuration which provides about 96% coverage including blockage from a combination of the payload doors, vertical stablizer, and wing

In summary a tabulation of percent coverage factors resulting from this evaluation are shown in Table 22 It clearly shows the significant advantage to be obtained by reorienting the antenna boom and gimbals.

	PRESENT ORIENTATION	OPTIMUM ORIENTATION
SINGLE ANTENNA	68%	78%
TWO ANTENNAS	82%	96%

Table 22. Percent Coverage Factors for Ku-Band Communication Antenna/s

Figures 45 and 46 illustrate the blockage imposed by a single left antenna in the baseline and optimum configurations. These figures were used to obtain the total blockage for two antennas and are included for completeness.

4.5.3 Detection Time/Probability of Detection

The detection time and probability of detection calculations are performed in this section assuming a fixed antenna power gain level of 32.74 dB. The beamwidths (BW) for a 32.74 dB antenna power gain level of a 20, 26, 30, and 36 inch dish are 2.06, 1.94, 1.90 and 1.65 degrees respectively at a frequency of 13.775 GHz. These beamwidths may be obtained from Section 4.1. The modified raster and conical scans are shown in Figures 47 and 48.

Raster Scan-detection time

The modified raster scan illustrated in Figure 49 gives the geometry used to calculate the minimum and maximum detection time employing a raster scan for the respective regions shown in this figure (MIN. and MAX.). The raster scan will begin at the top of the total scan region. The area "A" indicated in equation(23)is that which would be under the arc subtended by line AB for minimum detection, and the area for maximum detection of a vector would include the area under the arc A"B" plus the area between the two lines A"B" and A'B'. A designation error of 2.8° is assumed when detecting a vector.

The detection time for the raster scan, illustrated in Figure 49 is calcualted using the following equations: (derived from Reference F).

$$\theta_y = BW/1.3 \qquad (22)$$

where: θ_y = angular travel in y direction during reversal cycle in degrees

BW = beamwidth for 32.74 dB level

1.3 = beam overlap (typical)

The beam overlap refers to a number which is related to the difference beam overlapping the main beam.

$$L = \frac{A}{(\theta_y/1.3)} \tag{23}$$

where: A = area of region covered by the raster scan from beginning until detection (degrees squared)

L = length of the scan in degrees until detection

assume a scan rate = 10°/sec [Reference B]

$$T_s = \frac{L}{10°/sec} \tag{24}$$

where T_s = time for detection of a vector using raster scan (seconds)

$$D_v = D \pm D_e \tag{25}$$

where: D_e = designation error (assumed 2.8 degrees Reference B)

D = distance traveled by vector from the origin (degrees)

D_v = distance traveled by vector considering D_e (degrees)

$$V_d = \frac{D_v}{T_s} \tag{26}$$

V_d = Angular velocity of vector (degrees/second)

The HP 9821 A calculator and plotter program found in Figure 90 of Appendix B is used for evaluation of the detection time of a look angle vector passing through a raster scan procedure as a function of the look angle rate. Figures 50-53 illustrate the minimum and maximum time limits employing the raster scan for a 20, 26, 30, and 36 inch diameter reflector. The maximum time is obtained using a "+" in Equation (25) and the minimum time is obtained using a "-" sign in Equation (25). By comparing the figures it can be seen that the larger the reflector the larger the range between minimum and maximum detection time limits.

Table 23 lists the raster scan parameters for the respective reflector diameters at the fixed power gain level of 32.74 dB. This information was used to evaluate the detection time.

DISH SIZE (INCHES)	TOTAL SCAN LENGTH(DEG.)	TOTAL SCAN TIME FOR 20° CONE (SEC)
20	256.73	25 67
26	273 96	27.40
30	279.59	27 96
36	321.42	32 14

Table 23 Raster Scan Parameters (Common Power Gain)

Conical Scan - detection time

A conical scan will have a minimum detection time of zero seconds for no designation error with the maximum detection time being a function of look angle rate. The time required for a conical scan to lock-on will generally be shorter than the raster scan because the starting point for the raster scan is farther away from the actual Orbiter-to-TDRS look angle. The conical scan will have a point constantly moving towards its maximum radius from the center of the scan area in a circular fashion The detection time for the conical scan is a function of the designation error, maximum velocity of the scan procedure, and the angular velocity of the look angle between the Orbiter and the TDRS If a calculated vector is well within the specified maximum designation error or 2.8°, immediate lock-on may occur with the conical scan. The equation to calculate the detection time for a conical scan assuming a constant angular scan velocity is:

$$D_{tc} = \frac{D_e}{V_c - V_{la}} \qquad (27)$$

where: V_c = maximum angular velocity of the scan (degrees/second)

V_{la} = velocity of the look angle (degrees/second)

D_{tc} = detection time of a vector-conical scan (seconds)

Figure 91 in Appendix B contains the HP 9821A calculator program used to plot the conical detection time based on Equation (27). The plots for the four respective reflectors are shown in Figures 54-57.

Table 24 contains the parameters used to calculate velocities for the detection time of a vector employing the conical scan.

APERTURE (INCH)	MAXIMUM SCAN LENGTH (DEG).	TOTAL SCAN TIME FOR 20° CONE (SEC.)
20	332.60	33.26
26	356.70	35.67
30	363 80	36.38
36	417 90	41.79

Table 24 Conical Scan Parameters (Common Power Gain)

The conical scan scheme indicates that there will be a faster lock-on time than the raster scan, which is indicated in comparison of the detection time figures for the raster and conical scan (Figures 50-53 and Figures 54-57 respectively) employing a 20, 26, 30, or 36 inch diameter reflector.

Probability of Detection - raster and conical

The probability of detecting a target considering the worst case designation error (2.8 degrees) is calculated using equation (28) which is valid for $A_{rv} \geq (\frac{10°-D_e}{T_{st}})$:

$$P_d = \frac{(\frac{10°-D_e}{T_{st}})}{A_{rv}} \times 100\% \qquad (28)$$

T_{st} = total time for scan of complete scan region (seconds)

D_e = designation error (degrees-assumed 2.8)

A_{rv} = angular rate of vector (degrees per second)

The probability of detecting a target with a conical or raster scan decreases rapidly once the maximum look angle rate of the antenna is exceeded. The results are calculated using an HP 9821A Calculator Program found in Figure 92 of the Appendix B.

Detection probability curves for the raster and conical scan using 20, 26, 30, and 36 inch reflectors are found in Figures 58-65. The probability curves for the raster scan in each figure assumes the designation error of 2.8 degrees for one curve and zero degrees for the curve labeled "WO". The probability of detection is slightly higher for the raster scan than that for the conical scan for a fixed look angle rate. The probability of detecting a vector is found to fall off sharply for both scan procedures once the maximum look angle rate is exceeded (100% probability) for lock-on that is indicated by Figures 58-65. The time for detection of a slow changing look angle is significantly better for the conical scan even in the presence of a 2.8° designation error. Since the majority of the Shuttle activities will involve slow look angle rate changes, it appears that the conical scan should be selected

4.6 Multipath Signal Effects on the Communications Antenna

A communications system such as the Space Shuttle Ku-Band Orbiter/TDRS system is impacted by multipath. Multipath is defined as the reflected signal that may occur from the Orbiter body, Earth, or deployed payload causing the Orbiter Ku-Band antenna to receive two or more signals arriving at different times and magnitudes. The purpose of this section is to determine the possible effects of multipath signals on the operation of the acquisition and tracking system of the Space Shuttle Orbiter Ku-Band Communications Antenna Two cases are considered for multipath effects, the multipath due to the Earth and due to the Orbiter.

The multipath factor as a function of frequency and pointing angle is determined from the antenna pattern and modification effects from a simplified math model for a carrier frequency of 13.775 GHz $\pm$ 350 kHz, which includes the Doppler effect. The type of modulation which is currently baselined for the Ku-Band system is spread spectrum or pseudo random noise (PN) modulation. For the case of spread spectrum modulation the r.f. bandwidth may be as great as 50 MHz. The tracking error signal is currently baselined using a triple channel monopulse type feed system in which three antenna patterns will be formed. The output of the monopulse bridge will include the sum pattern, the azimuth difference pattern and the elevation difference pattern. The difference patterns have a null in the direction of the peak of the sum beam as shown in Figure 66, assuming no multipath effects. The effect of multipath reflection will be to produce ripples or scalloping effects in portions of both the sum and difference antenna patterns but mainly in the difference pattern. The ripple effects will change with angular pointing direction and will also be a function of frequency.

An idealized plane model for multipath determination is shown in Figure 67. For this study the specular multipath (worst case) is considered

Normally, the multipath signal has two components, specular and diffuse The specular component is a reflected signal from a smooth or ideal surface and the diffuse component is the sum of scattered signals from rough surfaces. These reflections cause the variations in both the sum and difference pattern as mentioned previously in this section The Orbiter antenna is assumed to be isotropic for the purpose of this discussion and the change in frequency of the received signal due to multipath, L_{MP}, is given by equation (29) such that:

$$L_{MP}\ (dB) = 20 \log \left\{ 1 - |R|\ e^{-j \frac{2\pi f}{c} \cdot \frac{2h_1h_2}{d}} \right\} \qquad (29)$$

where h_1 = height of Orbiter antenna (meters)

h_2 = height of TDRS antenna (meters)

f = frequency (Hz)

$\frac{2h_1h_2}{d}$ = path difference between reflected path (r_1+r_2) - (meters) and direct path (r) - (meters)

c = speed of light (meters/second)

d = distance between antennas measured along plane surface (meters)

$|R|$ = magnitude of the voltage reflection coefficient (no units)

The multipath factor as a function of frequency is calculated in which four voltage reflection coefficients ($|R|$) are considered: 0, -3, -6 and -10 dB which have magnitudes of 1,.707,.5, and .32 respectively. The HP 9821A calculator program used to evaluate this effect is found in Figure 93 of Appendix B. The height of the TDRS and Orbiter above the horizontal plane is assumed to be 19,323 n.mi. and 237.57 n.mi respectively. The multipath effect on the received signal due to Earth and Orbiter reflections as a function of frequency are shown in

Figures 68-71 and Figures 72-75 respectively for the four voltage reflection coefficients previously indicated. The frequency limits in these plots are chosen to be small in order to show detail effects. These results are typical for the frequency band of 13.75 GHz-13.80 Ghz which is the forward link between the TDRS and the Orbiter The spacing of the spread spectrum sidebands is 5.486 kHz. If the multipath nulls coincide with the PN sideband spacing, this may cancel sidebands of the received signal causing loss of communications Some of the multipath nulls of the Earth case shown in Figures 68-71 appear to come close to the sideband spacing of the spread spectrum signal from the TDRS to the Orbiter.

Equation (29) may also be used to account for the effect of pointing angle change ($\Delta\theta$) and is rewritten as:

$$L_{MP} = 20 \log \left\{ 1 - |R| \; e^{-j \frac{2\pi f}{c} \cdot 2 h_1 \tan \theta} \right\} \qquad (30)$$

where. h = height of Orbiter antenna above horizontal plane (meters)

θ = angle between horizontal plane and line connecting antenna center

c = speed of light (meters/second)

$|R|$ = magnitude of the voltage reflection coefficient (no units)

$2h_1 \tan \theta$ = path difference between the reflected path (r_1+r_2)-(meters) and the direct path (r)-(meters).
since $h_2 \gg h_1$; $\tan \theta = \frac{h_1 - h_2}{d} \approx \frac{h_2}{d}$

The assumed parameters for the multipath factors as a function of the Orbiter antenna pointing angle are the same as that for the effect of multipath as a function of frequency change from the TDRS to the Orbiter An HP 9821A calculator program found in Figure 94 of Appendix B is used to evaluate the multipath factor due to the Earth and Orbiter as a function of pointing angle. Figures 76-79 and Figures 80-83 show the Earth and Orbiter multipath factor as a function of pointing angle. It can be seen that the effect of multipath due to the Earth reflections will have a greater impact than that due to the Orbiter This is because the path difference of the direct and indirect signals is very small in comparison with that of the Earth

The spread spectrum is considered to be desirable for a multipath environment since in general only a small percentage of the power could be cancelled by the indirect signal. Suppression techniques such as increased antenna directivity, polarization, and the use of narrowband filtering are recognized as effective techniques for this problem [Reference W]

4.7 Single Versus Triple Channel Monopulse

Two possible implementations of the monopulse system for the Ku-Band Integrated Communications/Radar Antenna are the triple channel system and the single channel system. The triple channel system is presented in the Rockwell specification [Reference B] as a possible implementation. The triple channel system has seperate signals which are obtained from a sum feed and two difference feeds on a continuous basis. The single channel system has the sum and two difference channels time sequenced by changing the phase shift. The change in phase shift produces the three radiation patterns.

A single channel type system was used for the Apollo high gain antenna and it was found to be sensitive to incidental amplitude modulation (IAM) at the frequency associated with the phase shift change (50 Hz). PIN diode phase shifters were used to switch phase lines in and out of the circuit at a 50 Hz rate, which resulted in the formation of patterns for each of the channels on a time division multiplexed basis. The Apollo Unified S-Band ground stations were designed to transmit angle modulation, and a significant amount of incidental amplitude modulation was transmitted for large modulation indicies (i e. $\beta \geq 5$). This erroneous IAM resulted in a physical shifting of the antenna orientation while voice messages were sent on the S-Band link. The solution that was obtained before the first flight resulted in reduction of the modulation indicies in the ground transmitters.

Another factor to be considered in the single channel system is that all tracking information is carried in one transmission line. This inherently results in better phase coherence between the time division multiplexed channels of the single channel system. In the three channel system phase errors may result from differences in feed lines, amplifier characteristics, hybrid characteristics, etc. Also, implementation of a single channel system is somewhat simpler since all information is carried on one r.f. transmission

line, however, the losses associated with the single channel system are significantly greater in the difference channels, since a directional coupler is used to maximize the sum channel signal The level of degradation for the difference channel is typically 15 dB [Reference D], whereas, the level of degradation associated with the Apollo type antenna was 13 dB.

Since the signal-to-noise ratio margins in the spread spectrum bandwidth are marginal, the selection of the three channel system is favored over the single channel system. The major reason is that the losses in the difference channel are much less for the triple channel system. Also, there should be no adverse effects of incidental amplitude modulation (IAM) with the triple channel system.

5.0 RESULTS

The purpose of this section is to combine the factors from the previous discussion in order to make rational recommendations for the implementation of the Ku-Band tracking system.

The antenna patterns for 20, 26, 30, and 36 inch diameter parabolic dishes in Section 4.1 show that the power gain of the 36 inch dish is 5 dB above that of the baselined 20 inch dish. This added gain is shown in the signal-to-noise ratio Section 4.2 to be sufficient to permit use of the spread signal in the tracking loop with a 36 inch dish. Use of the spread signal is preferred since up to 5 minutes of time is required for synchronization with the despread signal. The extra time for synchronization necessitates a slower scanning rate of the antenna and requires more time than the specified 60 seconds for acquisition in the presence of a Doppler shift. The major disadvantages of the 36 inch dish is in the increased weight and size. The increased weight of the 36 inch dish will cause an approximate 400% increase, however, use of carbon fiber or other light weight materials could make the actual weight increase comparatively small. Also, the increased size makes stowage within the payload bay more difficult and may limit deployment mechanizations. The use of a dish smaller than 36 inches will result in the need for using the despread signal in the tracking loop which means excessive acquisition time. If a long acquisition time is determined to be acceptable than a 20 inch dish could be used.

In the spread spectrum Section 4.3 it is shown that the spread spectrum will consist primarily of sideband impulses with a spacing of 5.486 kHz over a 22.232 MHz r.f. bandwidth centered about the carrier frequency of 13.775 GHz. The impulse spacing will vary slightly due to Doppler shift variation over the bandwidth. Also, the Doppler is found to have a maximum shift of $\pm$ 358 kHz for a

100 n.mi. orbit with the Orbiter and TDRS in the same plane. This means that the frequency of the Orbiter receiver should be capable of tracking spread spectrum signals within ± 358 kHz. The Ku-Band specification allows for a ± 500 kHz shift which includes Doppler and local oscillator drifts in the Orbiter receiver and ground transmitter. If the accumulative drifts of the Orbiter receiver and ground transmitter are found to be less than ± 142 kHz, it would be desirable to change the Orbiter receiver tracking performance to a value closer to the actual maximum Doppler shift. Changing this value will minimize lock-on time for obtaining data during a search mode. Another suggestion resulting from the spread spectrum section is that a special filter in the tracking loop may be used to optimize the signal-to-noise ratio of the tracking signal. This filter would emphasize signal levels which are spaced 5.486 kHz corresponding to the spread spectrum sideband spacing. Use of this filter assumes that the carrier frequency shift due to Doppler is synchronized and that some tolerance for non-linear Doppler effects are included.

In the vehicle dynamics Section 4.4 it was found that the look angle variations will be relatively slow for inertial hold and local-vertical local-horizontal (LVLH) attitudes. Typical maximum rates during these activities are found to be .0124 degrees per second for inertial hold and .081 degrees per second for LVLH. The maximum look angle rates are found to occur during a fast maneuver and during "barbecue" which will comprise less than 10% of the on-orbit activities. The maximum Orbiter rate during a maneuver is 2.0 degrees per second and typical "barbecue" is 0.5 degrees per second. The results of the rates combined with blockage plots are used to show communications timelines for the attitudes considered. For a "barbecue" attitude, communications may be maintained 587 seconds out of a 720 second period and for LVLH communications may be typically

maintained 4163 seconds out of a 4444 second period of rotation. Each time communication is lost some time should be alloted for reacquisition in the above values.

The evaluation of scan parameters in Section 4.5 shows that a conical scan will give better performance than the raster scan even with the maximum designation error of 2.8 degrees. The major reason is that the minimum time to acquire for the conical scan is zero seconds and the possibility of quick acquisition is much greater for the low look angle rate changes for inertial hold and LVLH. It is further pointed out that some limits on the conical scan at the outer points of the search cone should be employed to slow down the antenna Other results in Section 4.5 show the desirability of deploying the antenna with an optimum gimbal orientation rather than with the baseline orientation It was shown that this will increase the spherical coverage of a single antenna from 68% to 77% and the coverage for two antennas is increased from 82% to 96%. This optimum orientation is obtained by overlapping the yoke blockage cone with the Orbiter vehicle blockage (See Figures 41 and 42)

A simplified evaluation of possible multipath effects was given in Section 4.6. It is found that Earth multipath may result in some loss of signal since the nulls produced by the multipath closely correspond to the spacing of the PN spread spectrum sidebands. Also, in the carrier only mode, loss of signal may occur from either Orbiter or Earth multipath. Some further study on this topic is recommended to obtain more specific conclusions with more accurate assumptions.

Finally in Section 4.7 the effects of using a single or triple channel monopulse were evaluated. The results show that a triple channel is preferred. The major reason is that the losses in the difference channels are much less for the triple channel. Also, there should be no adverse effects of incidental amplitude modulation (IAM) on the triple channel system. The major advantages of the

single channel system are (1) simpler implementation and (2) smaller phase errors since each channel is time synchronized. Since it is considered desirable to use the spread signal for tracking to minimize acquisition time, it follows that the triple channel is the favored implementation.

6.0 CONCLUSIONS AND RECOMMENDATIONS

As a result of this study the following communication oriented recommendations are made for the Ku-Band Integrated Communications/Radar Antenna tracking system.

(1) Use the maximum size 36-inch diameter parabolic dish to achieve an adequate signal-to-noise ratio in the tracking loop with a spread signal for tracking purposes. If a long acquisition time of up to 5 minutes is determined to be acceptable then a 20 inch dish could be used.

(2) Use a conical type search scan for acquisition which will result in minimum lock-on time compared with the raster scan.

(3) Reorient the antenna gimbals during deployment of the antenna boom to have a maximum overlap of the gimbal blockage and the Orbiter body blockage in order to significantly increase the percent spherical coverage for both the single antenna and dual antenna configurations.

(4) Use a triple channel monopulse system to obtain an adequate signal-to-noise ratio in the tracking loop and eliminate any undesireable effects of incidental amplitude modulation.

(5) A simplified evaluation has shown that multipath will have some limiting effects on the performance of the Ku-Band Communications System, however additional study is suggested to more accurately determine the effects.

(6) It is suggested that the Doppler specification of $\pm$500 kHz may be relaxed to reduce acquisition time if the cumulative local oscillator drifts can be reduced.

7.0 REFERENCES

(A). Anon, "Rockwell OV-102 Delta Preliminary Design Review," Rockwell No. SSV76-14-1, Vol II, p 213, 10 May 1976.

(B). Bologna, A W , "Ku-Band Integrated Communications and Radar Equipment Specification," Rockwell No MC409-0025, 15 March 1976

(C). Anon, "Integrated Rendezvous Radar/Wideband Data Communications System Study," Rockwell No. SD73-SH-066, November 1973.

(D). Anon, "Space Shuttle Integrated Rendezvous Radar/Communications System Study," Final Report Hughes No. D4148 SCG 60041R, March 1976.

(E). Anon, "Study to Investigate and Evaluate Means of Optimizing the Radar Function," Axiomatics Final Report No. R7511-3, November 1975.

(F). Walters, Glenn A , "Investigate and Evaluate Means of Integrating and Optimizing the Combined Radar/Communications Functions," D^2C Final Report Contract NAS 9-14615, May 1976.

(G). Eiane, B., "Orbiter and TDRS High Gain Antenna Acquisition," NASA (Lockheed) No. JSC-09112, September 1974.

(H). Carl, J R., "Ku-Band Communications System Antenna Acquisition and Autotrack Considerations," NASA (Lockheed) No. E33-75-104, October 1975.

(I). Rudnicki, J. F., "Theoretical Prediction of Ku-Band Radiation Patterns for the Integrated Communication/Radar Antenna," MDTSCO No 1.2-WP-B0403-031, 27 February 1976.

(J). Rudnicki, J F and J. F. Lindsey, "Ku-Band Communication System Tracking Loop Signal/Noise Evaluation," MDTSCO No. 1.2-WP-B0403-032, 18 March 1976

(K). Rudnicki, J. F., "Characteristics of the TDRS Spread Spectrum Ku-Band Signal," MDTSCO No. 1.2-WP-B0503-033, 29 April 1976.

(L). Rudnicki, J. F , J F. Lindsey, "Evaluation of Vehicle Dynamics Effects on Acquisition and Tracking of the Ku-Band Antenna," MDTSCO No. 1.2-WP-B0503-034, 27 May 1976.

(M). Rudnicki, J. F., "Evaluation of Scan Parameters for the Ku-Band Antenna," MDTSCO No. 1.2-WP-B0503-035, 1 July 1976.

(N). Rudnicki, J. F., "Multipath Signal Effects on the Ku-Band Communication Antenna," MDTSCO No. 1.2-WP-B0503-036, 13 August 1976

(O). Kraus, J. D., Antennas, McGraw-Hill, 1950.

(P). Glazer, G , "Spread Spectrum Concepts - A Tutorial," Proceedings of the 1973 Symposium on Spread Spectrum,"Tech Document No 271, Vol. I, pp. 5-8, March 1973.

(Q). Tu, K., "Updated Space Shuttle RF Link Margins," Lockheed No. 76-21X9-120, January 1976

(R). Trahan, W. H., "Preliminary Baseline Reference Mission 2 TDRS Look Angles and AOS/LOS Data," MDTSCO No. 1.4-TM-MIB-22, 17 March 1975.

(S). Filipowsky, R. F. and E. I. Muehldork, Space Communications Systems, Prentice Hall, 1965.

(T). Anon, Shuttle Operational Data Book, NASA No JSC-08934 (Vol I), June 1974

(U). Anon, "Space Shuttle Baseline Reference Missions," Vol II, Mission 2, Revision 2, NASA No JSC-07896, August 1975

(V). Anon, "OFT Functional Level Requirement," Vol. V, Book 3 NASA No. SS-P-002-530B, February 1976.

(W). Barton, D K , "Low Angle Radar Tracking," Proc. of the IEEE, Vol. 62, pp. 687-704, June 1974.

APPENDIX A

FIGURES

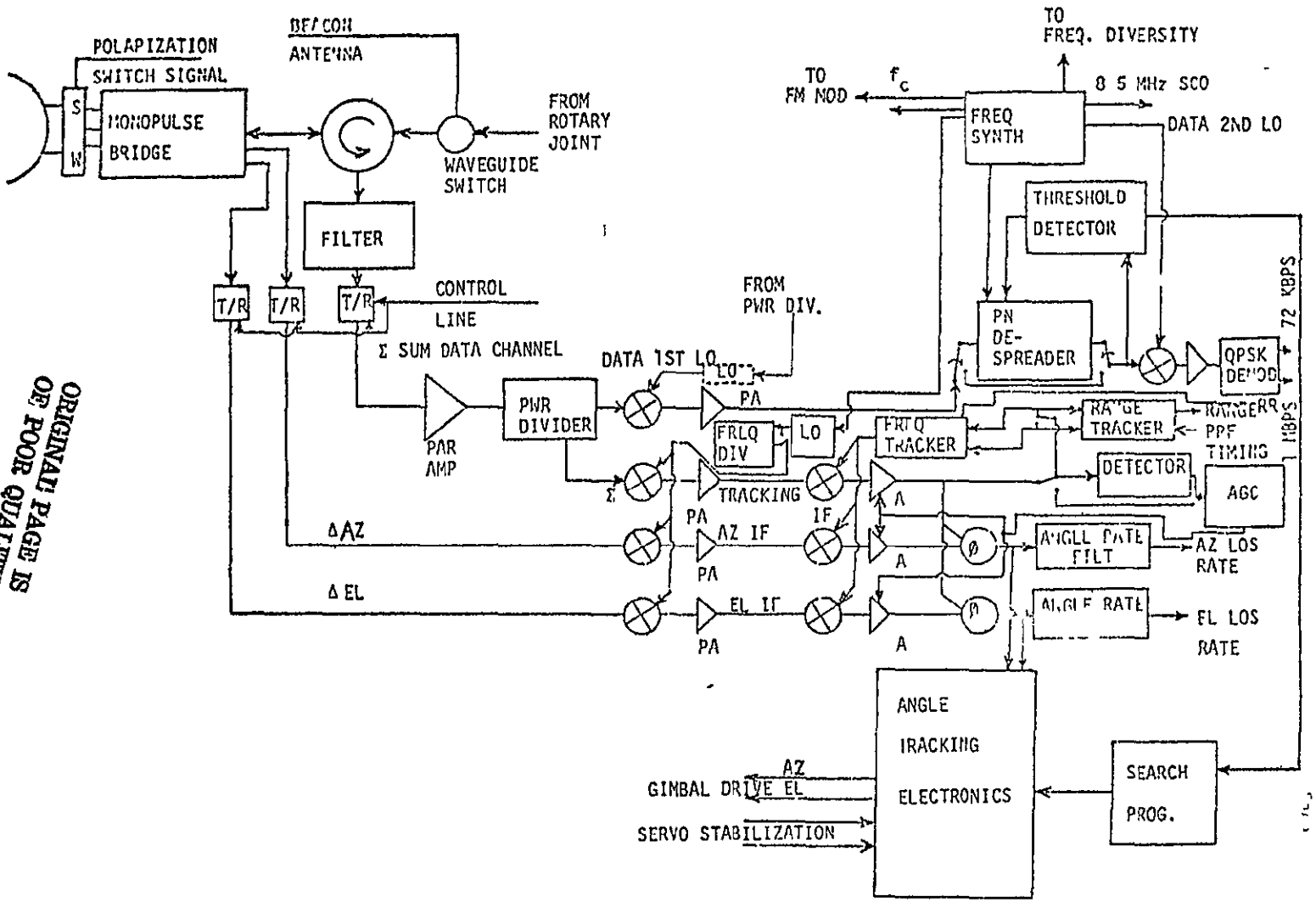

FIGURE 1 FUNCTIONAL BLOCK DIAGRAM FOR THE TRACKING LOOP OF THE COMMUNICATIONS/RADAR KU-BAND SYSTEM

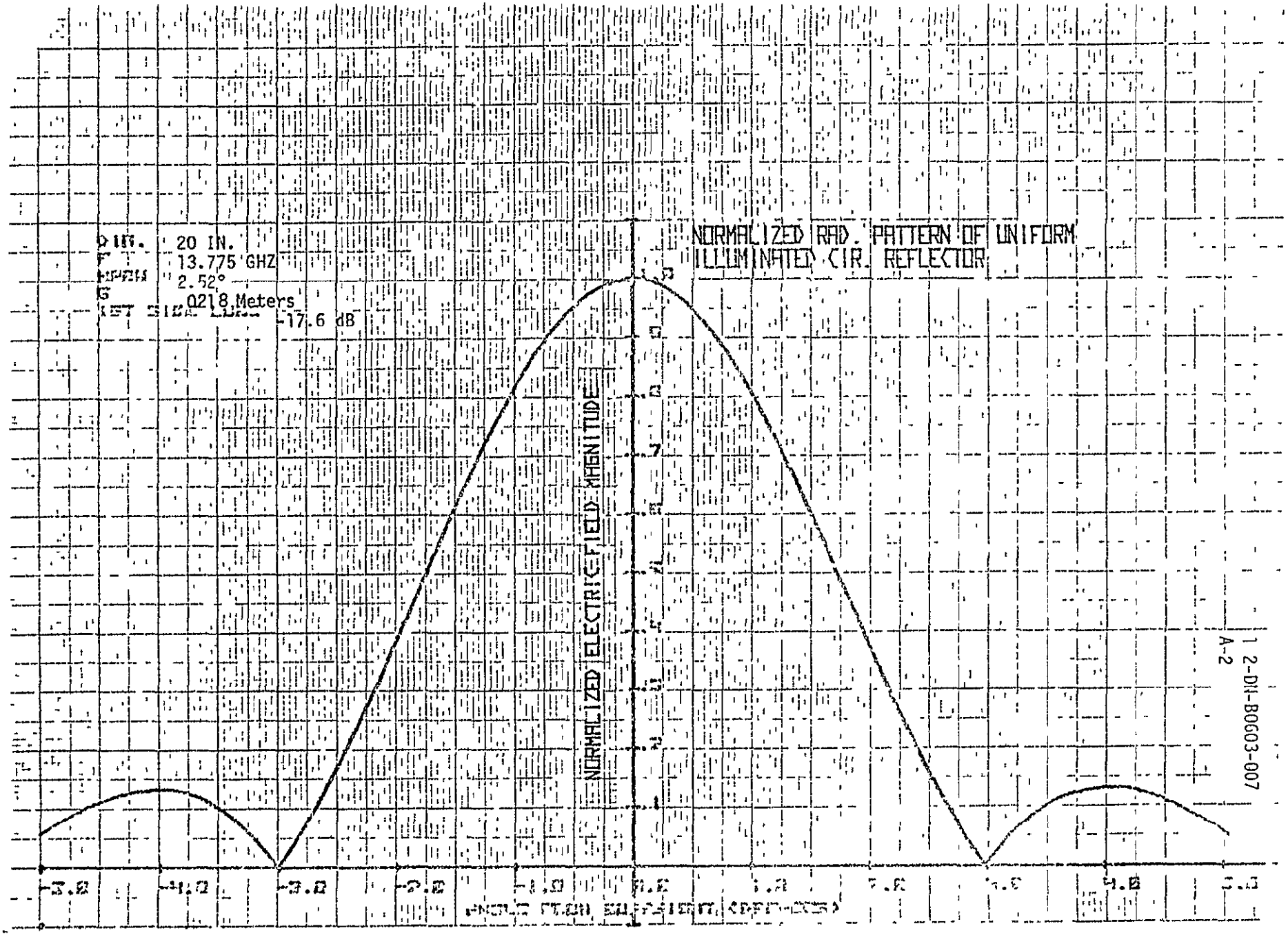
NORMALIZED RAD. PATTERN OF UNIFORM
ILLUMINATED CIR. REFLECTOR
20 IN.
13.775 GHZ
2.52°
.0218 Meters
-17.6 dB
NORMALIZED ELECTRIC FIELD MAGNITUDE
12-DH-B0603-007
A-2

Figure 2

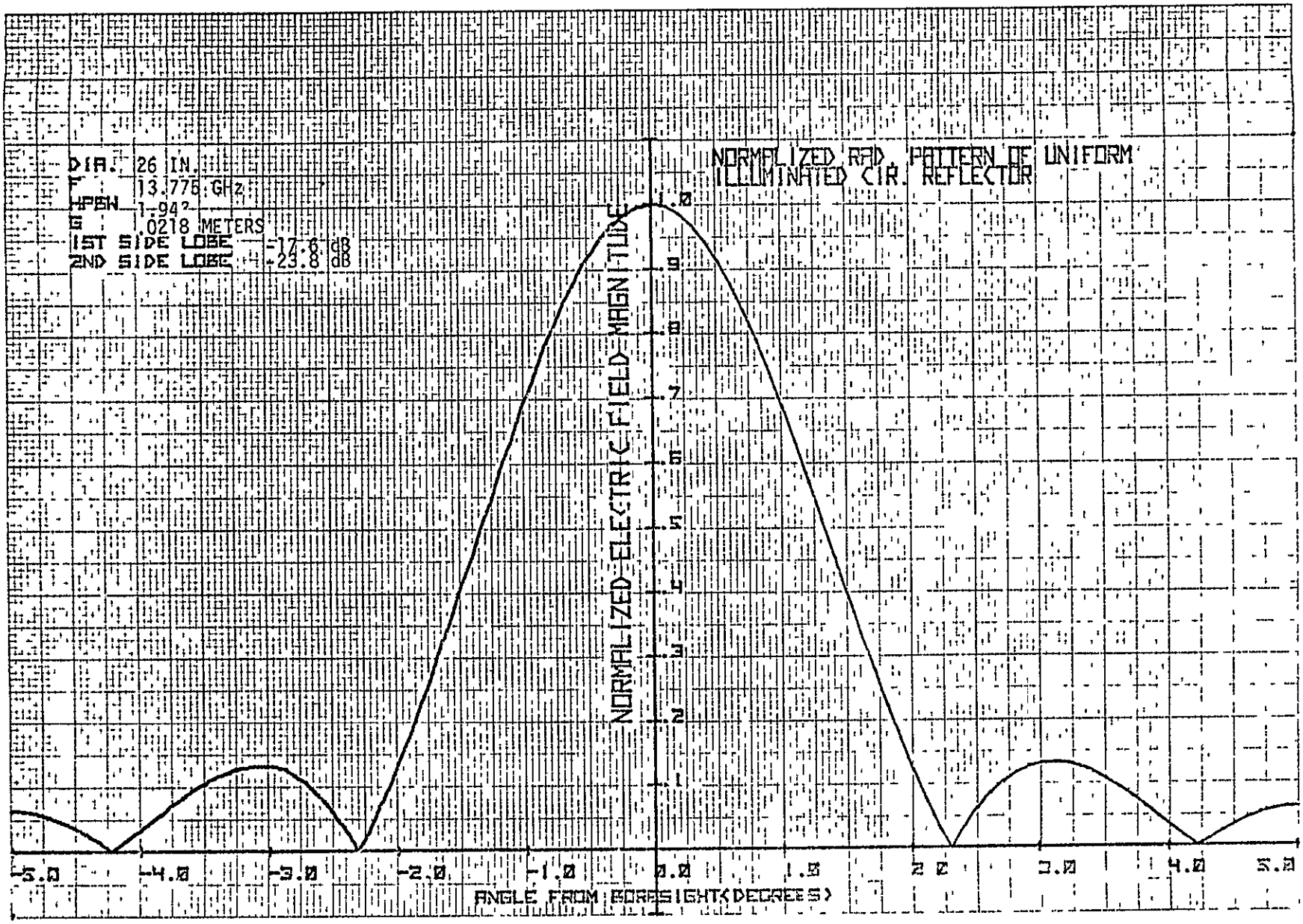

FIGURE 3

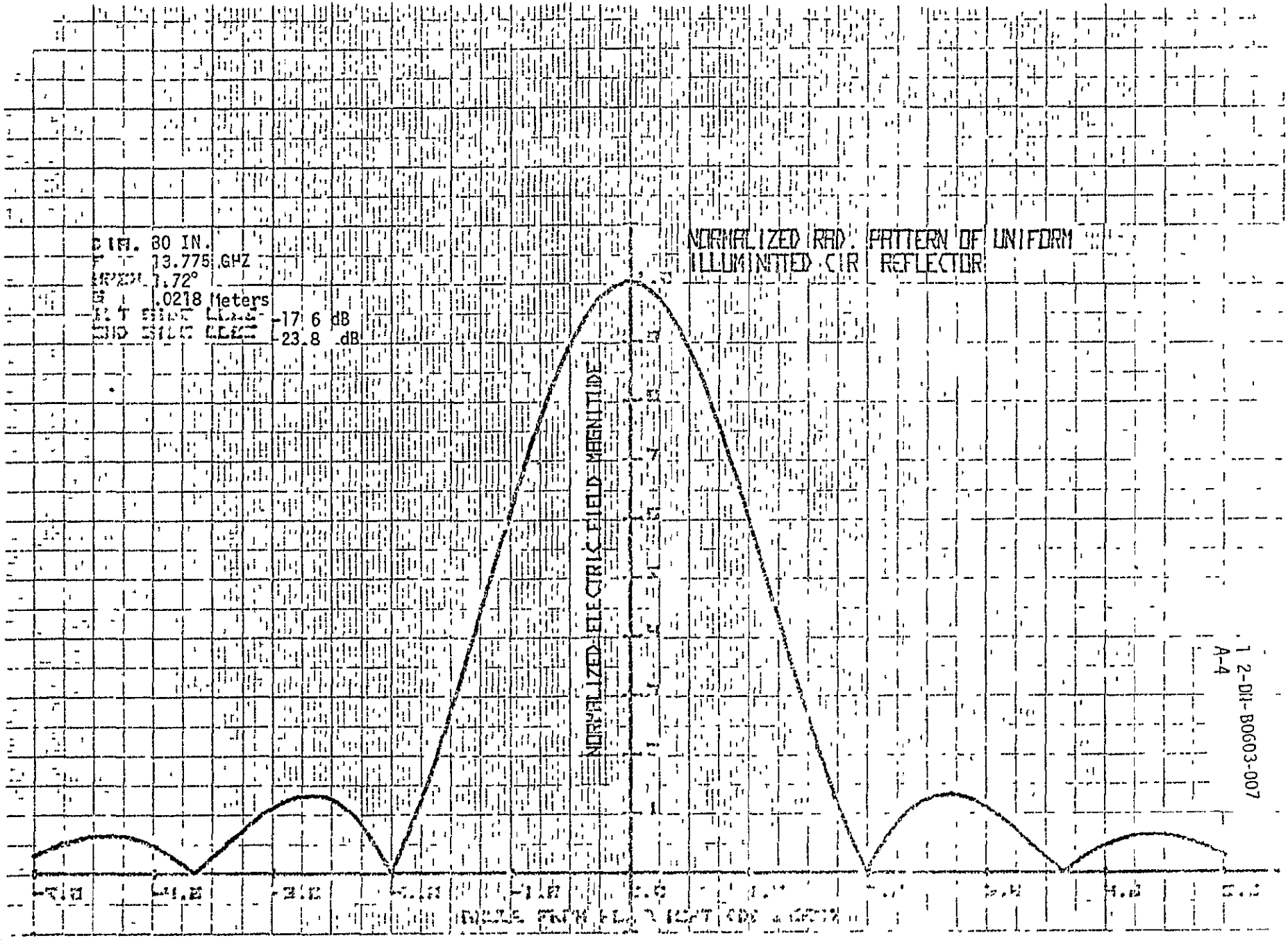
DIA. 80 IN.
13.775 GHZ
.0218 Meters
-17.6 dB
-23.8 dB
NORMALIZED RAD. PATTERN OF UNIFORM
ILLUMINATED CIR REFLECTOR
NORMALIZED ELECTRIC FIELD MAGNITUDE
12-DH-B0603-007
A-4

Figure 4

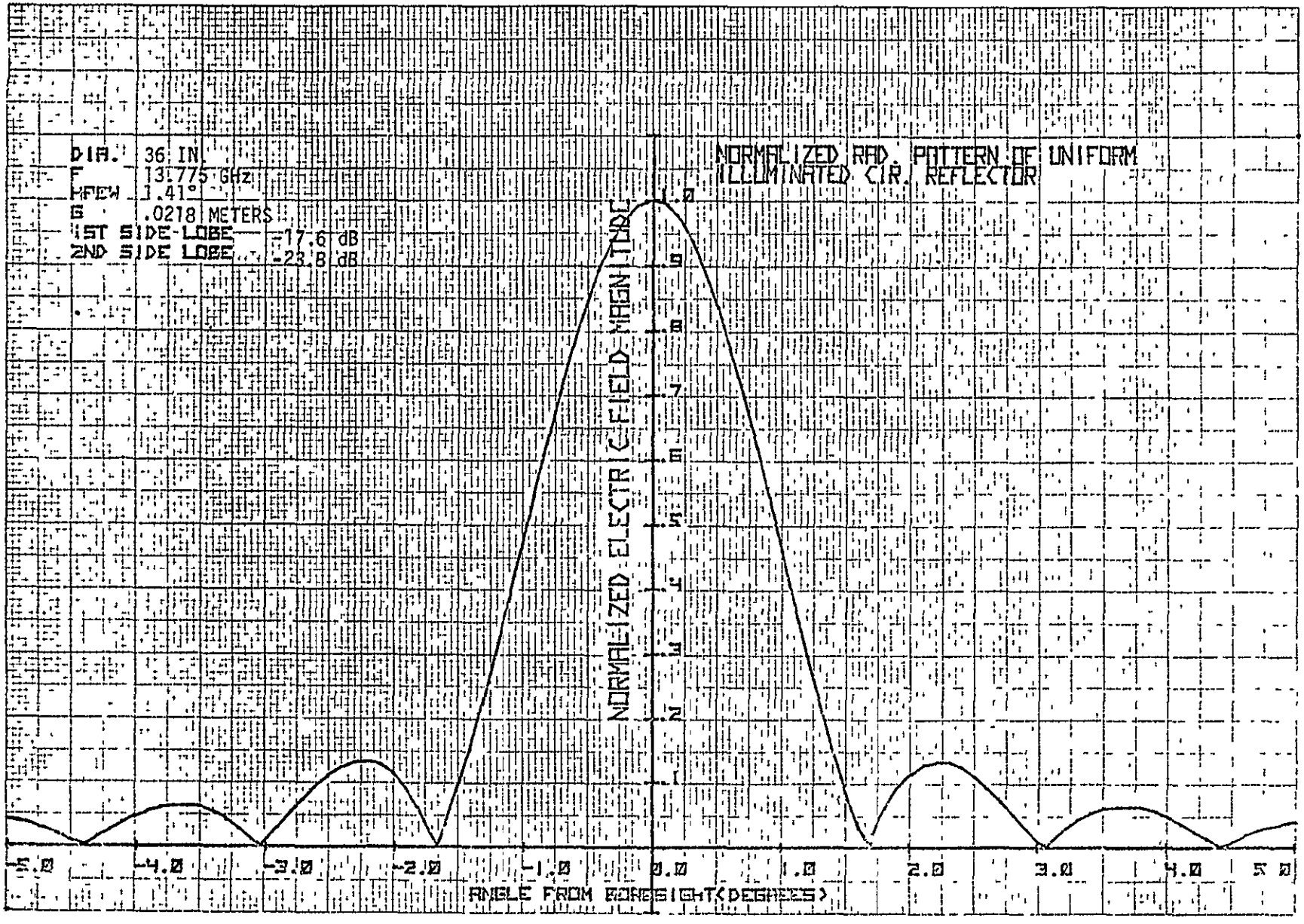

FIGURE 5

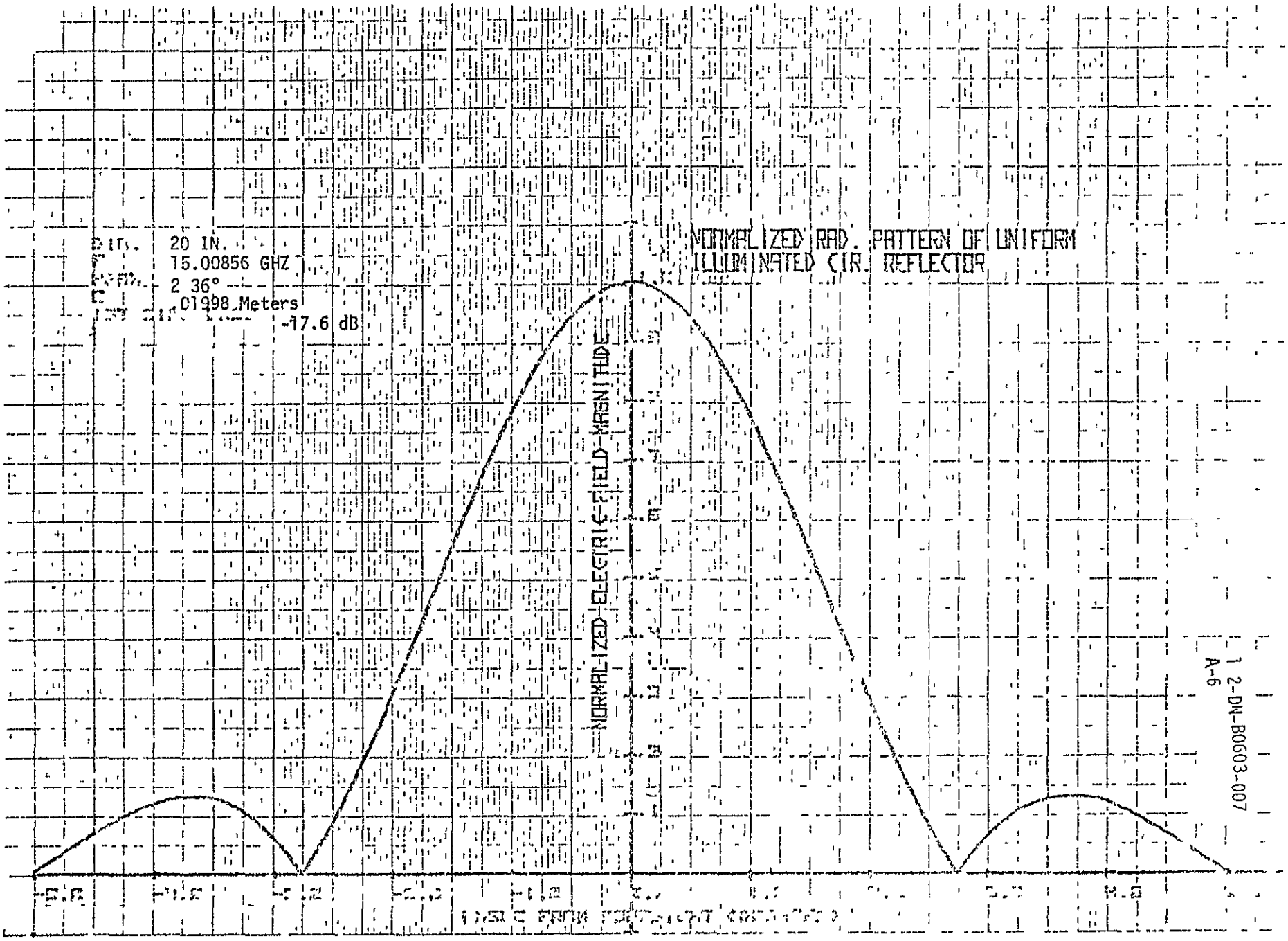
20 IN.
15.00856 GHZ
2 36°
.01998 Meters
-17.6 dB
NORMALIZED RAD. PATTERN OF UNIFORM ILLUMINATED CIR. REFLECTOR
NORMALIZED ELECTRIC FIELD MAGNITUDE
1 2-DN-B0603-007
A-6

Figure 6

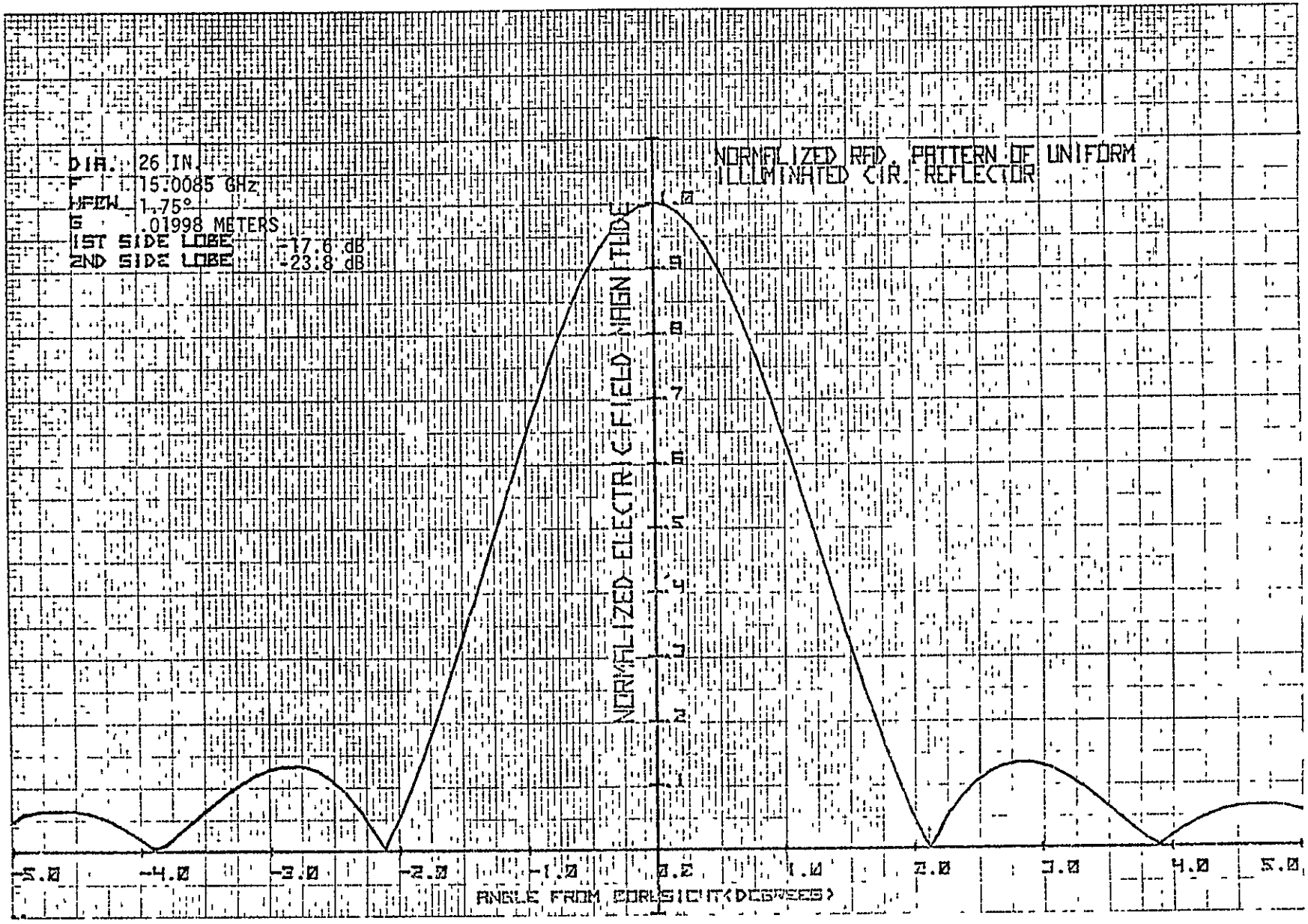

FIGURE 7

NORMALIZED RAD. PATTERN OF UNIFORM
ILLUMINATED CIR. REFLECTOR
DIA. 30 IN.
15.0085 GHZ
1.54°
.0998 Meters
-17.6 dB
-23.8 dB
NORMALIZED ELECTRIC FIELD-MAGNITUDE
-5.0
-4.0
-3.0
-2.0
-1.0
0.0
1.0
2.0
3.0
4.0
5.0

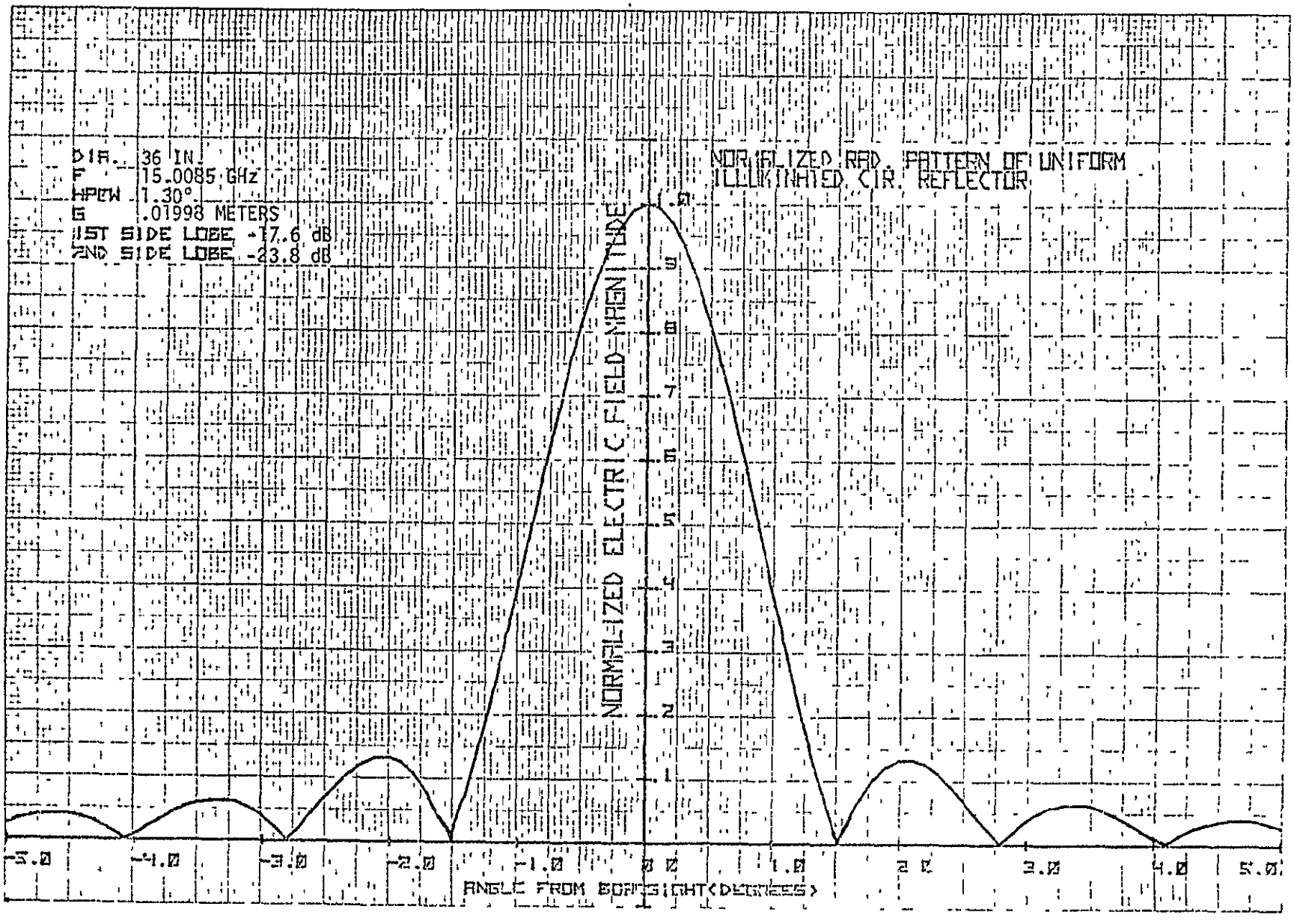

FIGURE 9

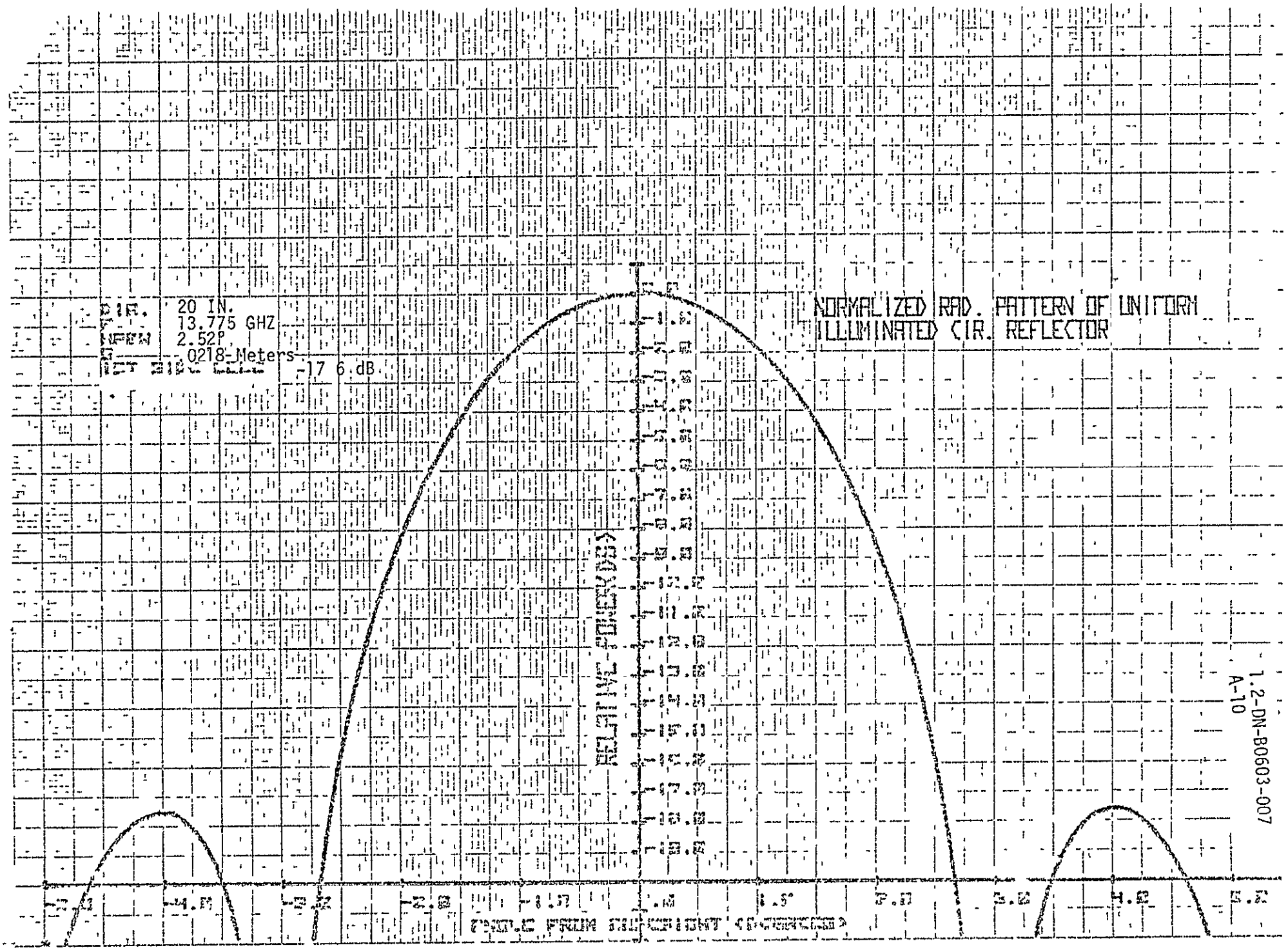
NORMALIZED RAD. PATTERN OF UNIFORM ILLUMINATED CIR. REFLECTOR
DIA. 20 IN.
13.775 GHZ
2.52°
0218-Meters
-17.6 dB
1.2-DN-B0603-007
A-10

Figure 10

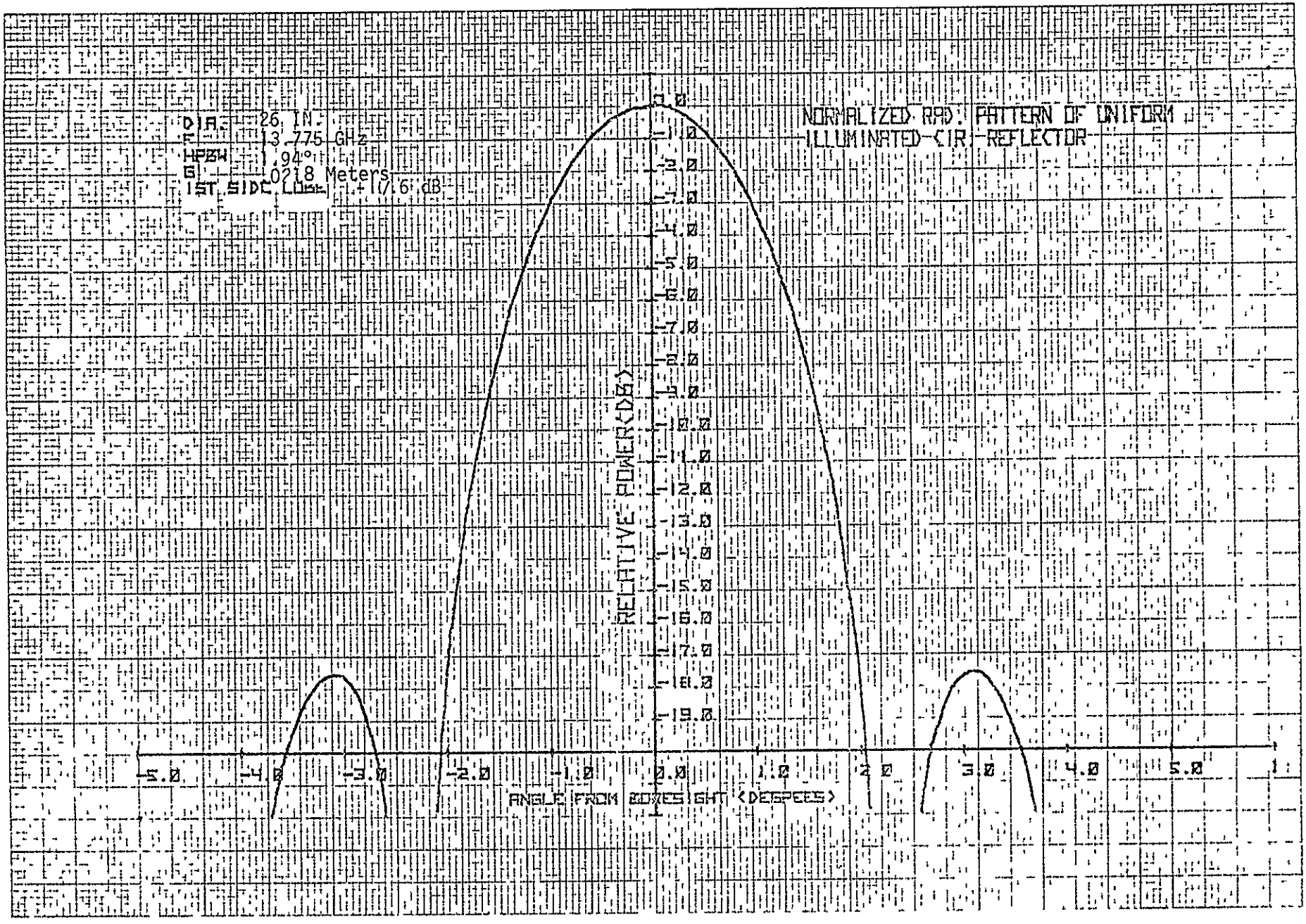

FIGURE 11

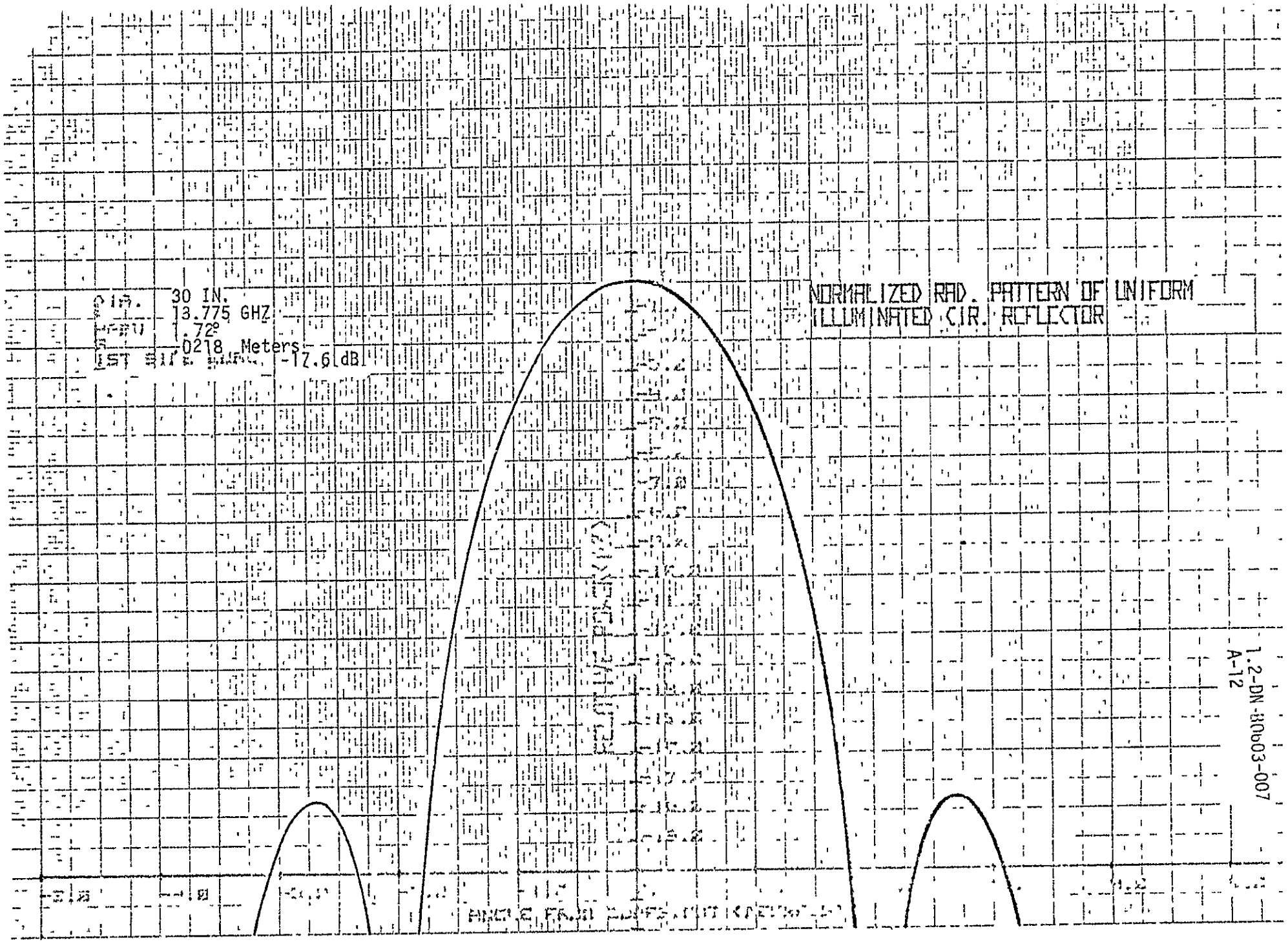
NORMALIZED RAD. PATTERN OF UNIFORM
ILLUMINATED CIR. REFLECTOR
30 IN.
13.775 GHZ
1.72°
.0218 Meters
-17.6 dB
1.2-DN-80603-007
A-12

Figure 12

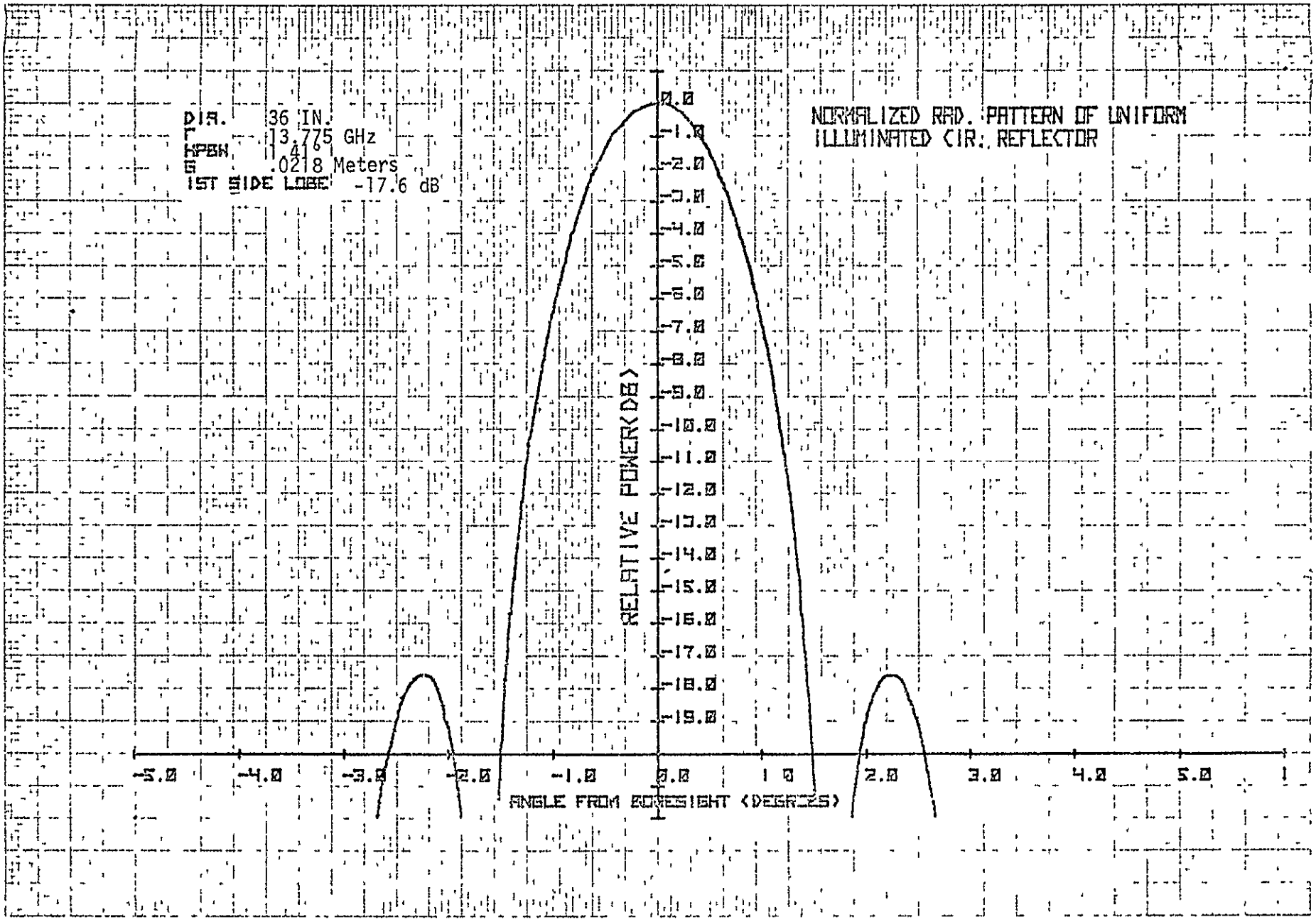

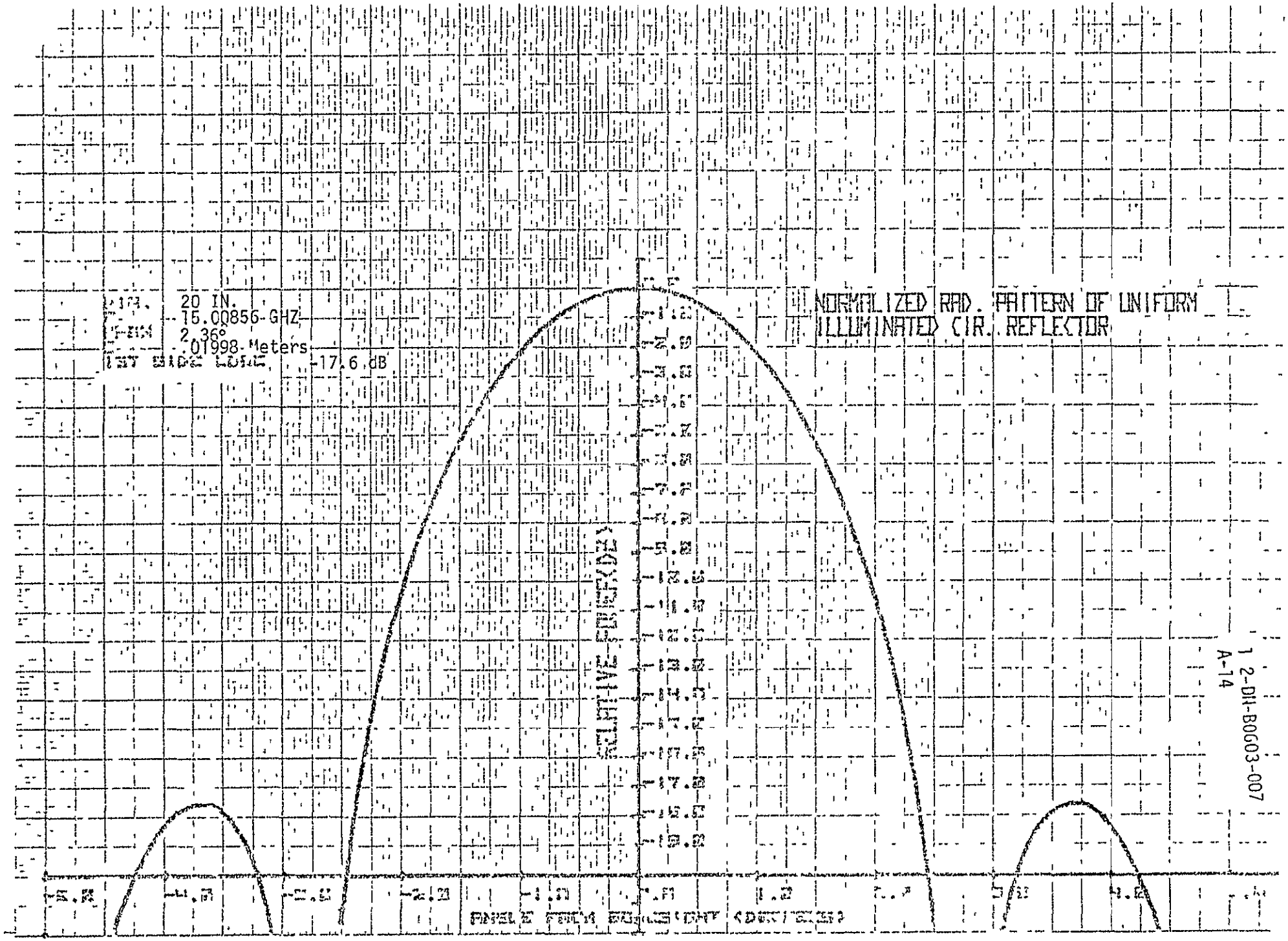
20 IN.
15.00856-GHZ
2.36°
.01998-Meters
-17.6 dB
NORMALIZED RAD. PATTERN OF UNIFORM
ILLUMINATED CIR. REFLECTOR
RELATIVE STRENGTH (DB)
12-DH-B0603-007
A-14

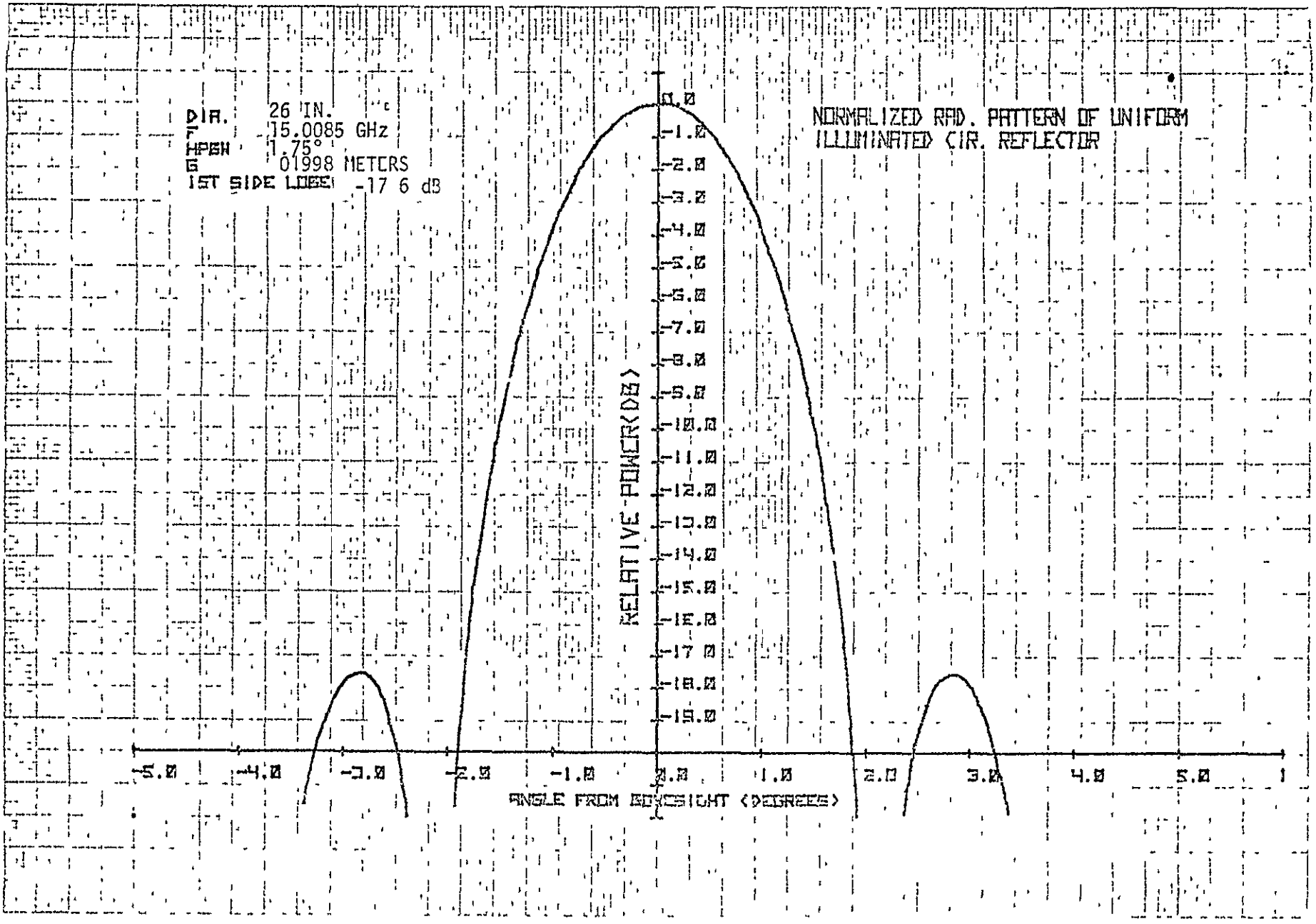

DIA. 30 IN.
15.0085 GHZ
1.54°
.01998 METERS
-17.6 dB
NORMALIZED RAD. PATTERN OF UNIFORM
ILLUMINATED CIR. REFLECTOR
1.2-DN-B0603-007
A-16

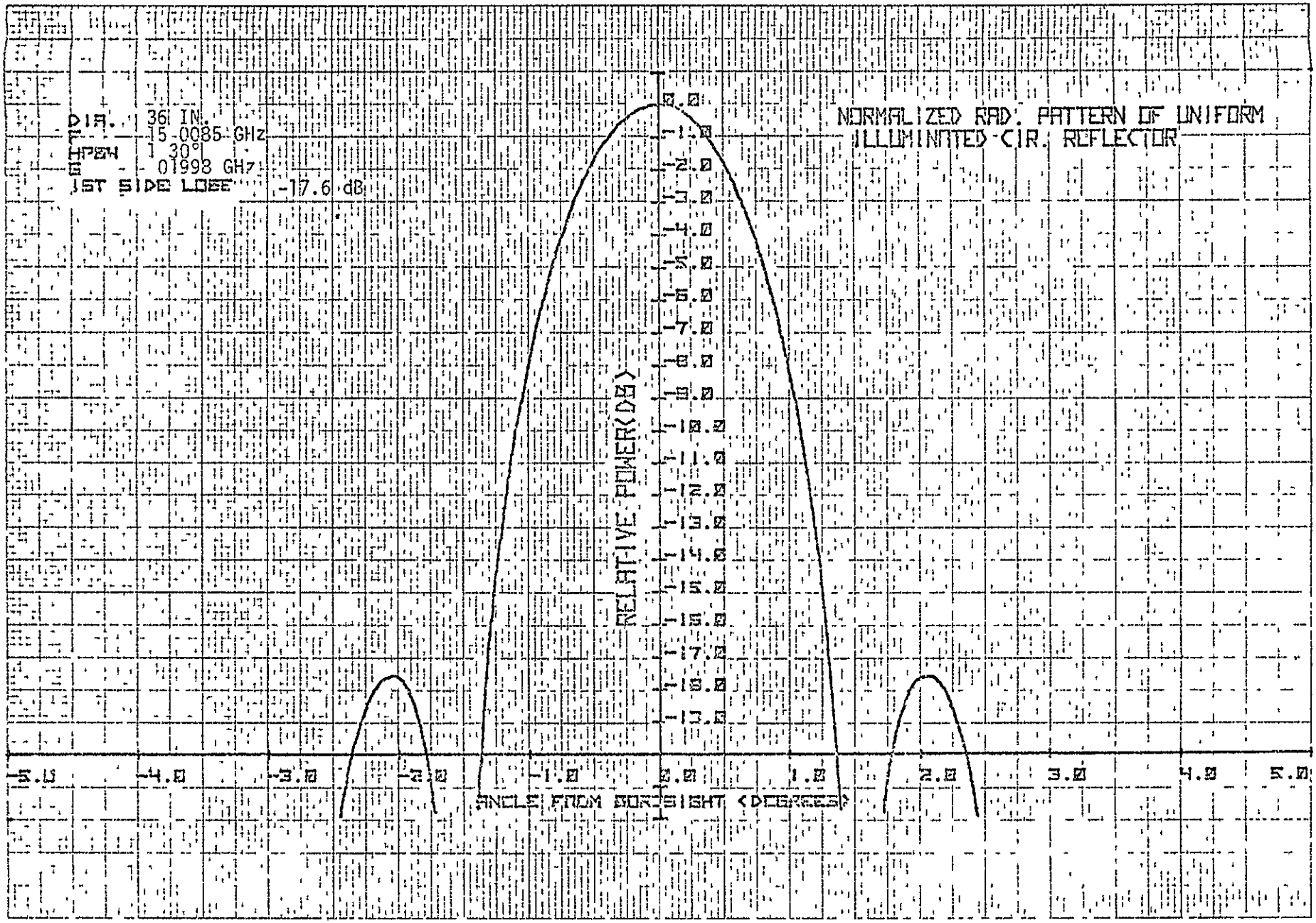

Figure 17

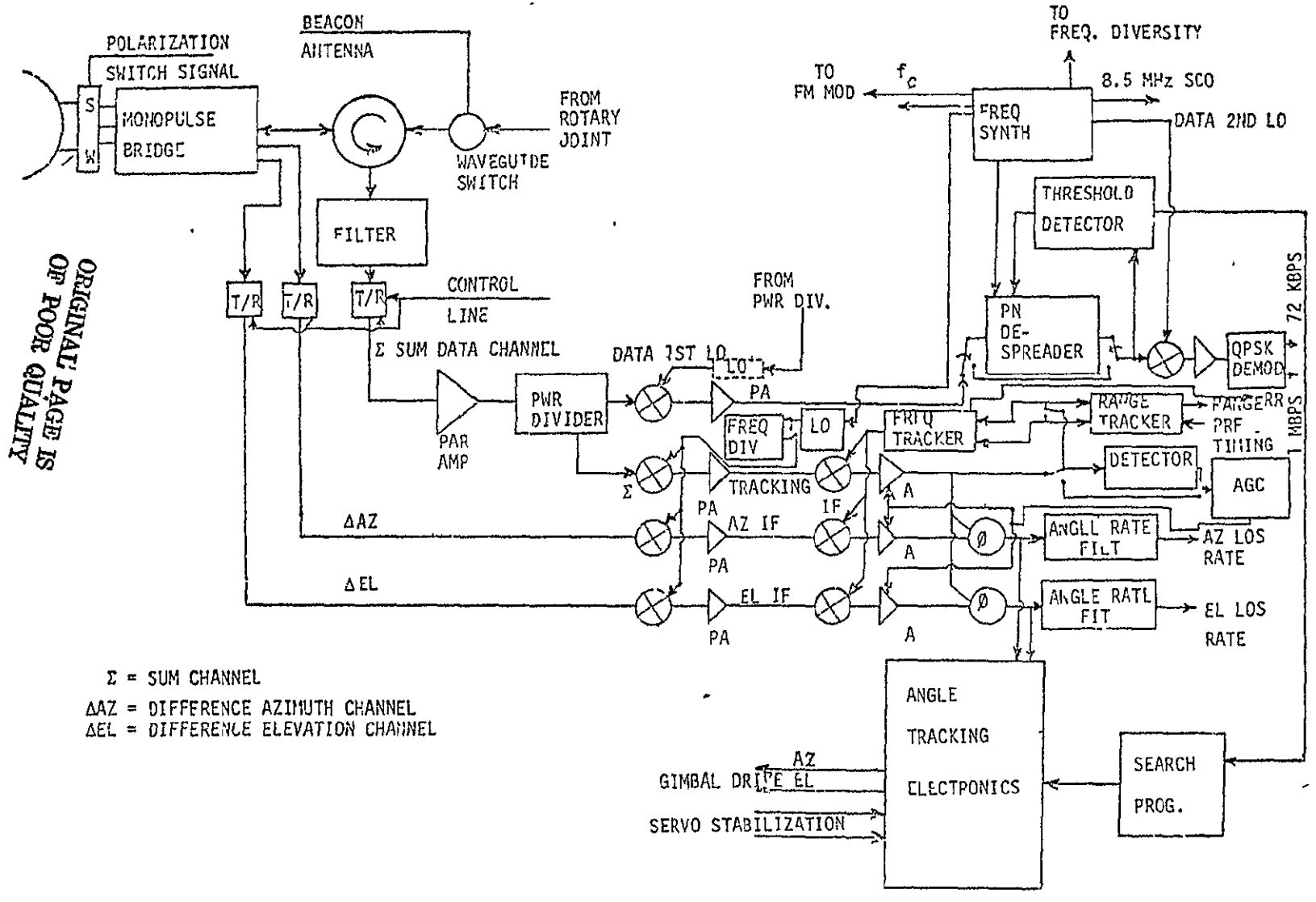

ORIGINAL PAGE IS
OF POOR QUALITY

Figure 18 CANDIDATE ORBITER TRACKING CONFIGURATION

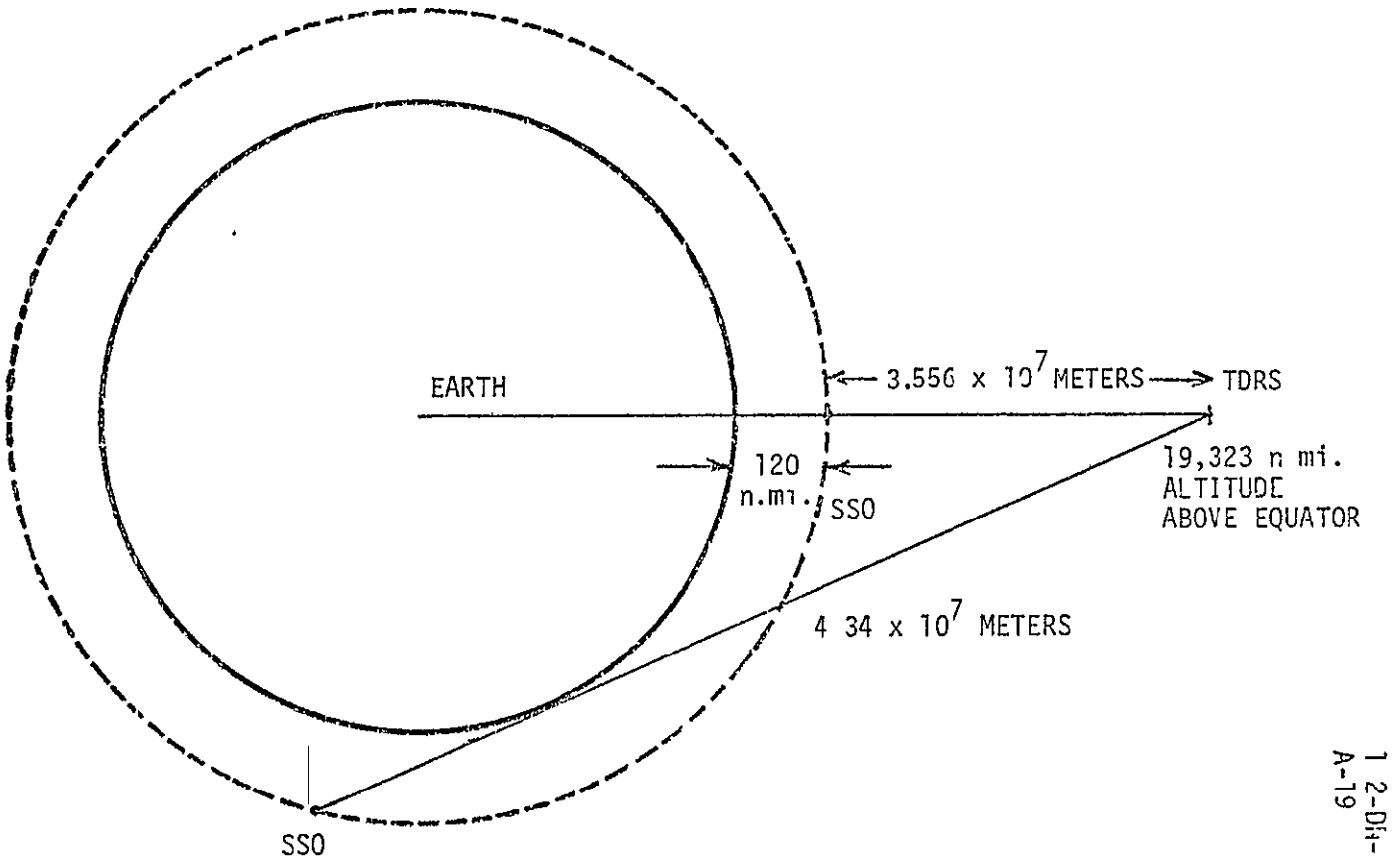

FIGURE 19 MIN. & MAX. SLANT RANGE PARAMETERS

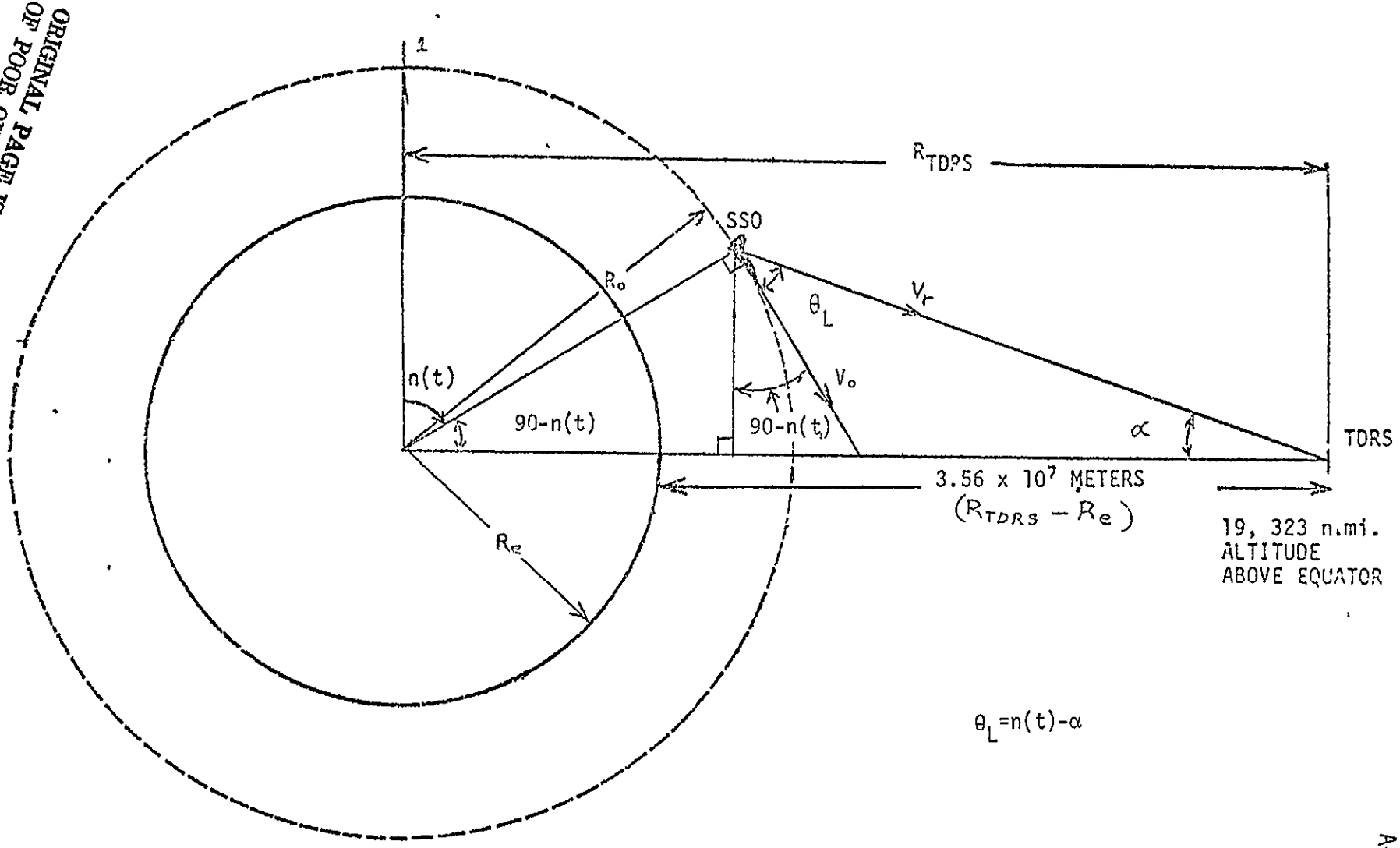

FIGURE 20 SSO/TDRS DOPPLER GEOMETRY

DOPPLER SHIFT AT AN ALTITUDE OF 100N MI
AOS
MAX
KILOHERTZ
TIME (MIN)
LOS
MIN.

FIGURE 21

DOPPLER SHIFT AT AN ALTITUDE OF 237.57 N.MI.
MAX
LOS
MIN
T (MEC/MIN)
DOPPLER SHIFT (KHZ)

FIGURE 22

DOPPLER SHIFT AT AN ALTITUDE OF 600N.M.
AOS
DOPPLER SHIFT (KHZ)
TIME (MIN)
MIN.
LOS

FIGURE 23

DOPPLER RATE AT AN ALTITUDE OF 100N MI
DOPPLER RATE(KHZ/MIN)
TIME(MIN)
AOS
LOS

FIGURE 24

ORIGINAL PAGE IS
OF POOR QUALITY

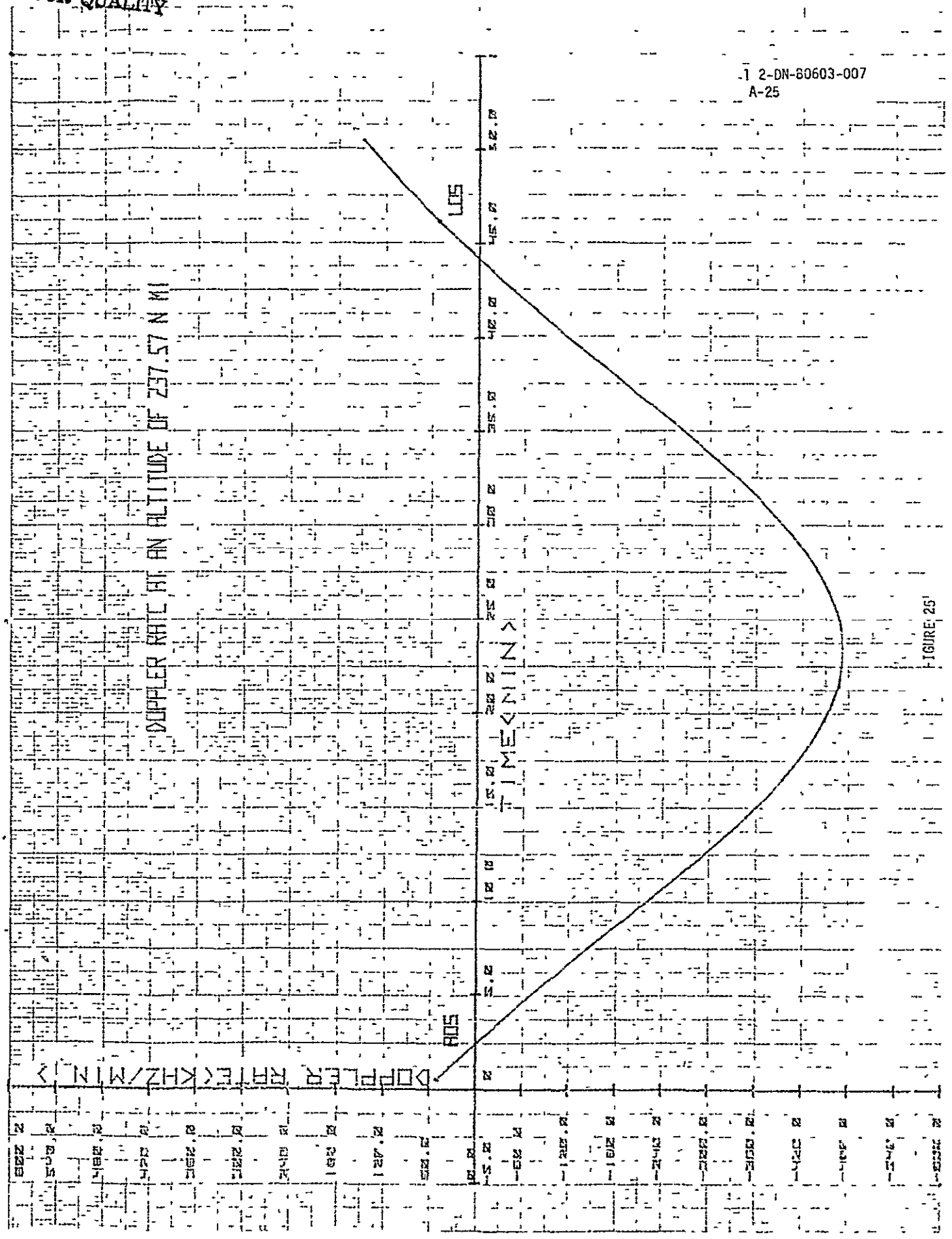

FIGURE 25

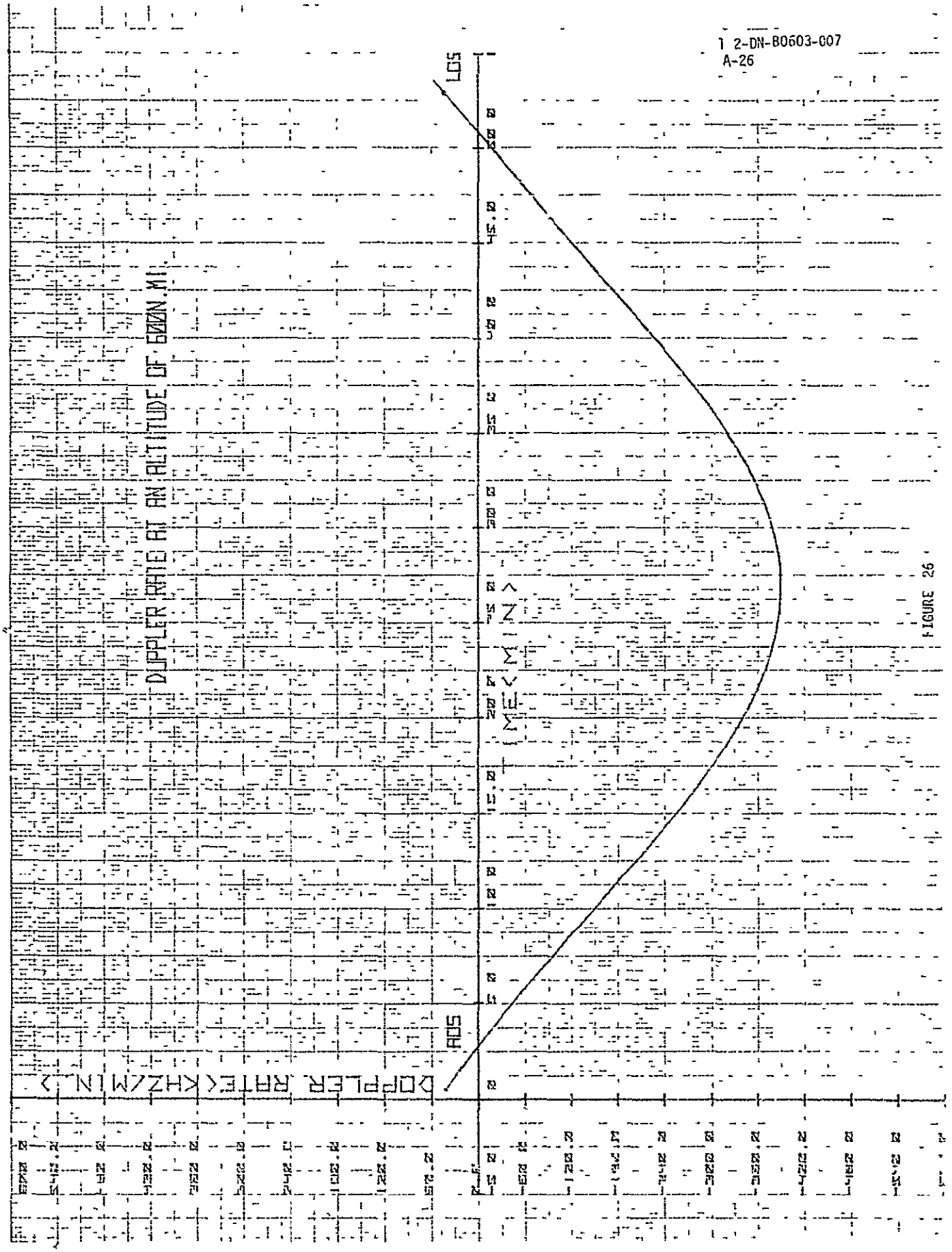

FIGURE 26

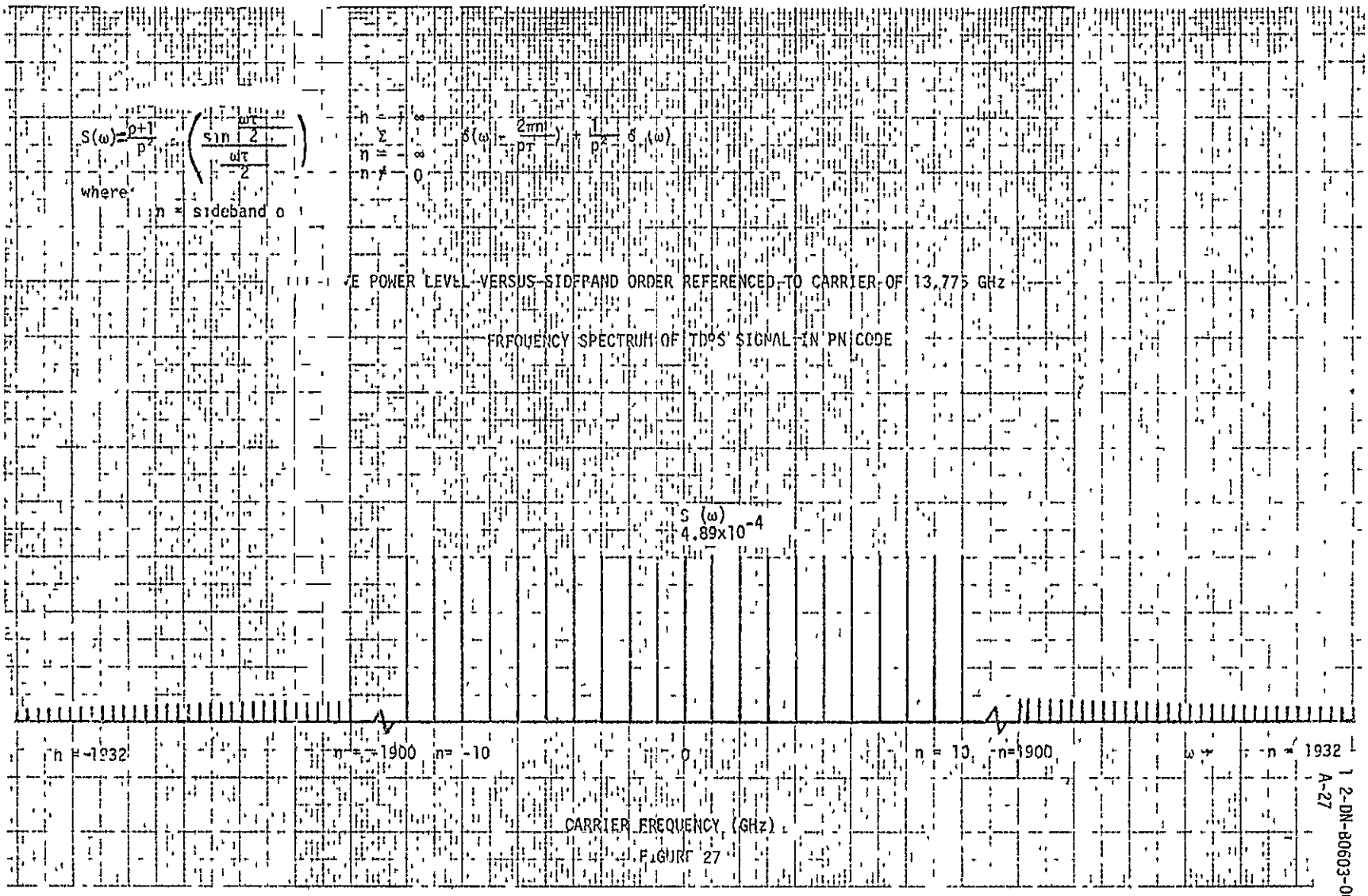

FIGURE 27

2-DN-B0603-007

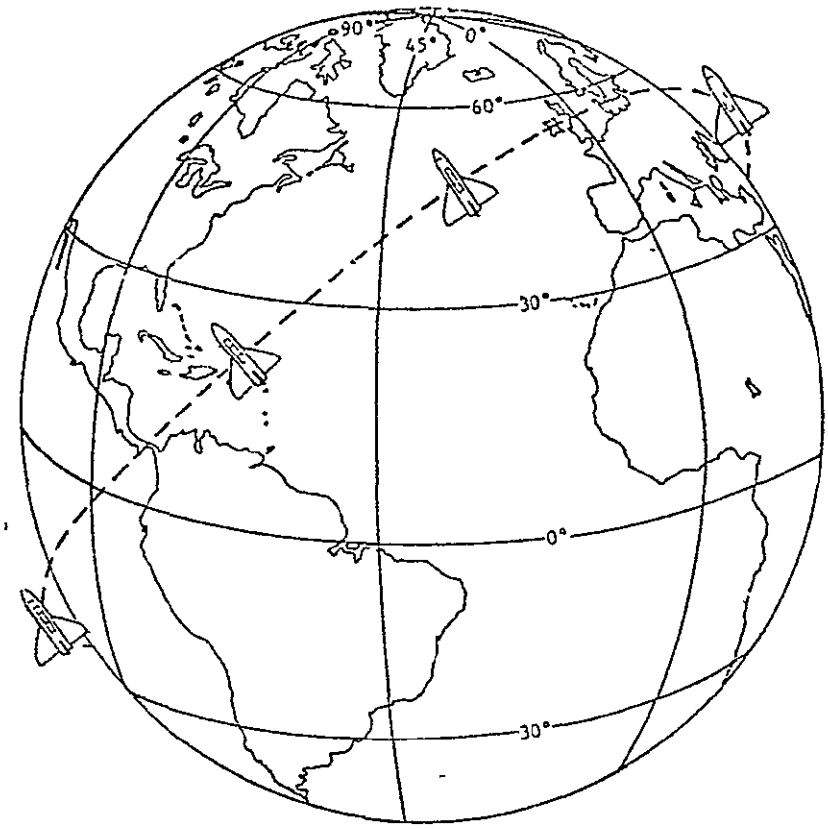

Figure 28 Inertial Hold Configuration

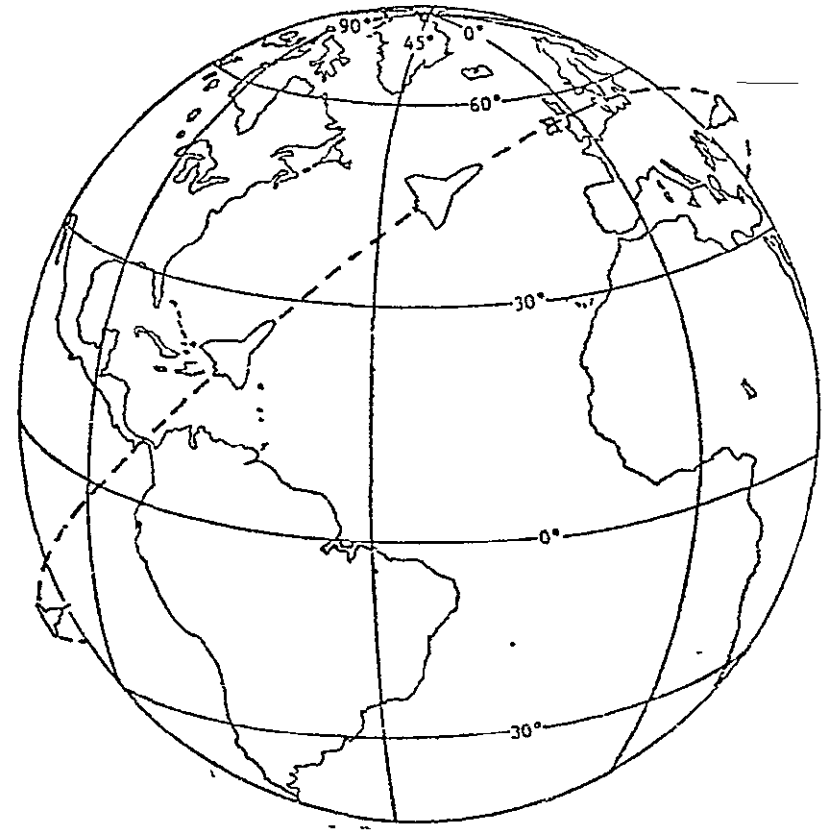

Figure 29 LVLH Configuration

ORBITER LOOK ANGLE VARIATION AT AN ALTITUDE OF 100N.MI. (LVLH)
ORBITER RATE<DEG/MIN>
TIME<MIN>
AOS
LOS

Figure 30

Figure 31

12-DN-80603-007

ORBITER LOOK ANGLE VARIATION AT AN ALTITUDE OF 600N.MI.(LVLH)
ORBITER RATE(DEG/MIN)
TIME(MIN)
LOS
A-31
12-DN-B0603-007

Figur

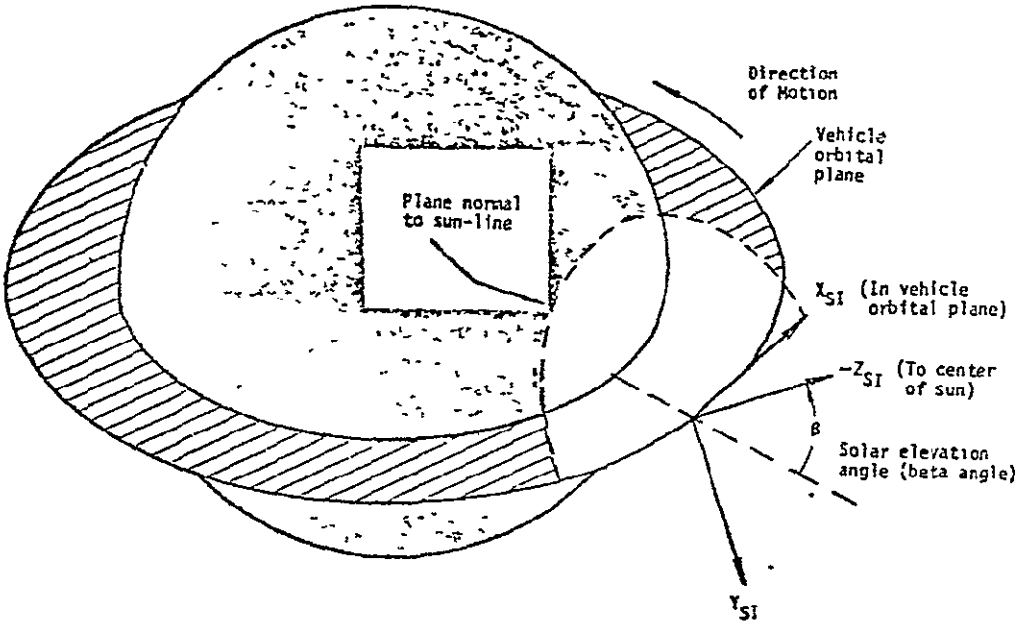

β , the solar elevation angle, is the angle between the vehicle sun-line and the vehicle orbital plane at orbital noon. It is positive when the sun is above (north of) the vehicle orbital plane.

SI = Solar inertial

For "barbecue", Orbiter axis of rotation remains in plane normal to sun-line

Figure 33 "Barbecue" Configuration

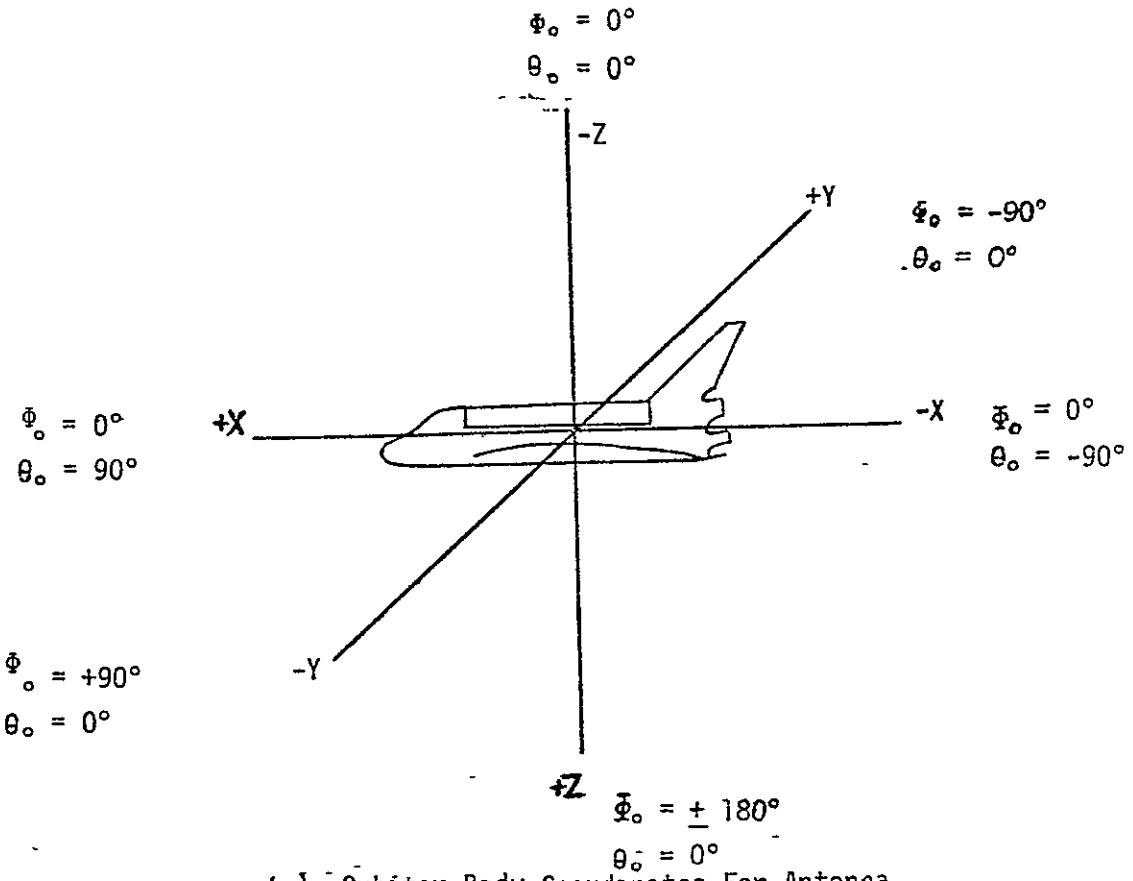

(a) Orbiter Body Coordinates For Antenna

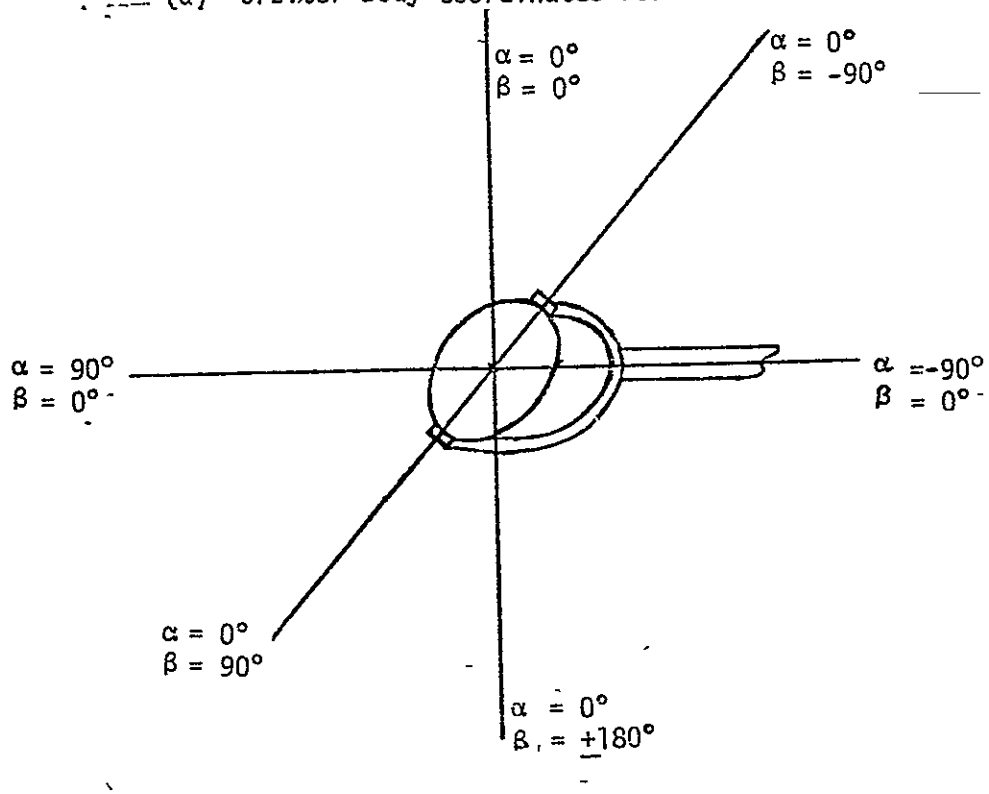

(b) Antenna Gimbal Coordinates (Antenna Pointed α=β = 0°)

Figure 34 Antenna Gimbal Transformation Coordinates

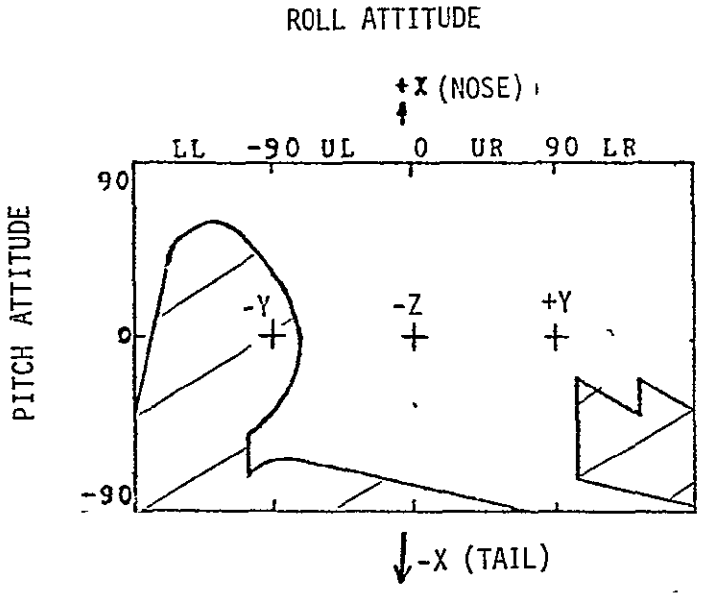

LL = LOWER LEFT
UL = UPPER LEFT
UR = UPPER RIGHT
LR = LOWER RIGHT

NOTE See coordinate system in Figure 34 (a).

Figure 35 Antenna Management Display (Vehicle Blockage)

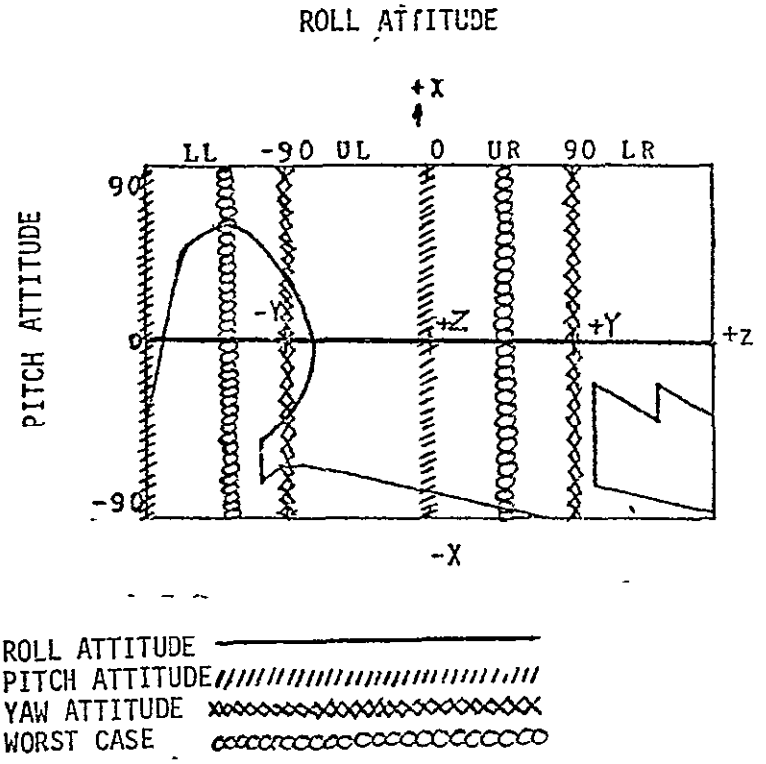

Figure 36 Path/Attitude Look Angle Variation

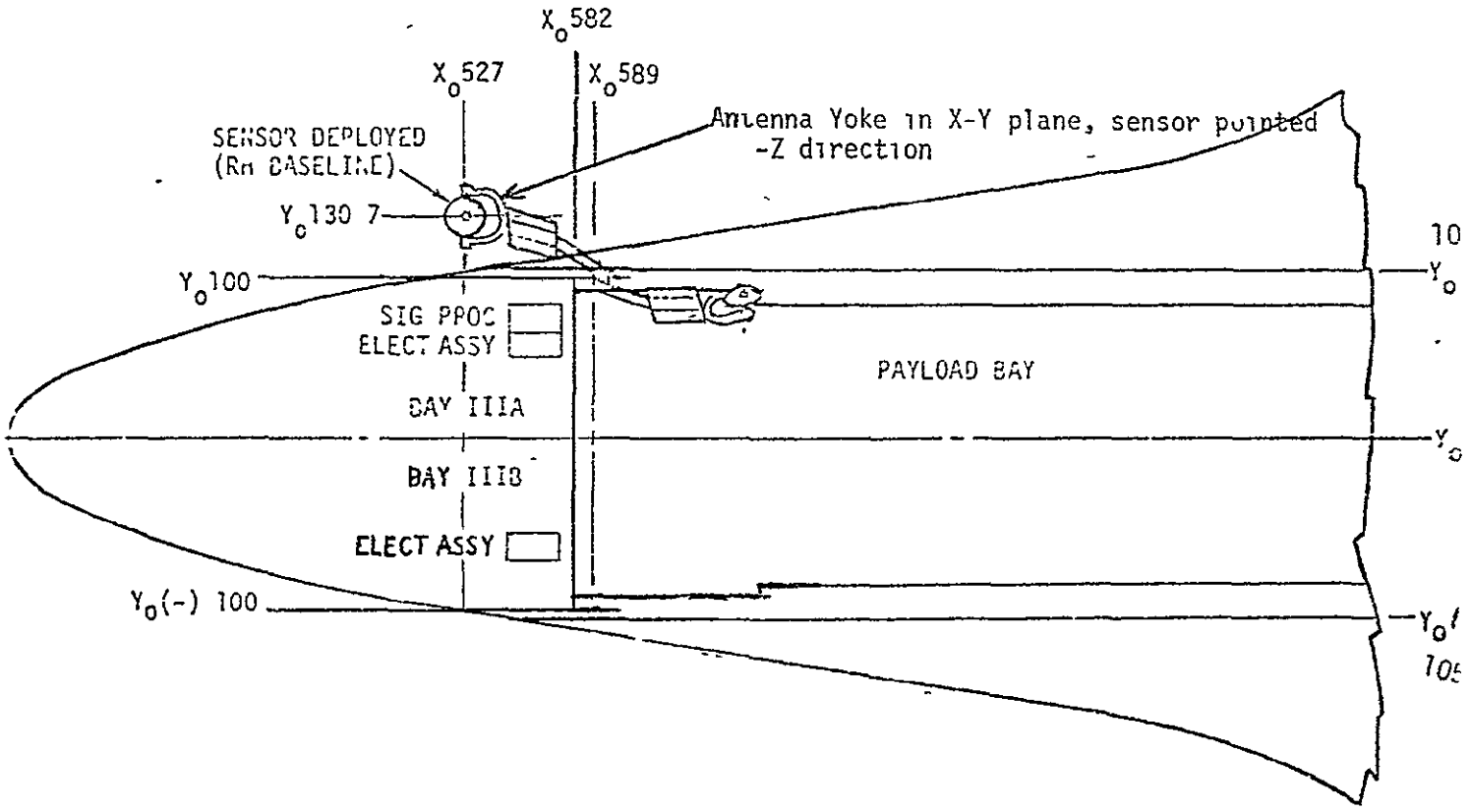

Figure 37 Orbiter Ku-Band Antenna Baseline Configuration (single antenna)

Shown for $\alpha = \beta = 0°$

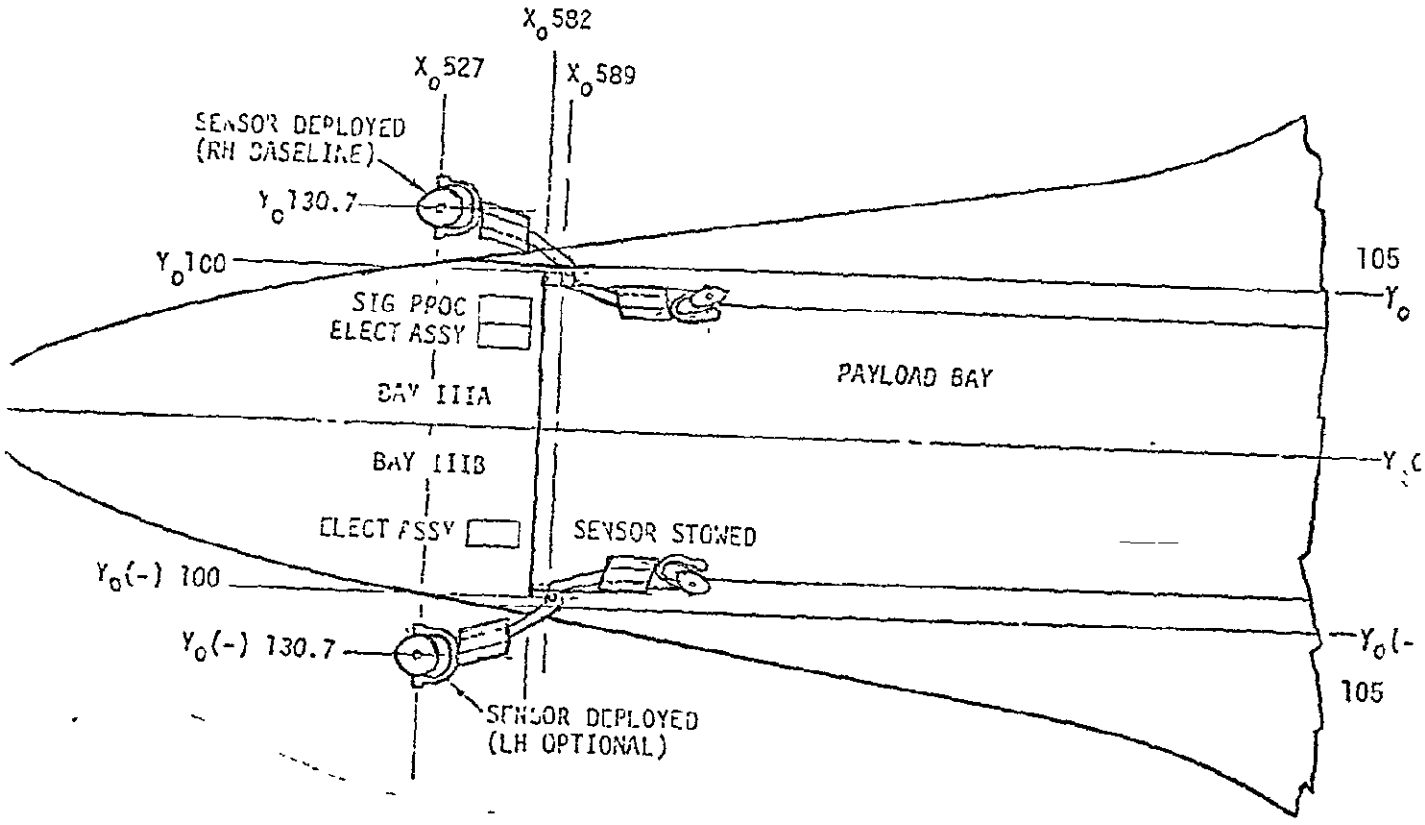

Figure 38 Orbiter Ku-Band Dual Antennas Baseline Configuration

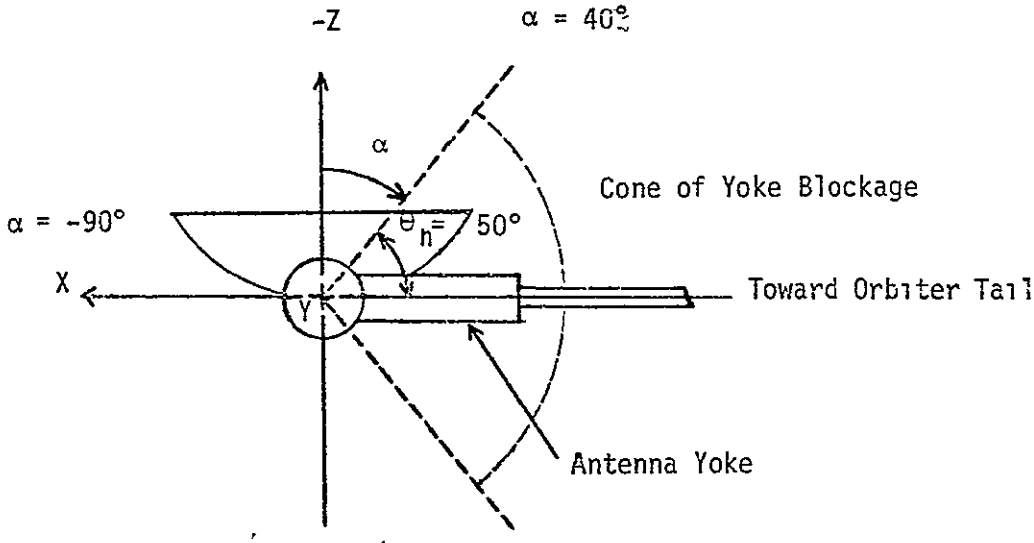

Figure 39 Yoke Blockage

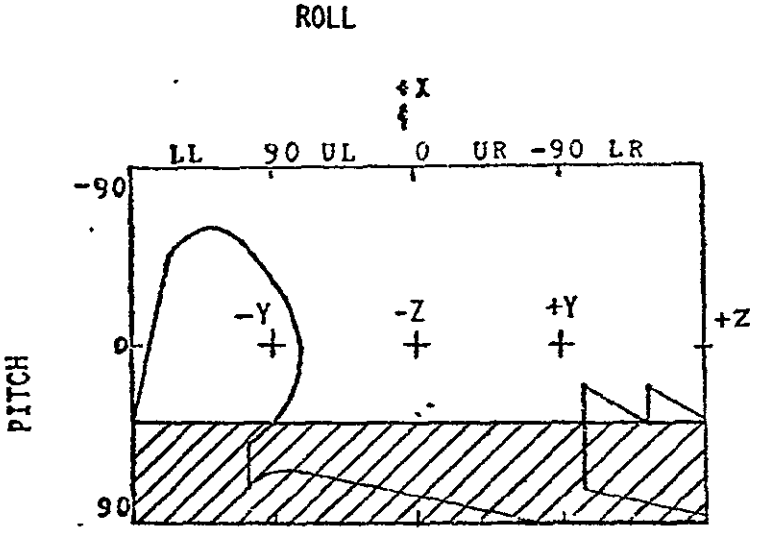

Figure 40 Ku-Band Single Antenna, Yoke and Vehicle Blockage (Baseline Configuration)

▨ Yoke Blockage

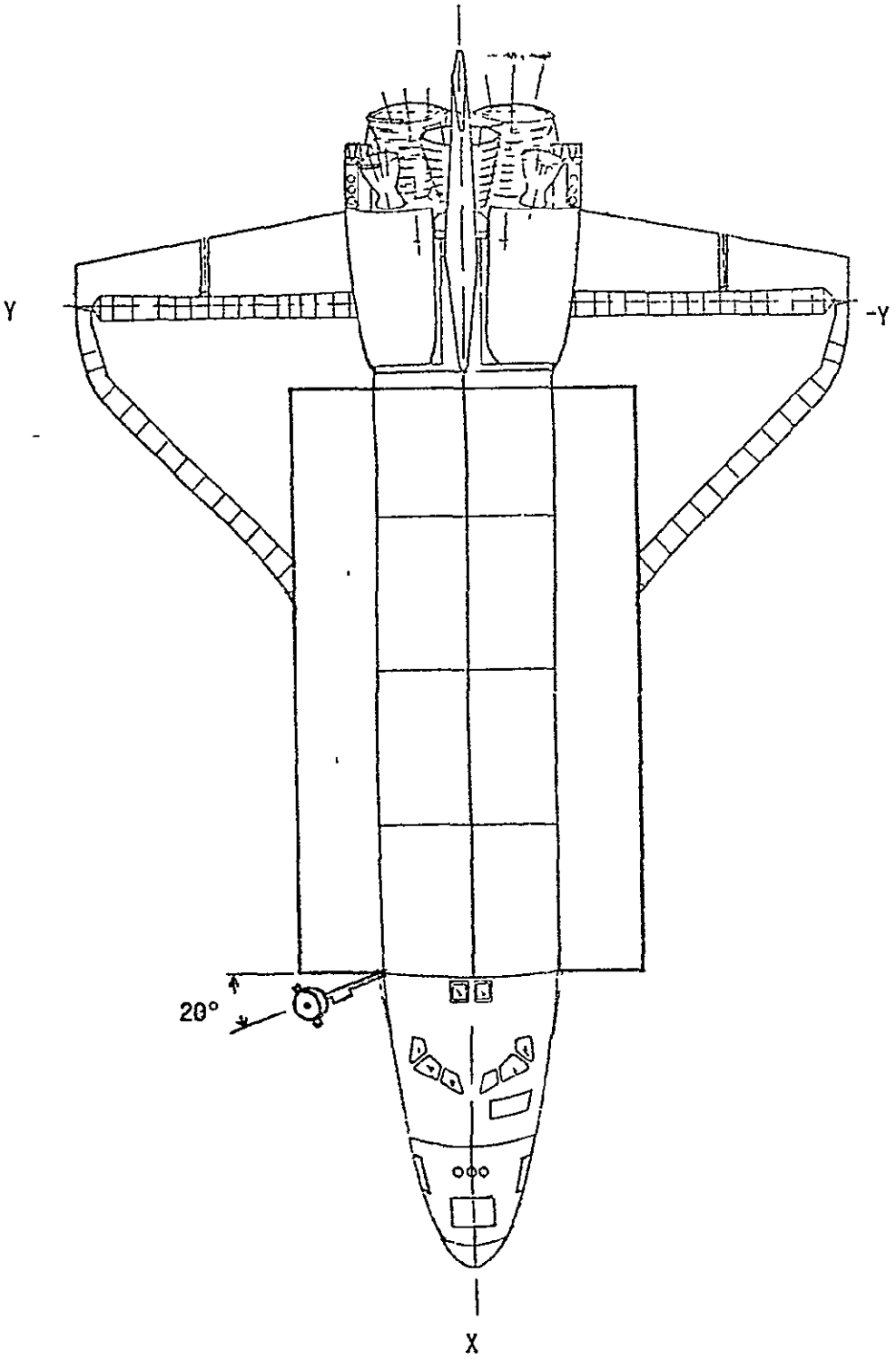

Figure 41 Optimum Deployment Configuration (Single Antenna)

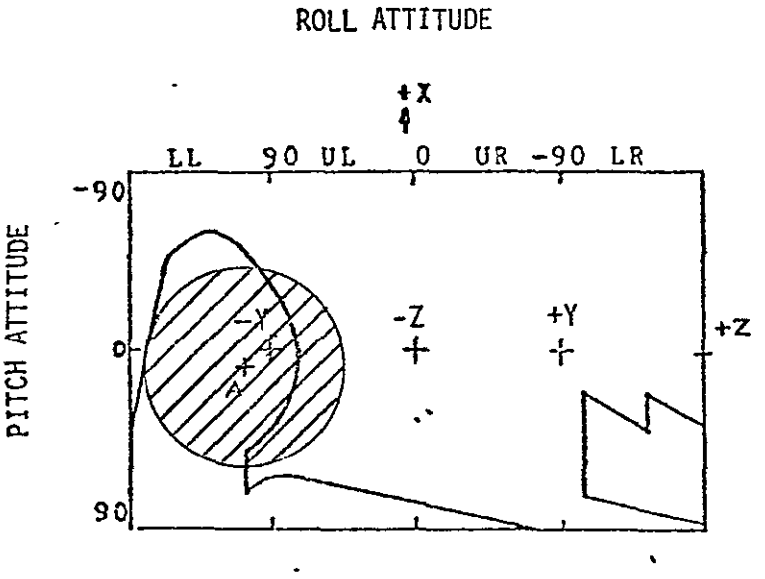

Figure 42 Optimum Deployment Configuration Blockage (Single Antenna)

Yoke Blockage

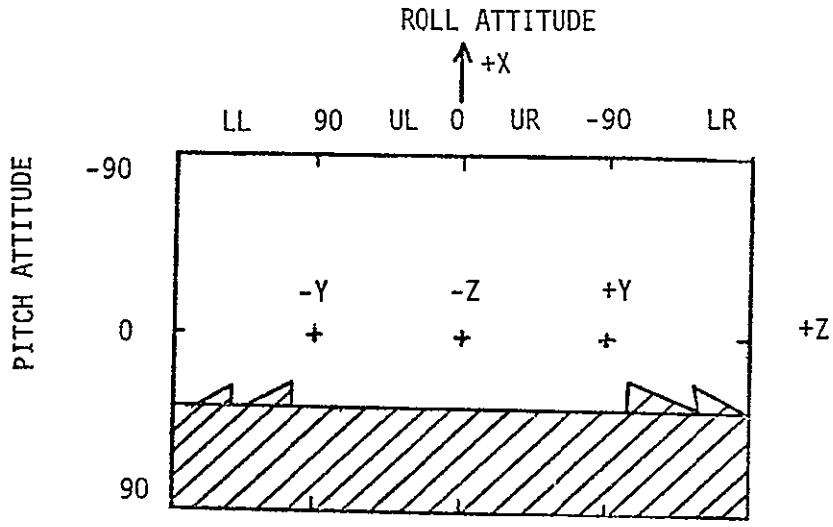

Figure 43 Baseline 2-Antenna Ku-Band System Blockage

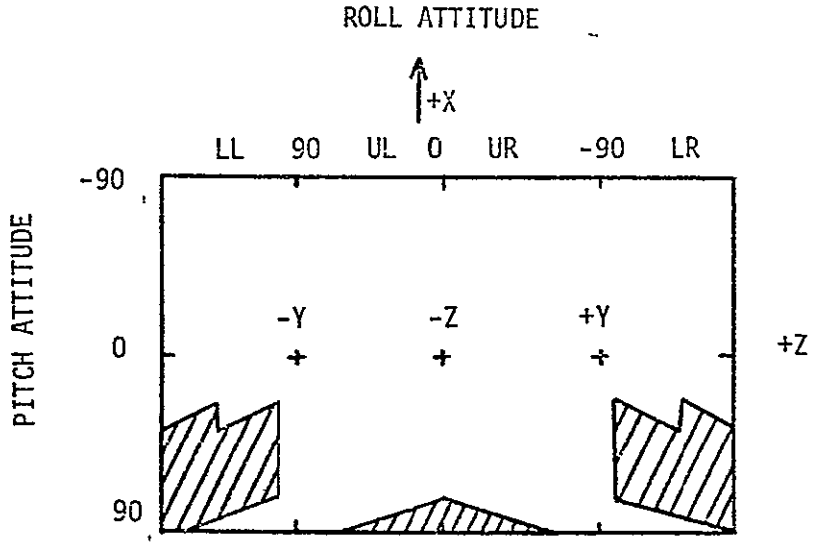

Figure 44 Optimum 2-Antenna System Blockage

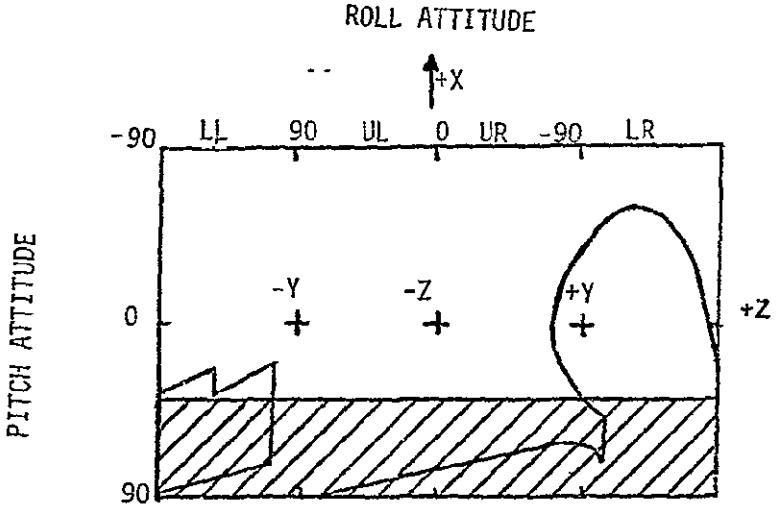

Figure 45 Left Antenna Blockage Baseline Configuration (Information only)

▨ Yoke Blockage

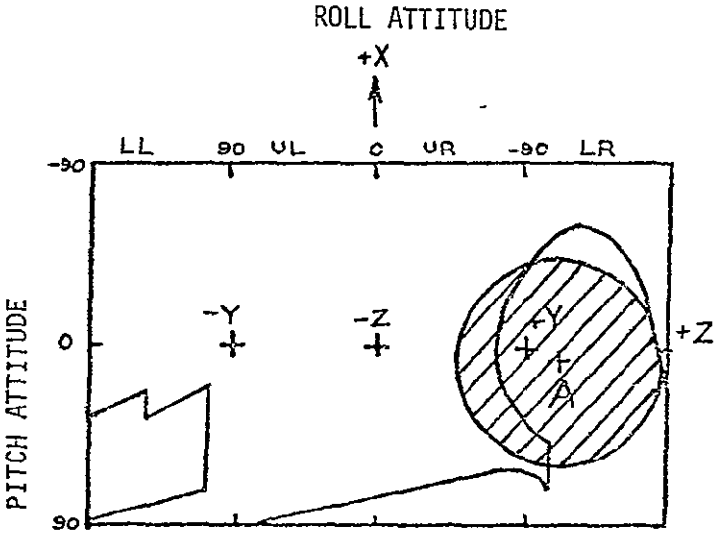

Figure 46 Left Antenna Blockage Optimum Configuration (information only)

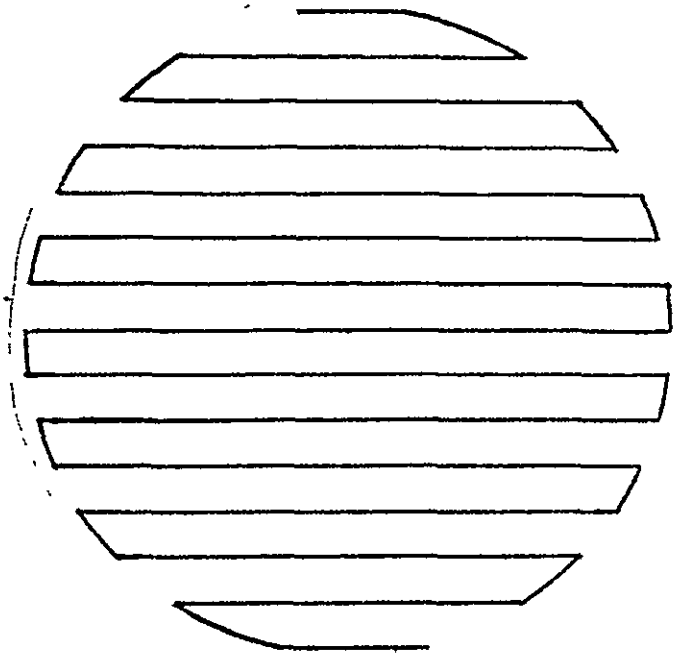

Figure 47 Raster Scan

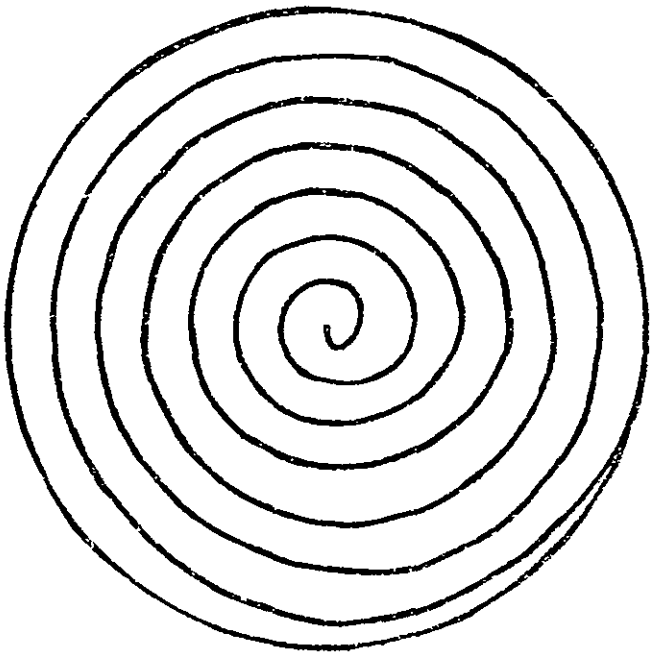

Figure 48 Conical Scan

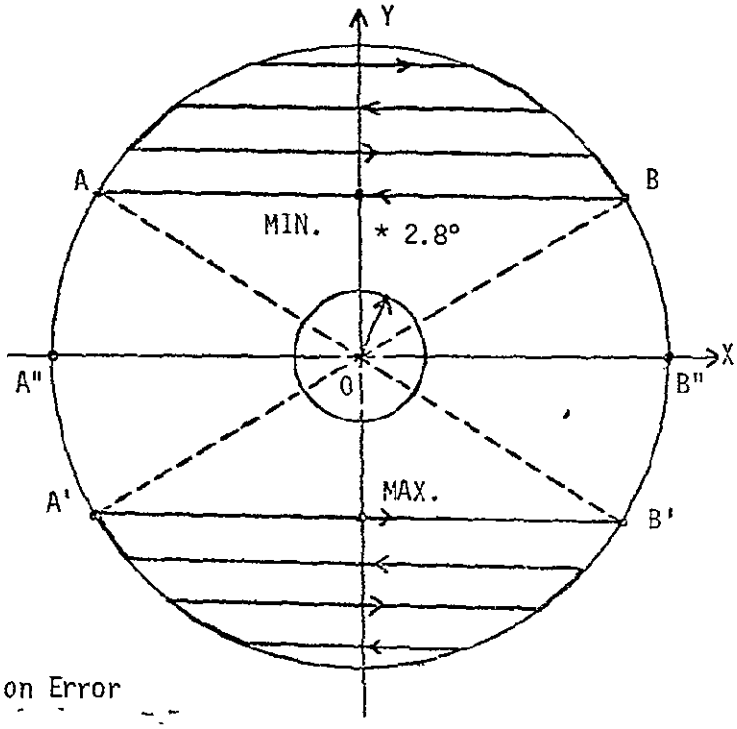

* Designation Error

Figure 49 Geometry for Detection Time Calculations For Raster Scan

(20 IN. REFLECTOR)
25.0
20.0
15.0
10.0
5.0
MAX
MIN
DETECTION-TIME (SEC)
0.0
.1
.2
.3
.4
.5
.6
LOCK ANGLE VELOCITY (DEG/SEC)

(26 IN REFLECTOR)
25.0
20.0
15.0
10.0
5.0
MAX
MIN
DETECTION TIME (SEC)
.1
.2
.3
.4
.5
.6
LOOK ANGLE VELOCITY (DEG./SEC.)

REFLECTOR
MAX.
MIN
25.0
20.0
15.0
10.0
5.0
0.0
1
2
3
4
5
6

(BEAN REFLEKTOR)
25.0
20.0
15.0
10.0
5.0
0.0
MAX.
MIN
DETECTION TIME(SEC)
1
2
3
4
5
6
LOOK ANGLE VELOCITY(DEG./SEC.)
1.2-DN-B0603-0 7
A-50

Z-DN-B0603-007

TIME OF TARGET DETECTION FOR CONICAL SCAN
(26 IN. REFLECTOR)
DETECTION TIME (SEC)
30.0
25.0
20.0
15.0
10.0
5.0
MAX
MIN.

TIME OF TARGET DETECTION FOR CONICAL SCAN
(30 IN. REFLECTOR)
DETECTION TIME (SEC)
30.0
25.0
20.0
15.0
10.0
5.0
0.0
MAX.
MIN.
1
2
3
4
5
6

TIME OF TARGET DETECTION FOR CONICAL SCAN
(30 IN. REFLECTOR)
DETECTION TIME (SEC.)
30.0
25.0
20.0
15.0
10.0
5.0
MAX.
MIN.
.1
.2
.5
1
2
5
10
LOOK ANGLE VELOCITY (DEG/SEC.)

Figure 53

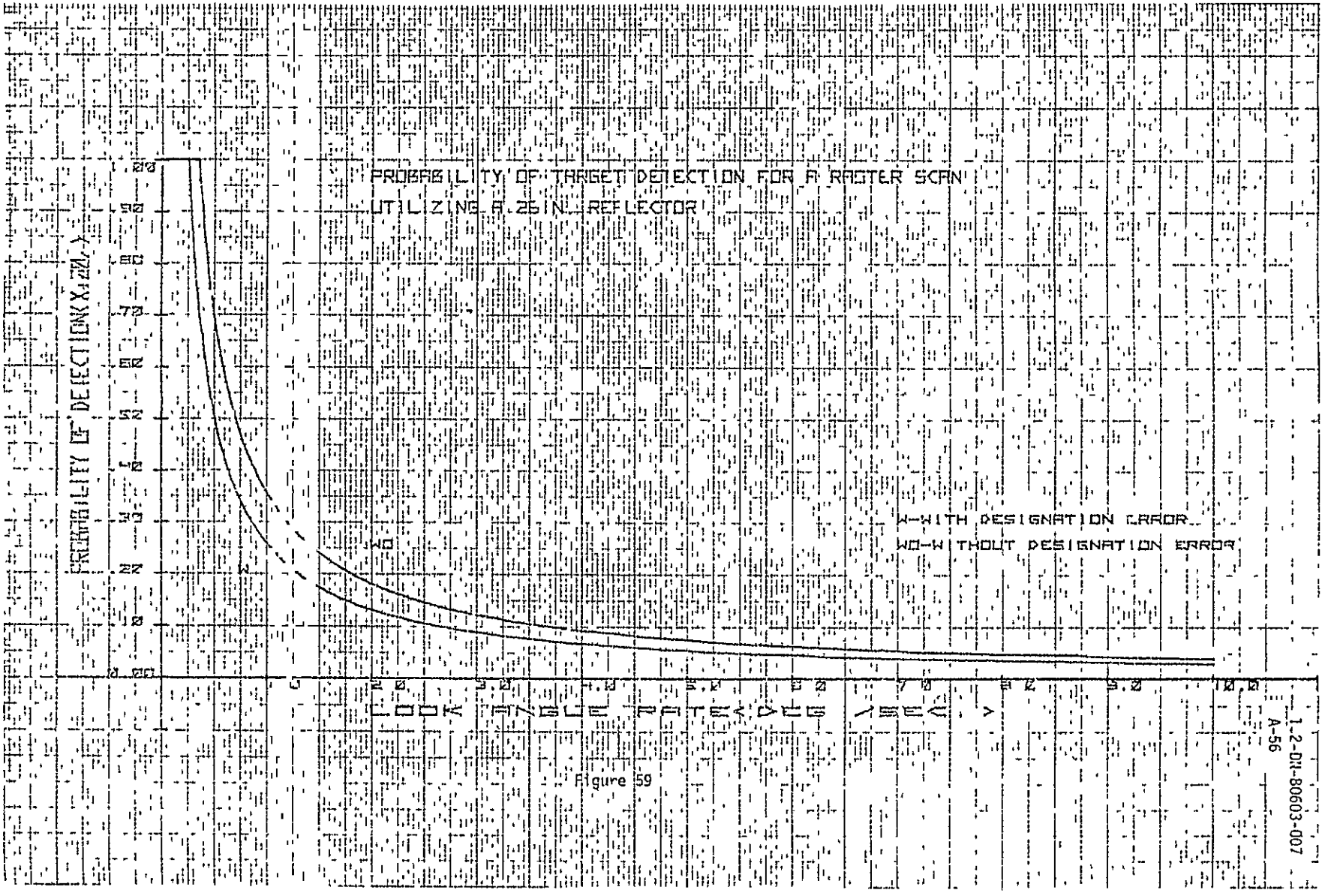

Figure 59

Figure 60

ORIGINAL PAGE IS
OF POOR QUALITY

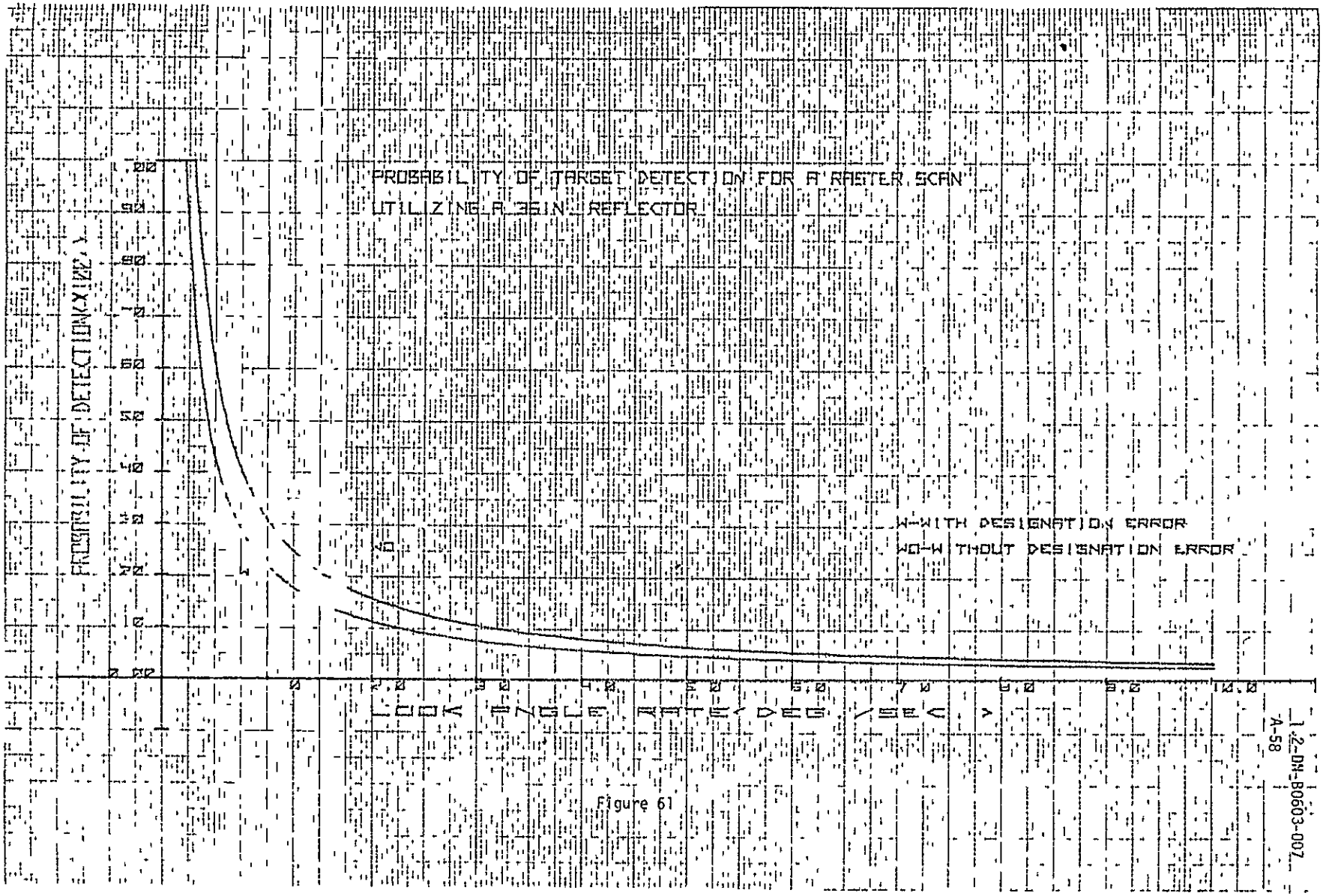

Figure 61

PROBABILITY OF TARGET DETECTION FOR A CONICAL SCAN
UTILIZING A 20 IN. REFLECTOR
W-WITH DESIGNATION ERROR
PROBABILITY OF DETECTION (%)
1.2-DI-80603-007-
A-59

Figure 62

ORIGINAL PAGE IS
OF POOR QUALITY

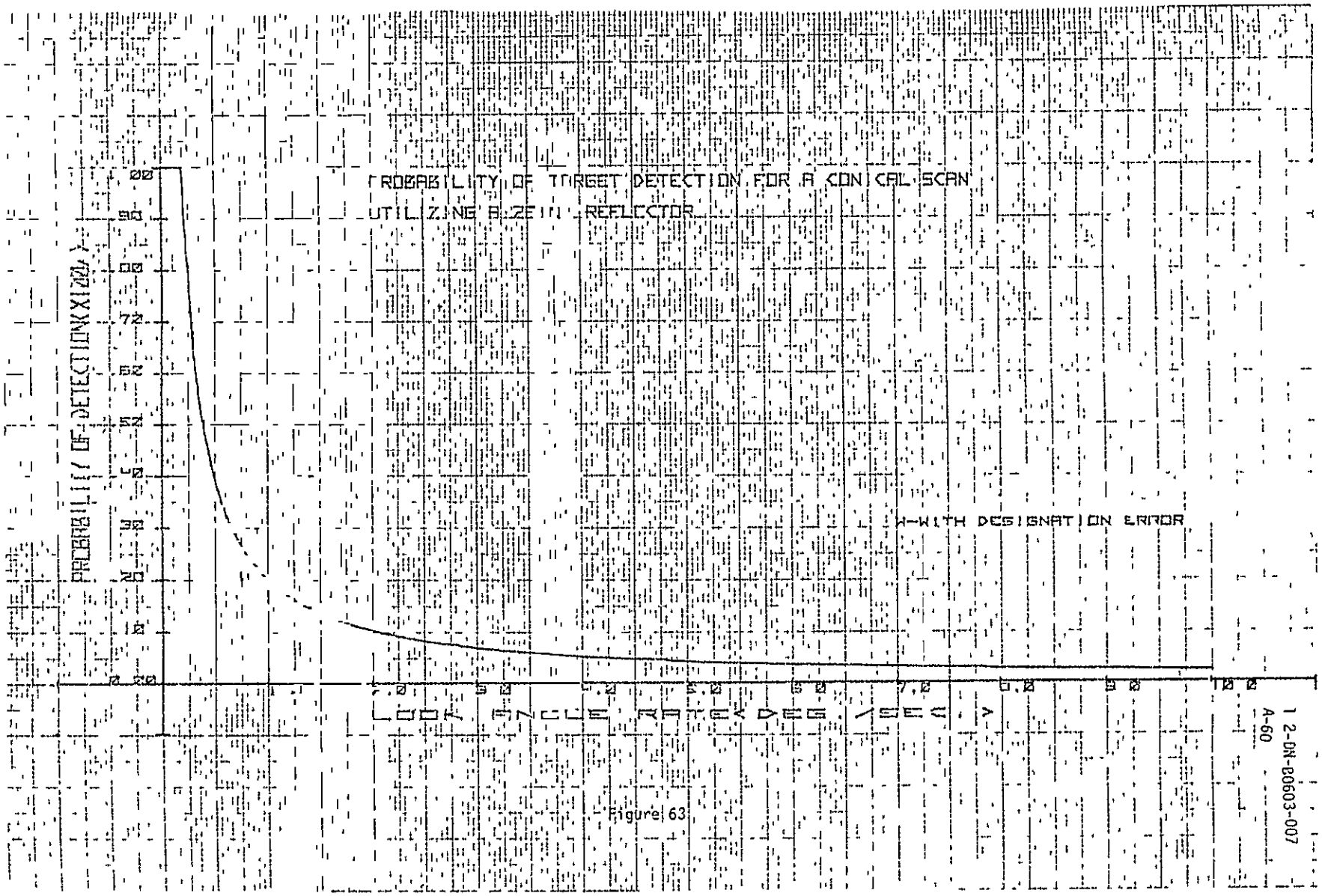

Figure 63

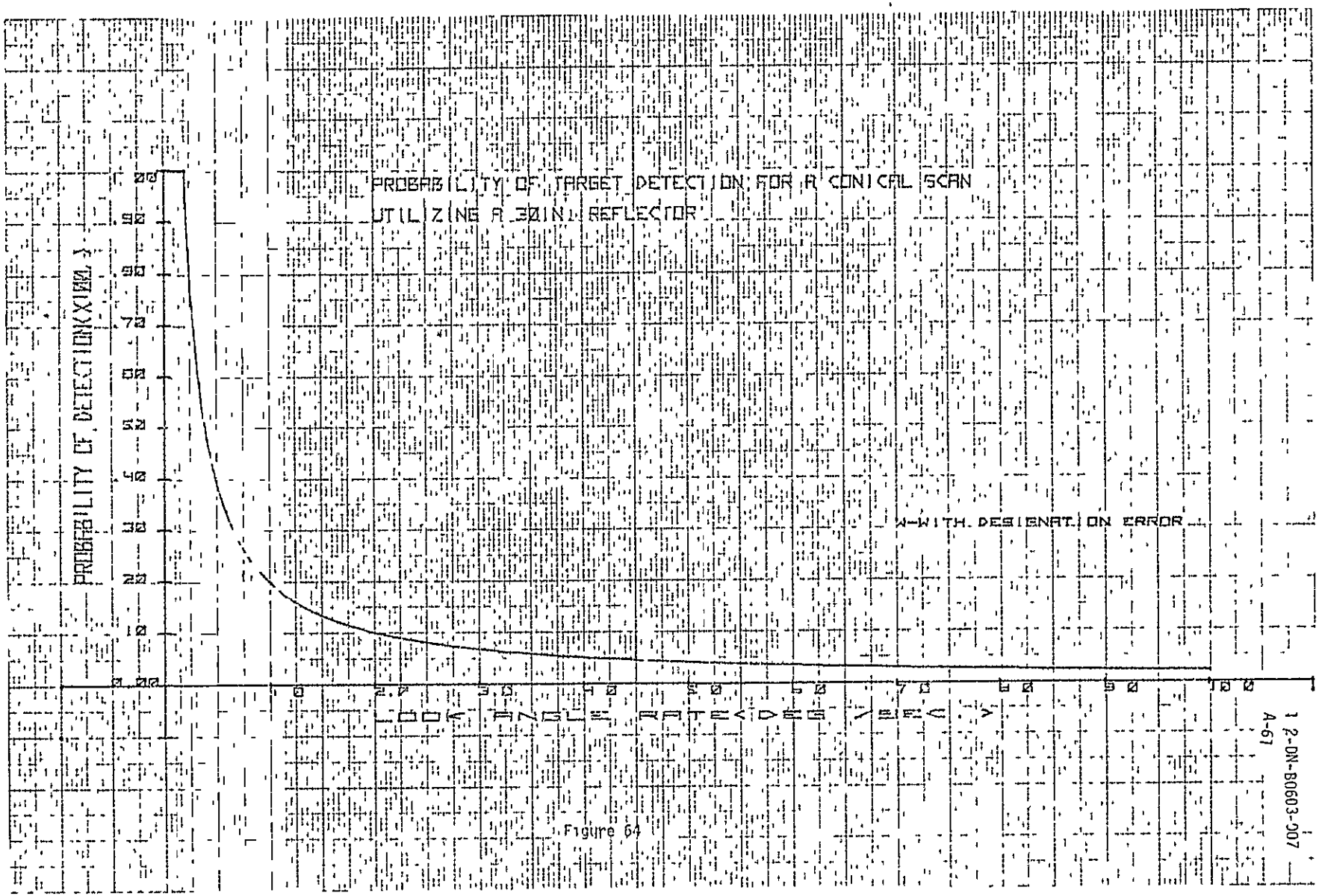

Figure 64

ORIGINAL PAGE IS
OF POOR QUALITY

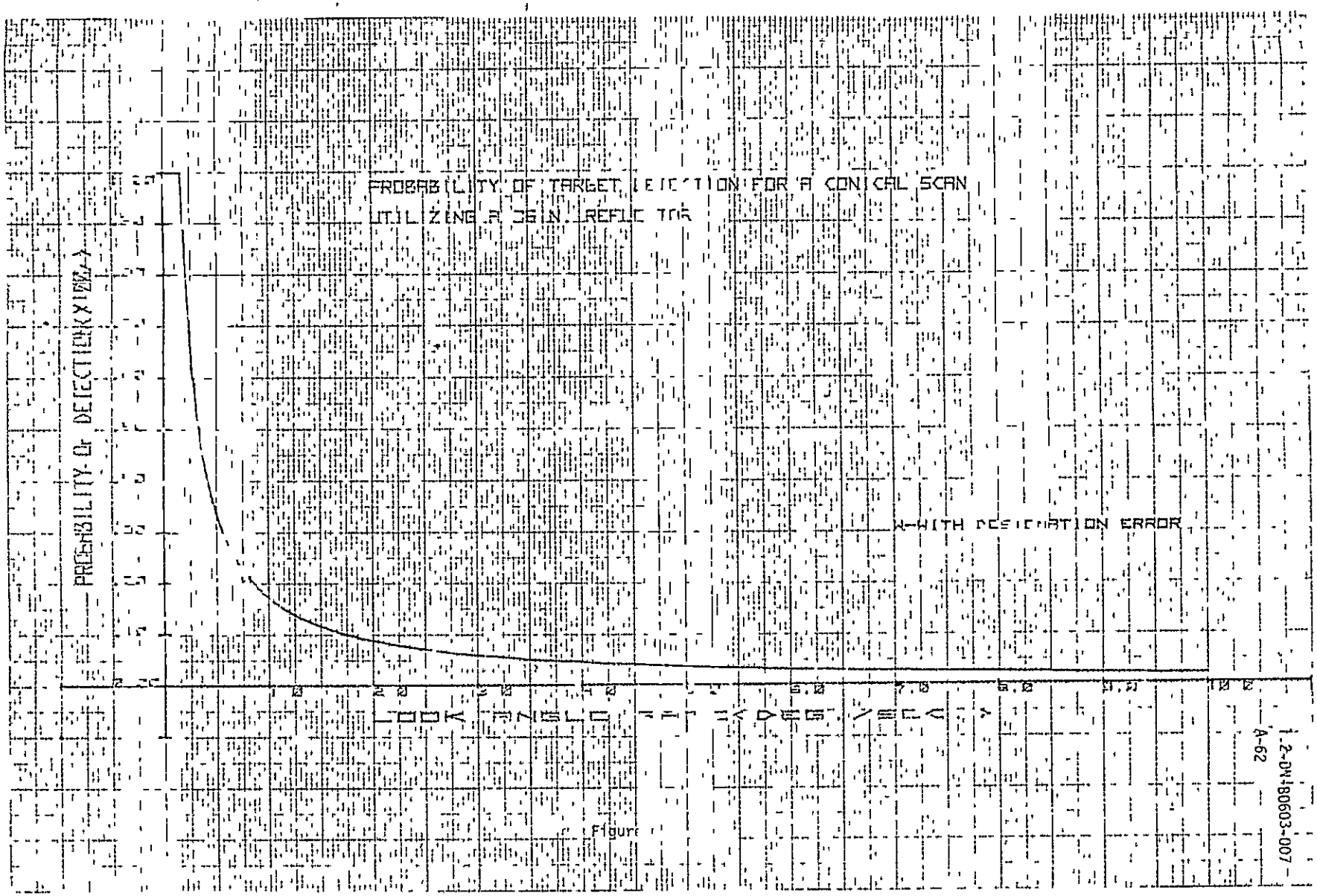

Figure

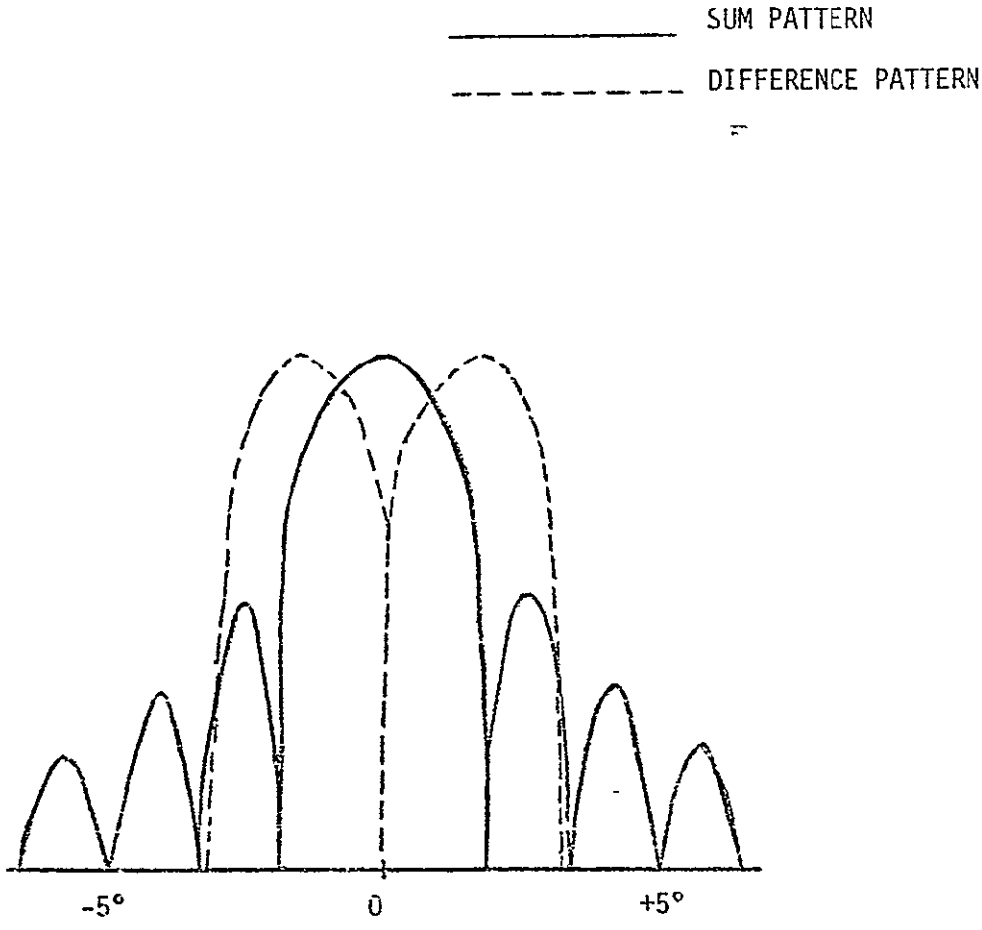

FIGURE 66 TYPICAL ANTENNA PATTERN FOR Ku-BAND MONOPULSE FEED

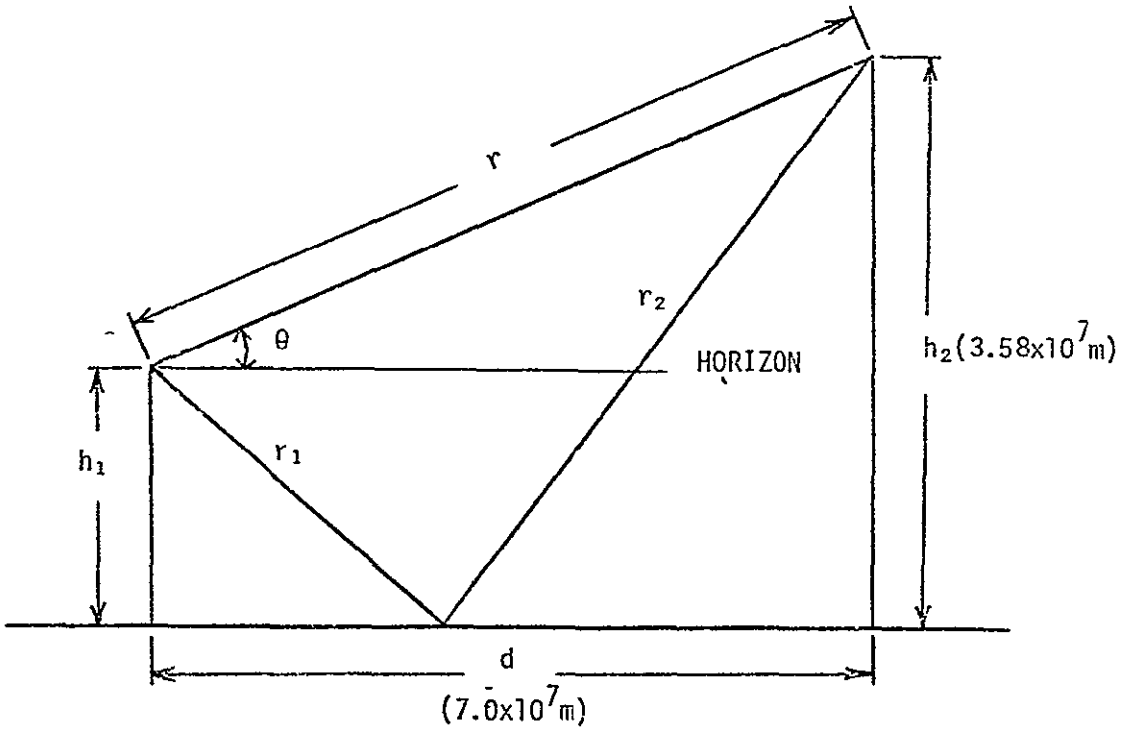

FIGURE 67 IDEALIZED PLANE SURFACE MODEL FOR MULTIPATH CALCULATIONS

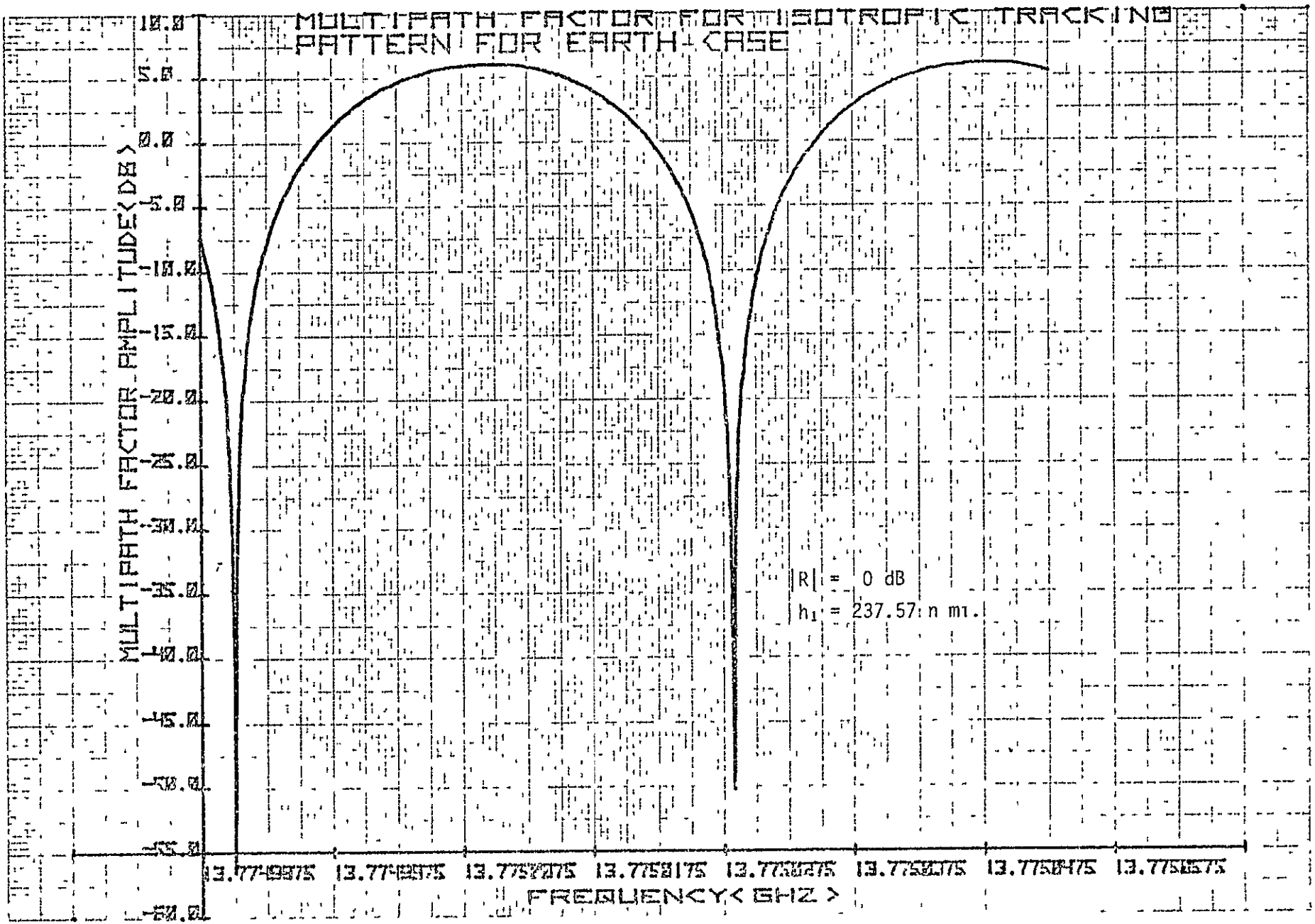

1.2-D1-B0603-017
A-65

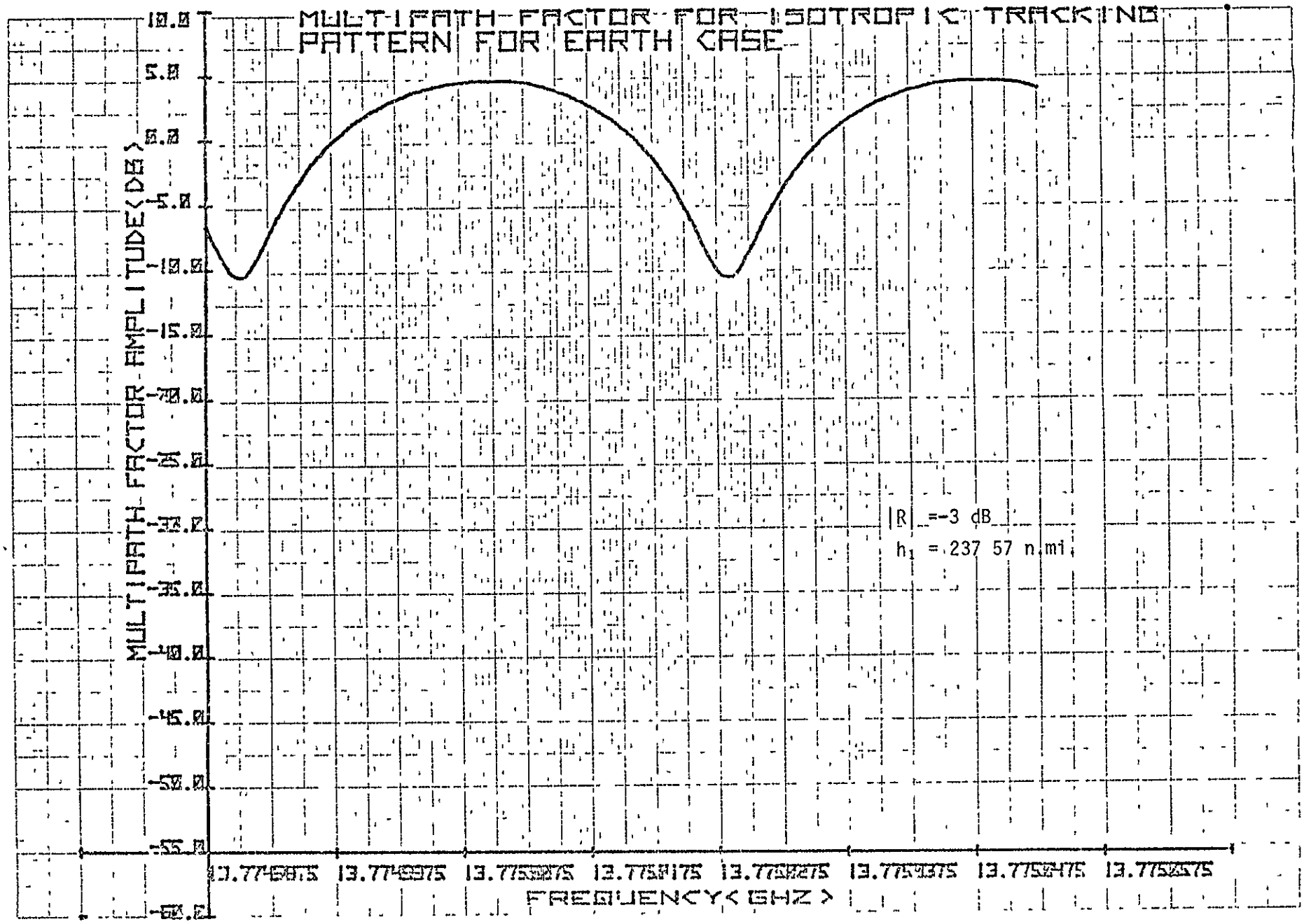
MULTIPATH FACTOR FOR ISOTROPIC TRACKING PATTERN FOR EARTH CASE
MULTIPATH FACTOR AMPLITUDE (DB)
10.0
5.0
0.0
-5.0
-10.0
-15.0
-20.0
-25.0
-30.0
-35.0
-40.0
-45.0
-50.0
-55.0
-60.0
|R| =-3 dB
h1 = 237 57 n.mi
13.774
13.774
13.775
13.775
13.775
13.775
13.775
13.775
FREQUENCY (GHZ)

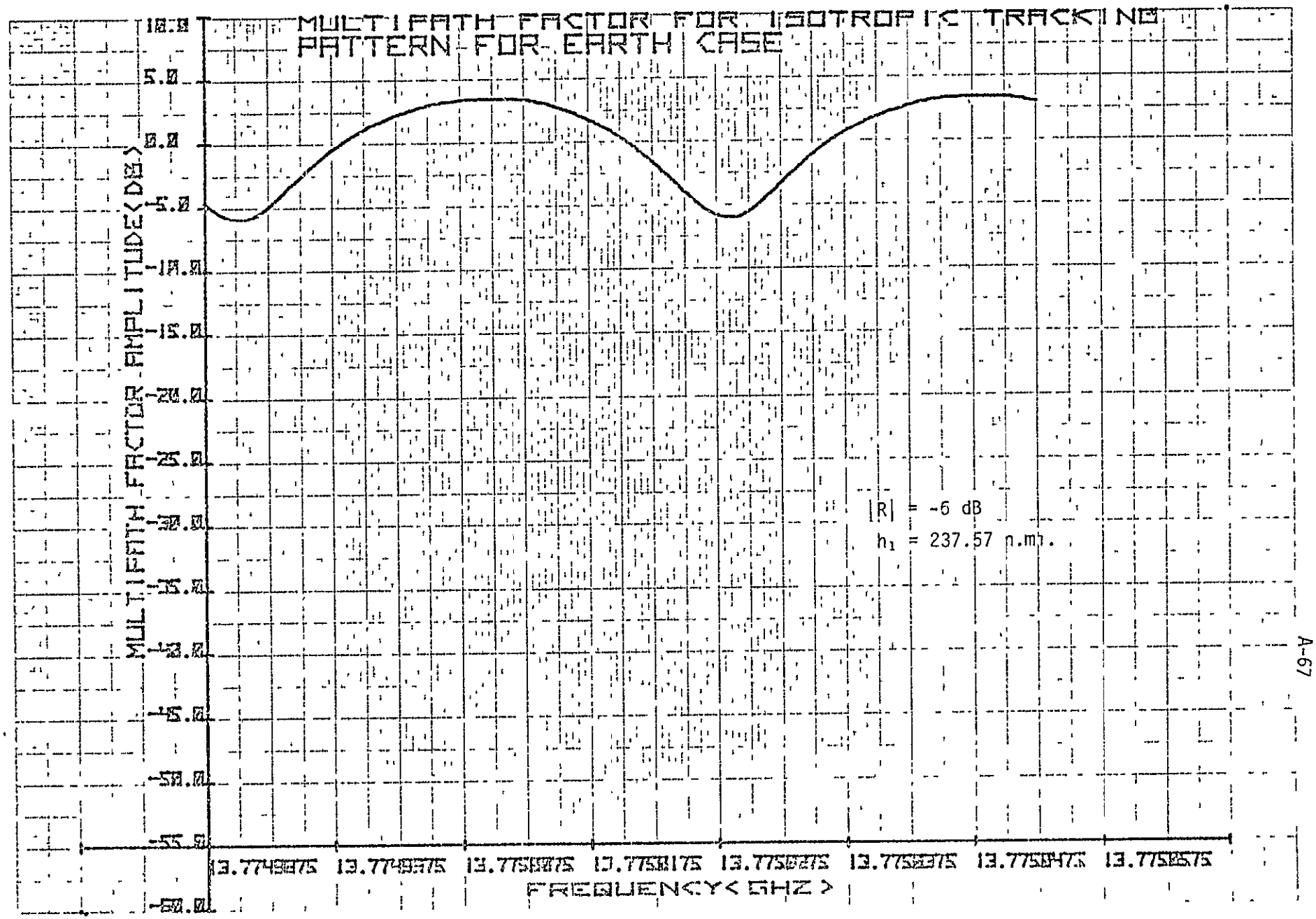

FIGURE 70

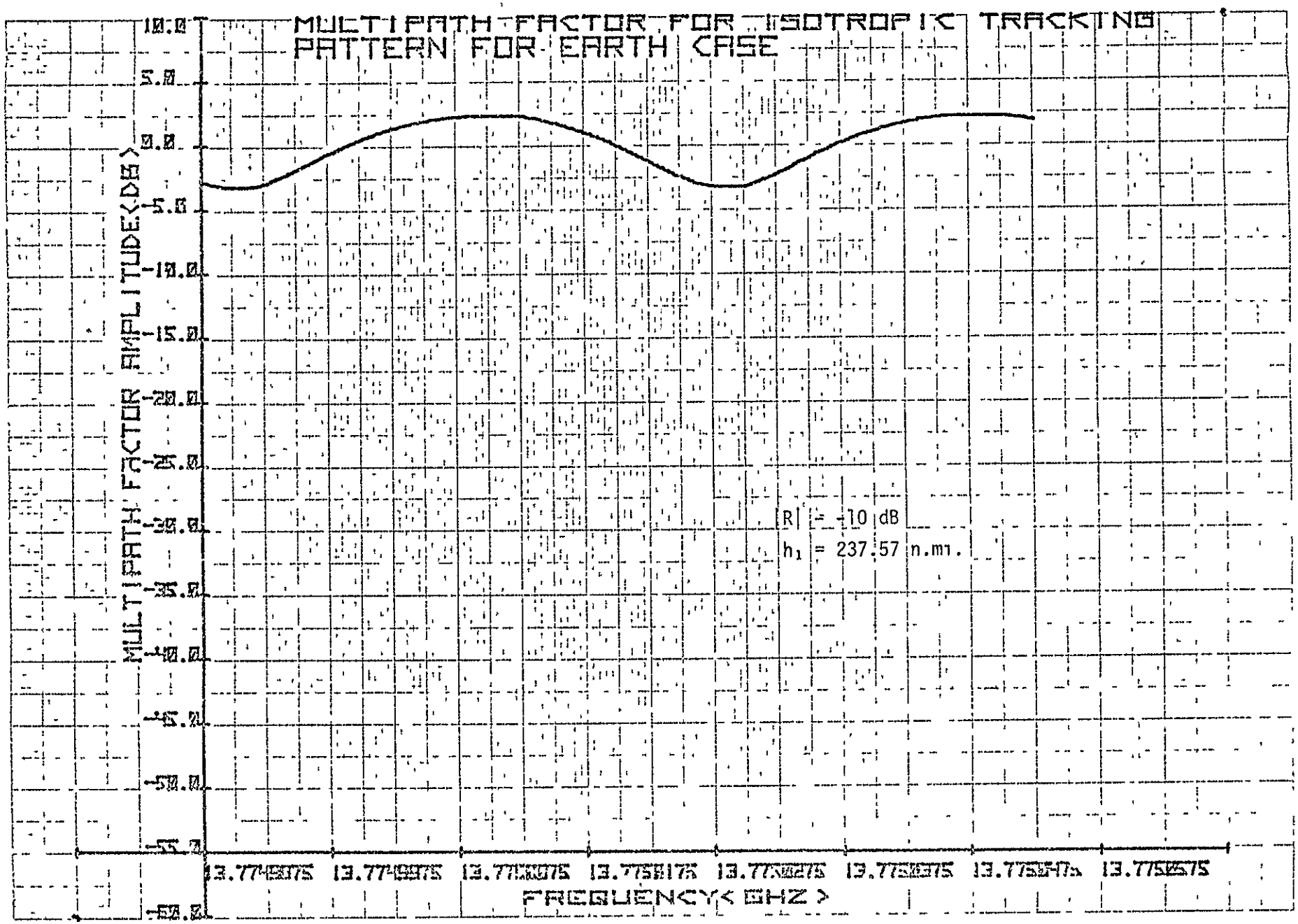

12-DI-B0603-007
A-68

MULTIPATH FACTOR FOR ISOTROPIC TRACKING PATTERN FOR ORBITER CASE
MULTIPATH FACTOR AMPLITUDE (DB)
10.0
5.0
0.0
-5.0
-10.0
-15.0
-20.0
-25.0
-30.0
-35.0
-40.0
-45.0
-50.0
-55.0
-60.0
-65.0
-70.0
-75.0
FREQUENCY (GHz)
14.4
14.9
15.4
15.7
|R| = 0 dB
h = meter
17-DH-B0603-007
A-69

MULTIPATH FACTOR FOR ISOTROPIC TRACKING
PATTERN FOR ORBITER CASE
MULTIPATH FACTOR AMPLITUDE(DBX)
10.0
5.0
0.0
-5.0
-10.0
-15.0
-20.0
-25.0
-30.0
-35.0
-40.0
-45.0
-50.0
-55.0
-60.0
-65.0
-70.0
-75.0
12.9
13.4
13.9
14.4
14.9
15.4
15.7
FREQUENCY(GHZ)
-3 dB
meter
1.2-D1-B0603-007
A-70

MULTIPATH FACTOR FOR ISOTROPIC TRACKING PATTERN FOR ORBITER CASE
MULTIPATH FACTOR AMPLITUDE(DB)
FREQUENCY (GHZ)
RI = -6 dB
h1 = 1 meter
12.9
13.4
13.9
14.4
14.9
15.4
15.7
10.0
5.0
0.0
-5.0
-10.0
-15.0
-20.0
-25.0
-30.0
-35.0
-40.0
-45.0
-50.0
-55.0
-60.0
-65.0
-70.0
-75.0
1.2-ON-80603-007
A-71

MULTIPATH FACTOR AMPLITUDE(DB)
FREQUENCY(GHZ)
12.9
13.4
13.9
14.1
14.3
15.4
15.7
-5.0
-10.0
-15.0
-20.0
-25.0
-30.0
-35.0
-40.0
-45.0
-50.0
-55.0
-60.0
-65.0
-70.0
-75.0
|R| = -10 dB
h = 1 meter
MULTIPATH FACTOR FOR ORBITER ISOTROPIC TRACKING
FOR ORBITER CASE

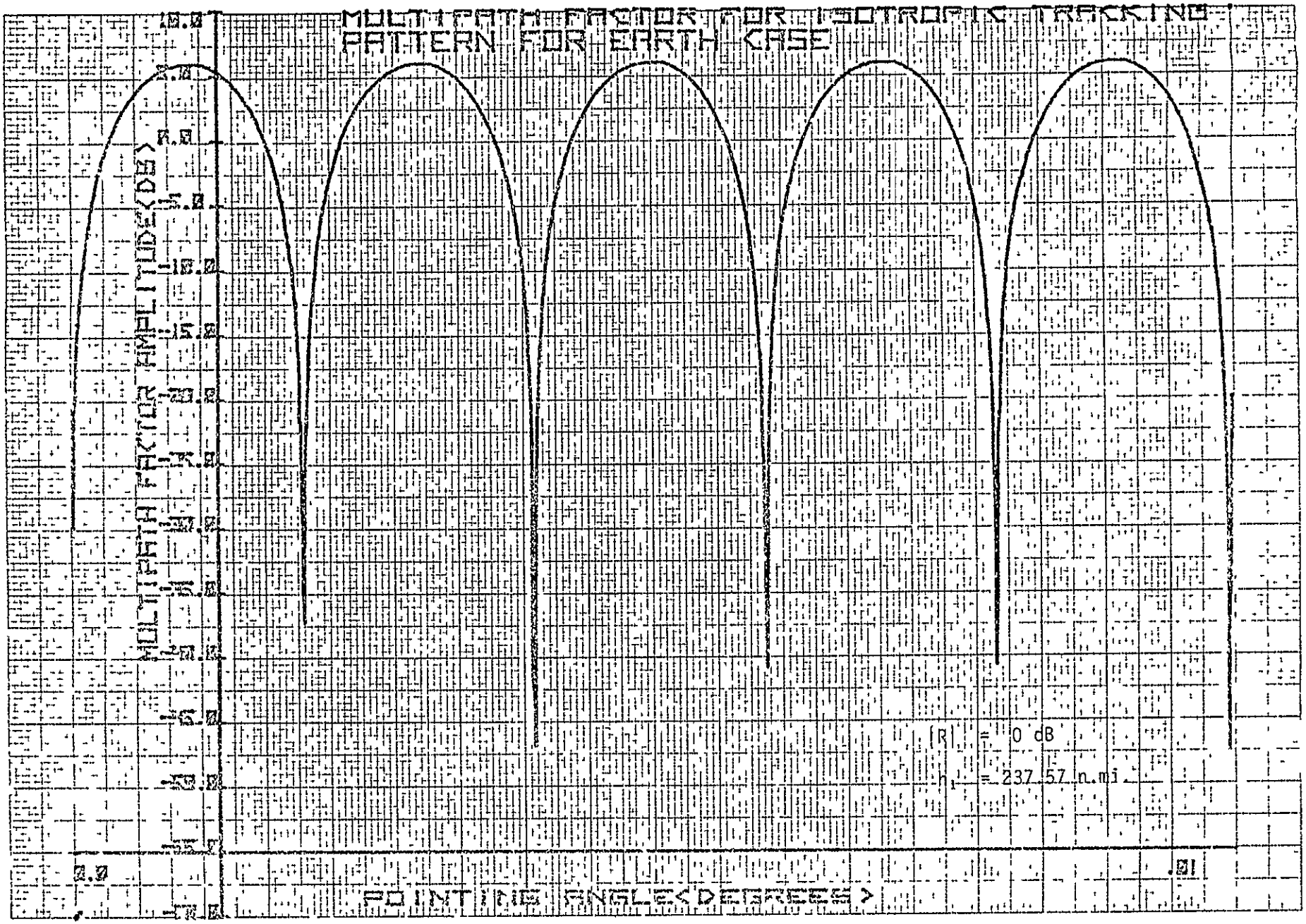

FIGURE 76

FIGURE 78

NO 340 10½ DIETZGEN GRAPH PAPER
10 X 10 PER HALF INCH

DIETZGEN CORPORATION
MADE IN U.S.A.

A-76

1.2-DI-B0603-007

FIGURE 80

FIGURE 81

FIGURE 22

NO 340 10% DIETZGEN GRAPH PAPER
10 X 10 PER HALF INCH

DIETZGEN CORPORATION
MADE IN U.S.A.

1.2-DH-B0603-007
A-80

FIGURE 93

APPENDIX B

HP 9821A CALCULATOR PROGRAMS

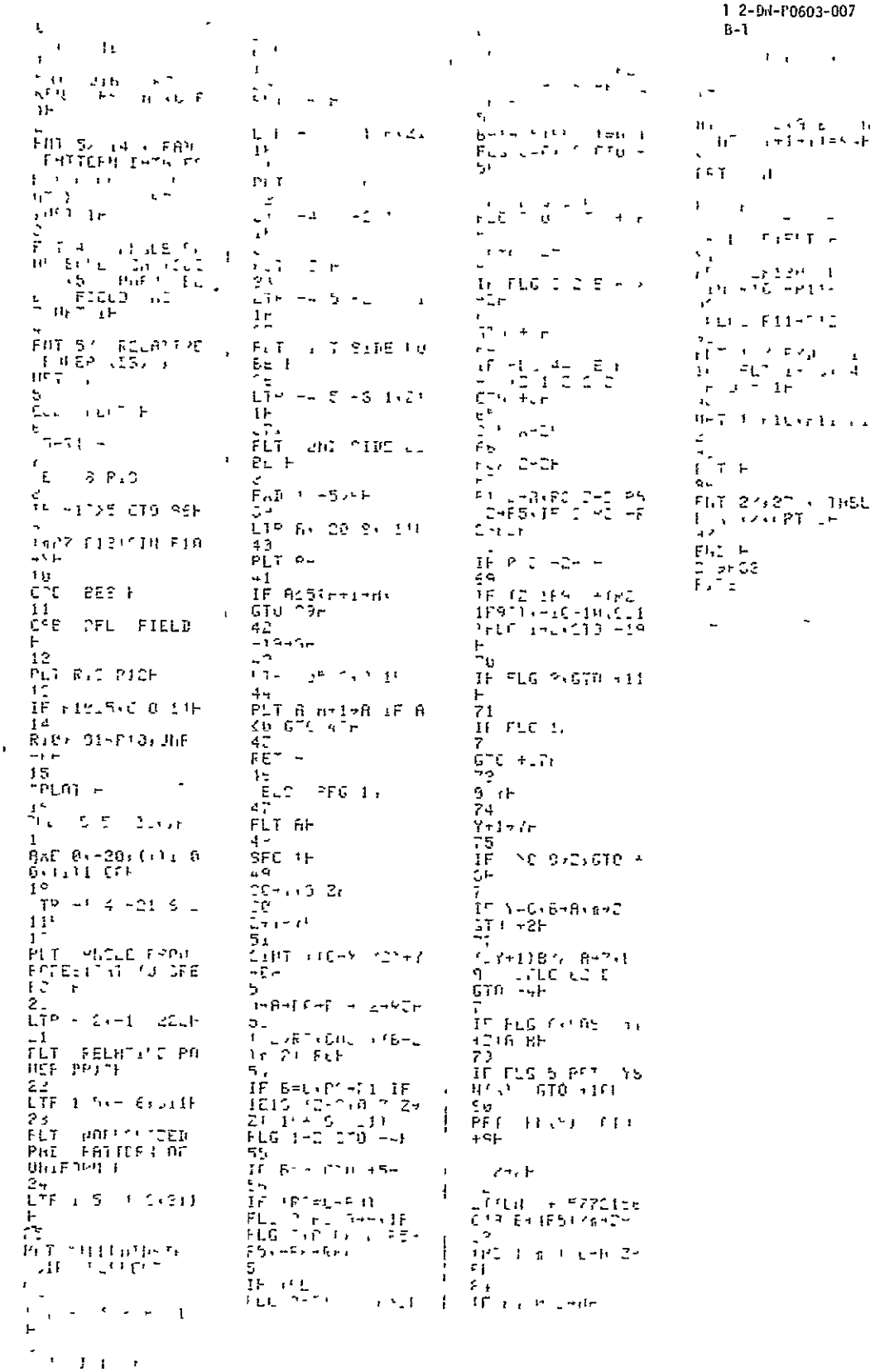

Figure 84 Antenna Radiation Program For Circular Isotropic Reflector

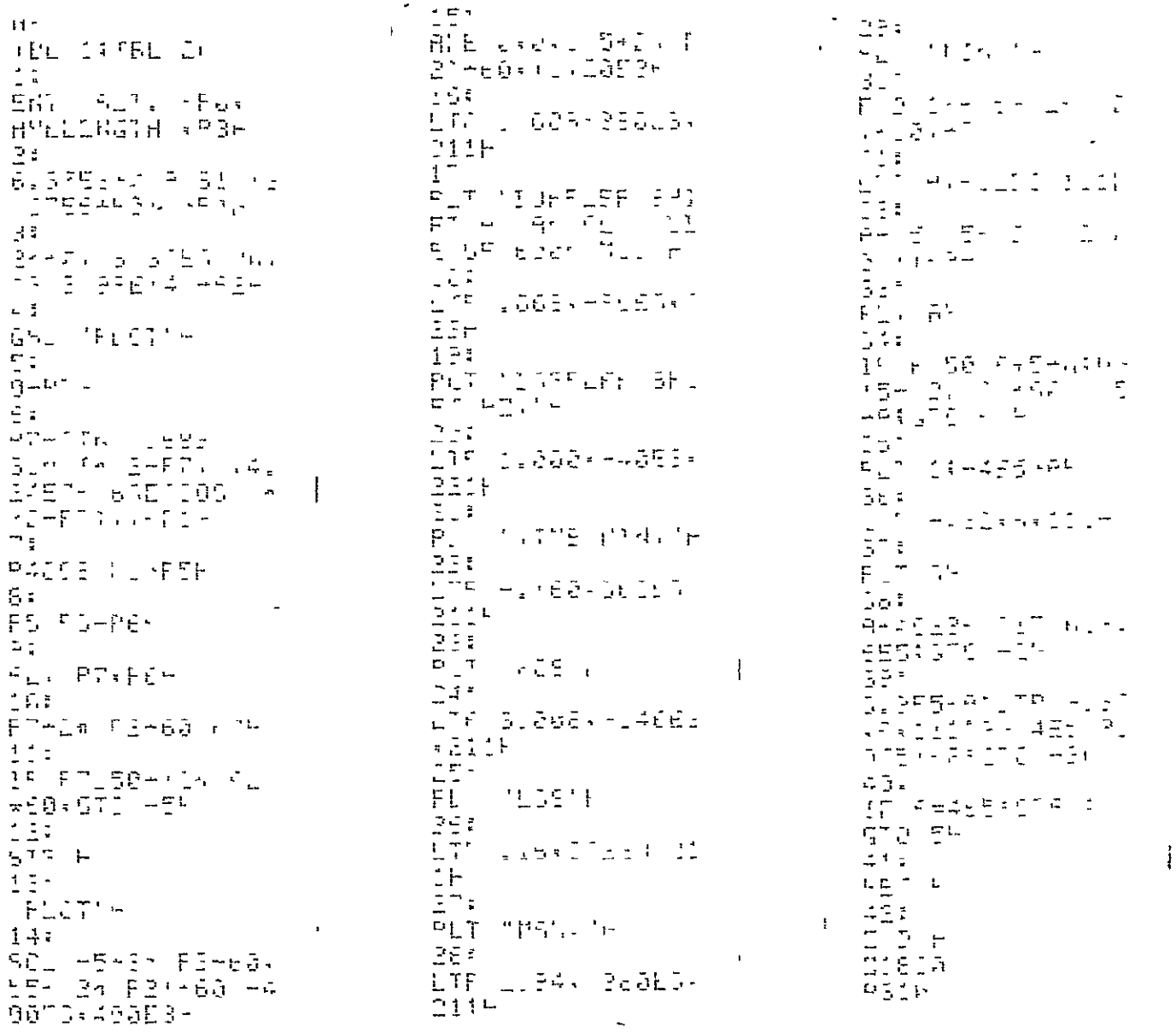

ORIGINAL PAGE IS
OF POOR QUALITY

Figure 85 Doppler Shift Plot Program

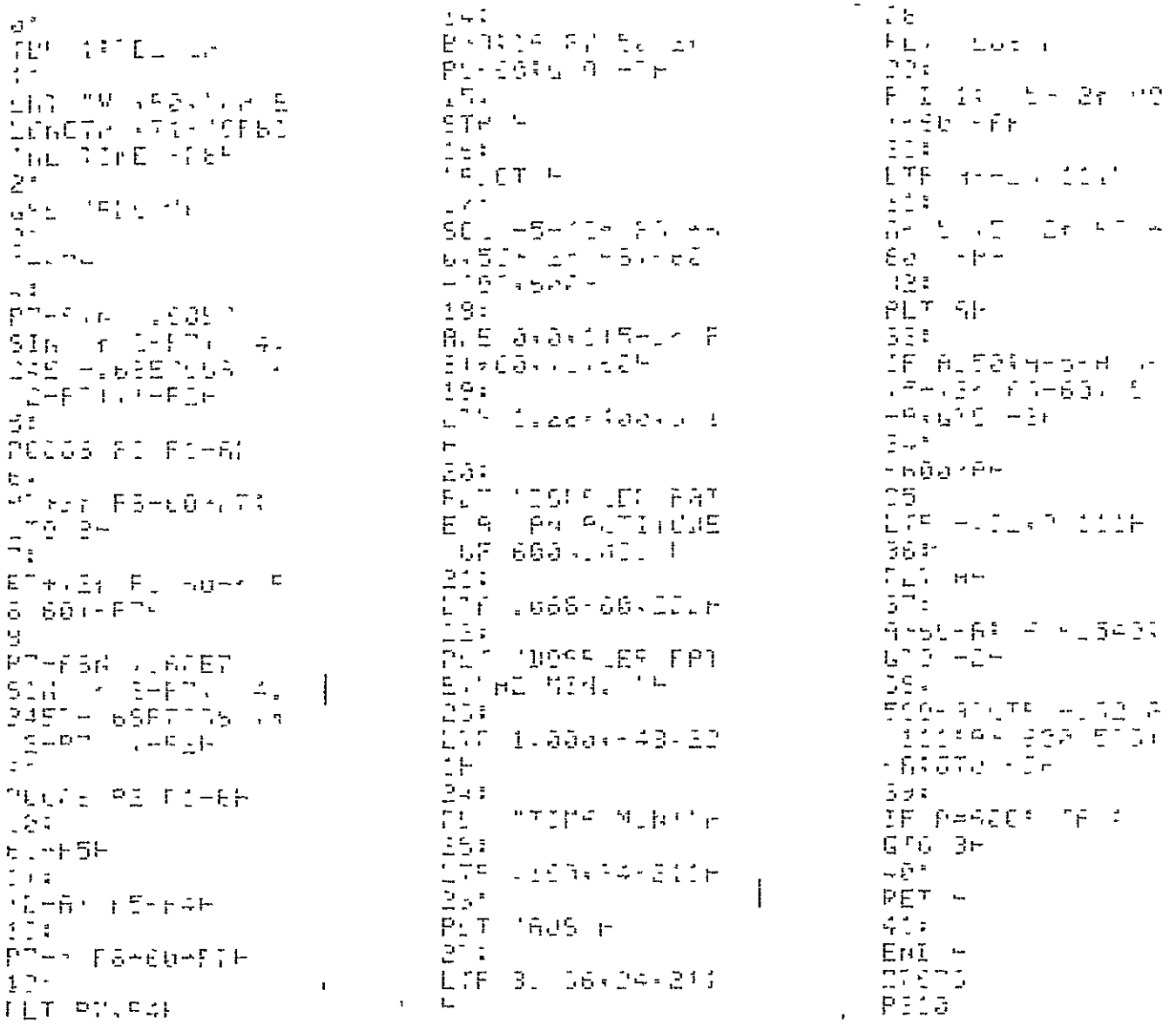

ORIGINAL PAGE IS
OF POOR QUALITY

Figure 86 Doppler Rate Plot Program

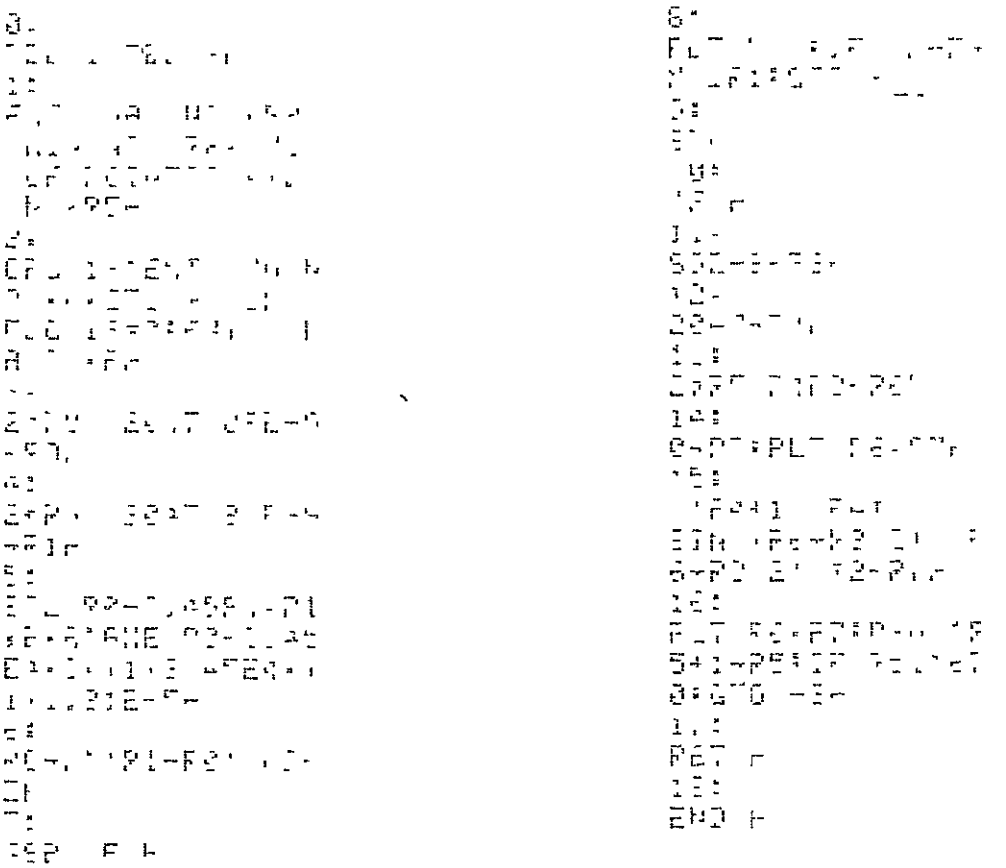

ORIGINAL PAGE IS
OF POOR QUALITY

Figure 87 Plot of Program Double-Sided Spread Frequency Spectrum From the TDRS to the Orbiter

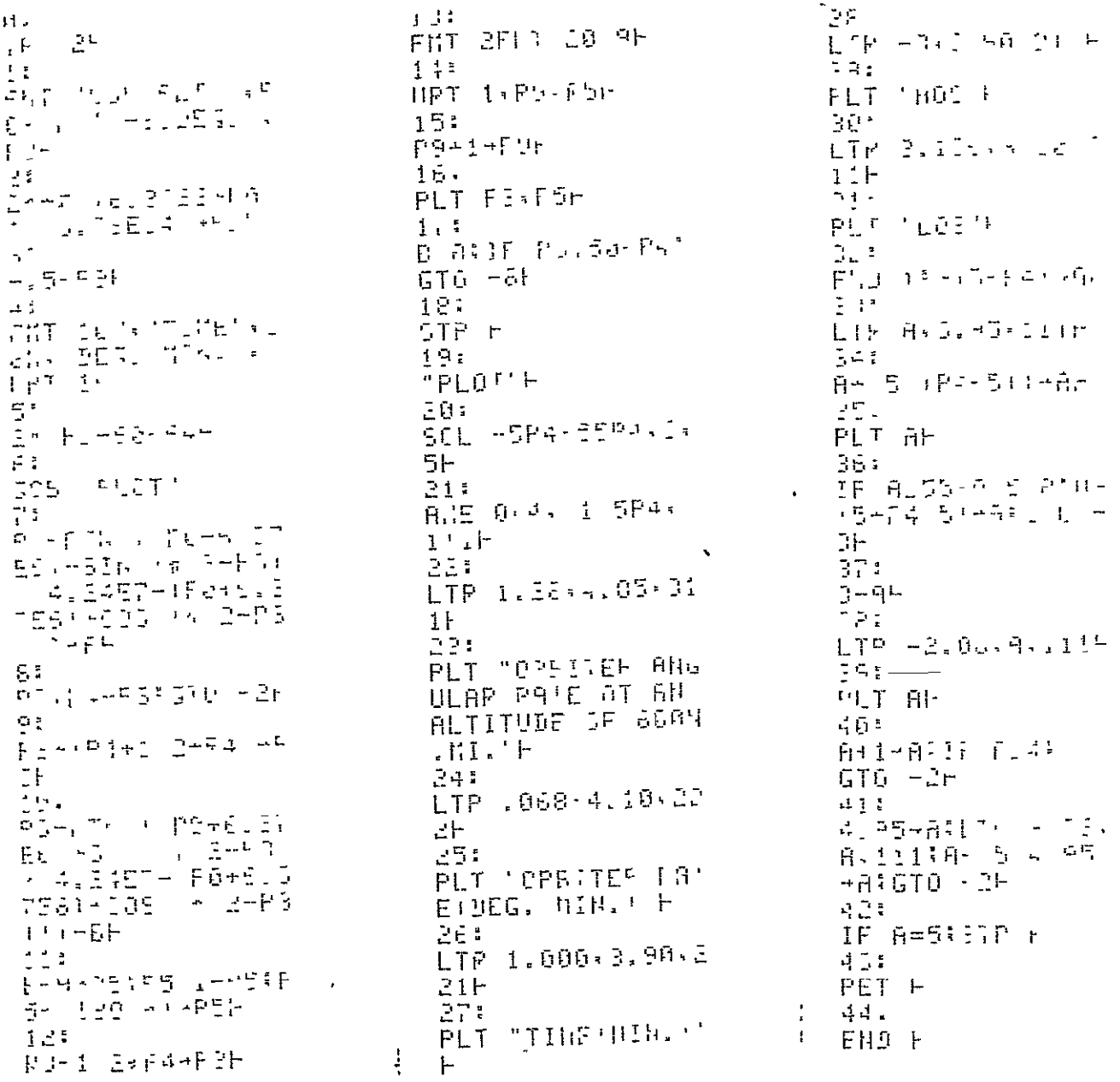

Figure 88 Orbiter Look Angle Variations in IH & LVLH Configuration

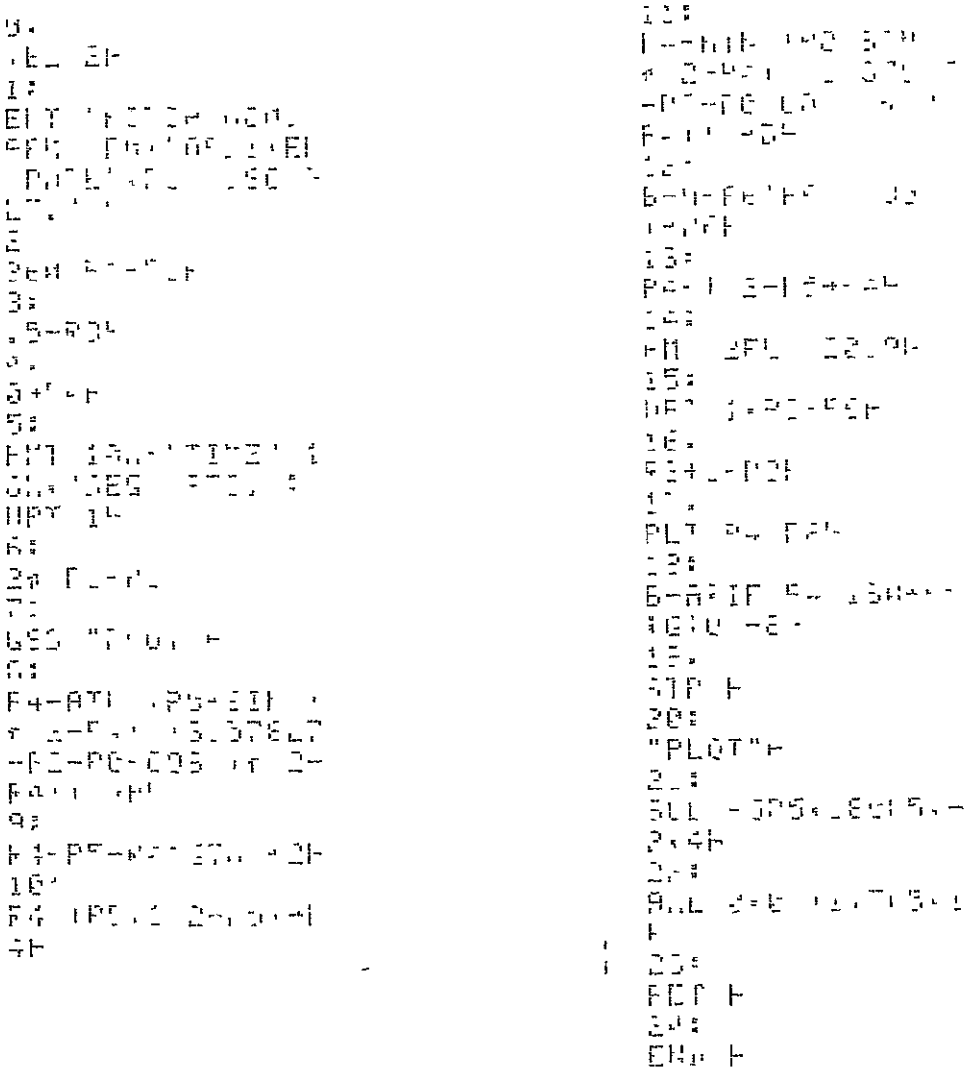

Figure 89 Calculation of Roll, Pitch and Yaw Attitudes of the Ku-Band Antenna

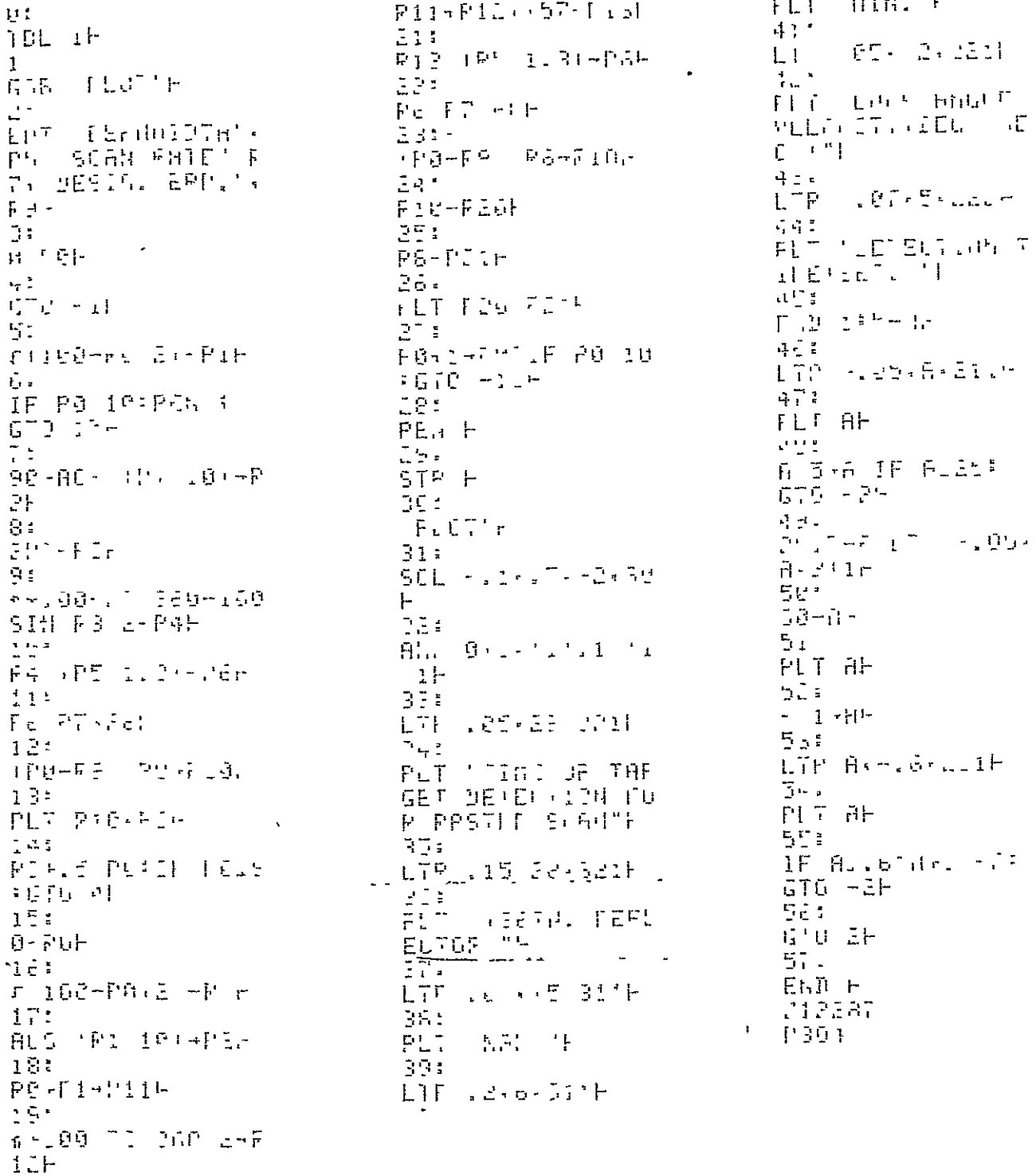

ORIGINAL PAGE IS
OF POOR QUALITY

Figure 90 Detection Time As A Function Of Look Angle Rate For Raster Scan

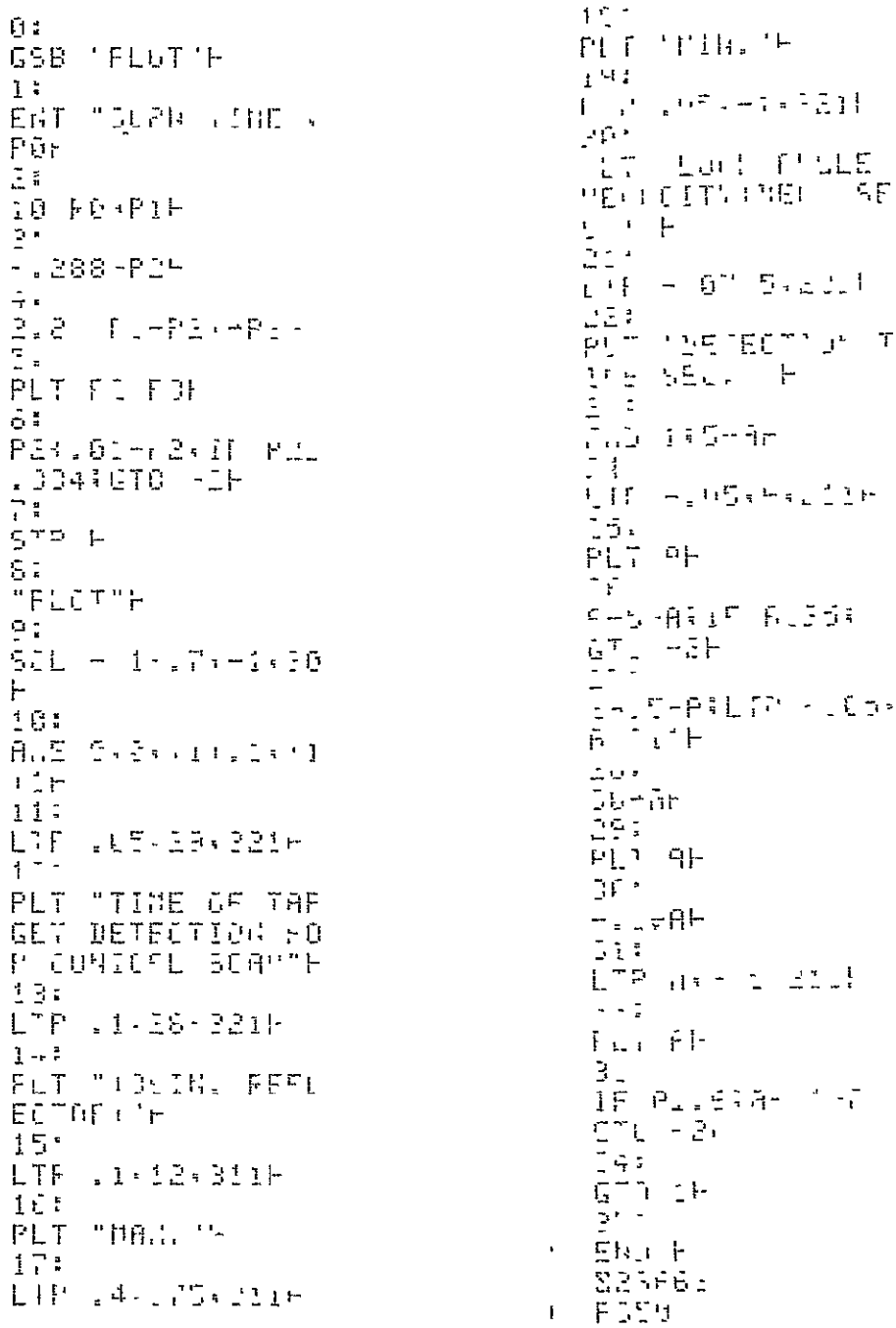

ORIGINAL PAGE IS
OF POOR QUALITY

Figure 91 Detection Time As A Function Of Look Angle Rate For Conical Scan

```
0:
ELL 1⊢
1:
GSB "FLAT"⊢
2:
ENT "MA' 'AP -PS
, SLUB TJLE ,r1-
'LSIC ET','FL
'SCAN FAL ,PI
3:
0→P6⊢
4:
'F6-PE' F1-P7'FS
-1-F6⊢
5:
IF F4_F6;F3·P7⊢
6:
PO F4-F5⊢
7:
PLT F4·F5⊢
8:
IF F4__6;GTO -4⊢
9:
STP ⊢
10:
 FLOT'⊢
11:
SCL -1,11,-,1,1⊢
 2:
AXE 0-0,·1·1- 1·
.1⊢
13:
LTP 2·,35·311⊢
14:
PLT 'PROBABILITY
 OF TARGET DETEC
TION FOR A RASTE
R SCAN'⊢

15:
LTP 2·,5·311⊢
16:
PLT 'UTILIZING A
 DBIN AFFLECTOR
'⊢
17:
LTP 3·-,07,311⊢
18:
FLT 'LOOK ANGLE
RATE,DEG/SEC. '
⊢
19:
LTP -,7-,3-,2,⊢
20:
PLT 'PROBABILITY
 OF DETECTION(
PERCENT)'⊢
21:
LTP 75· 3·211⊢
22:
FLT '1'⊢
23:
LTP 3·,35·211⊢
24:
PLT 'NO'⊢
25:
LTP 7·,3 211⊢
26:
PLT 'W-WITH DESI
GNATION ERROR'⊢
27:
LTP 7·,25·211⊢

28:
PLT 'NO-NO AUG'
DESIGNATION ERRO
R'⊢
29:
FXD '.-A⊢
30:
LTP 9· ,02 ,1 ⊢
31:
PL' A⊢
32:
IF A__1;A 1-A⊢
GTO -2⊢
33:
FXD 2,,0-,⊢
34:
LTP -,5·A·2,⊢
35:
FLT A⊢
36:
IF A_,6;A+,1-A⊢
GTO -2⊢
37:
.90-A;LTP -,5·A·
211⊢
38:
1→A⊢
39:
PLT A⊢
40:
GTO 2⊢
41:
END ⊢
215_33
R323
```

**ORIGINAL PAGE IS
OF POOR QUALITY**

Figure 92 Probability of Detection As A Function Of Angular Rate

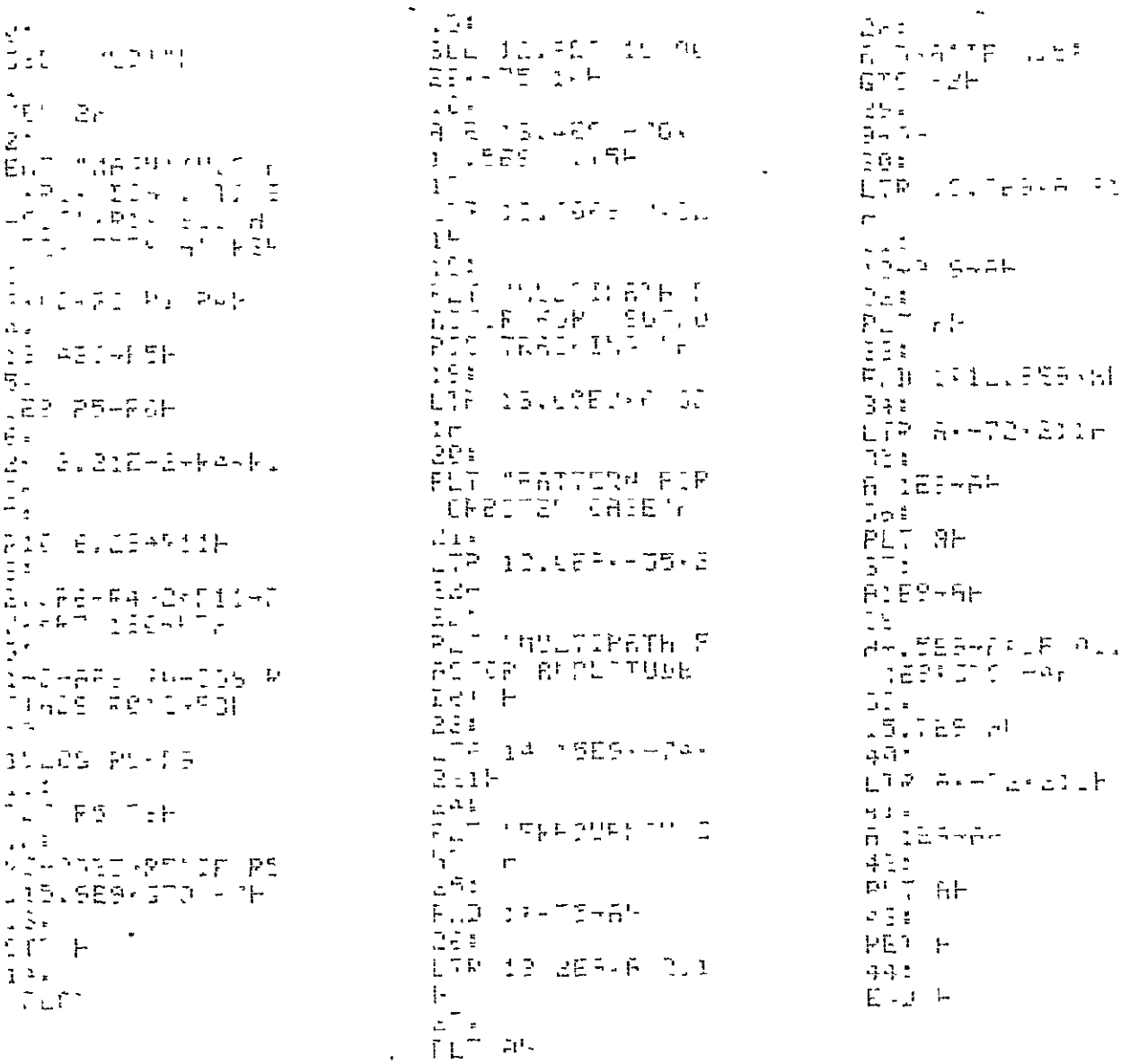

ORIGINAL PAGE IS
OF POOR QUALITY

Figure 93 Multipath Factor As A Function Of Frequency

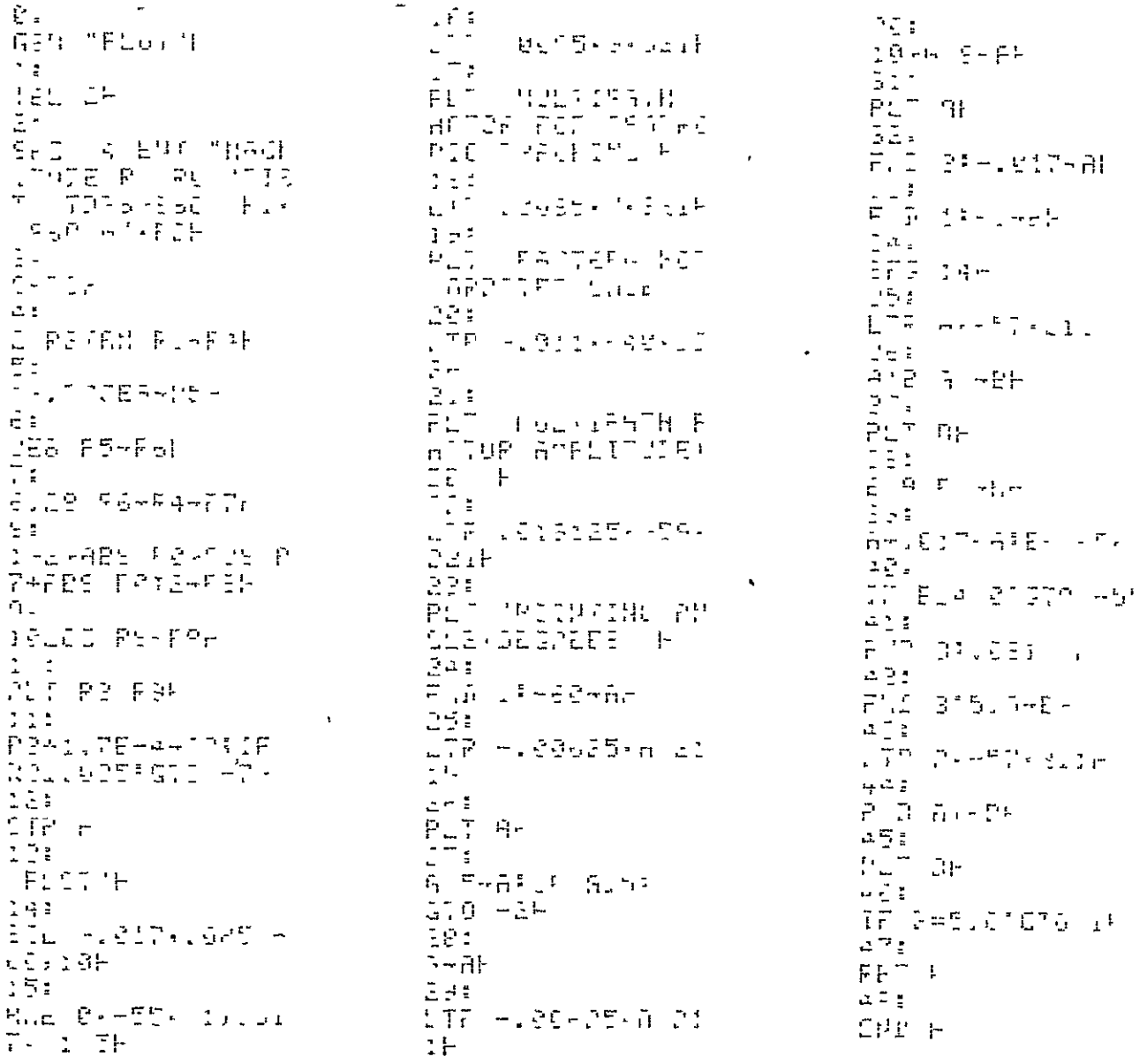

ORIGINAL PAGE IS
OF POOR QUALITY

Figure 94 Multipath Factor As A Function Of Pointing Angle